Grundvåg Sten-Andreas (Orcid ID: 0000-0002-4309-898X)
Pohl Florian (Orcid ID: 0000-0003-1008-8467)
Spychala Yvonne Therese (Orcid ID: 0000-0002-3896-9234)

Deep-water sand transfer by hyperpycnal flows, the Eocene of Spitsbergen, Arctic Norway

STEN-ANDREAS GRUNDVÅG[1,2], WILLIAM HELLAND-HANSEN[3], ERIK P. JOHANNESSEN[4], JORIS EGGENHUISEN[5], FLORIAN POHL[6] and YVONNE SPYCHALA[7]

[1]*Department of Geosciences, UiT The Arctic University of Norway, P.O. Box 6050 Langnes, N-9037 Tromsø, Norway (E-mail: sten-andreas.grundvag@uit.no)*

[2]*Department of Arctic Geology, University Centre in Svalbard, P.O. Box 156, N-9171 Longyearbyen, Norway.*

[3]*Department of Earth Science, University of Bergen, P.O. Box 7800, N-5020 Bergen, Norway.*

[4]*EP Skolithos, Sisikveien 36, N-4022 Stavanger, Norway*

[5]*Department of Earth Science, University of Utrecht, 3584 CS Utrecht, NL*

[6] *Marine School of Biological and Marine Sciences, University of Plymouth, Drake Circus, PL4 8AA Plymouth, UK*

[7]*Institute of Geology, Leibniz Universität, Hannover, Germany*

Associate Editor – Fabrizio Felletti

Short title – Deep-water hyperpycnites

ABSTRACT

Flood-generated hyperpycnal flows are dense, sediment-laden, turbulent flows that can form long-lived, bottom-hugging turbidity currents, which undoubtedly transport large volumes of fine-grained sediments into the ocean. However, their ability in transferring sand into deep-water basins is debated. This study presents sedimentological evidence of sandy hyperpycnal flow deposits (hyperpycnites) in a series of basin floor lobe complexes associated with a progradational shelf margin in the Eocene of Spitsbergen, Arctic Norway. Four coexisting types of sediment gravity flow deposits are recognized: (i) sandy hyperpycnites deposited by quasi-steady hyperpycnal flows; (ii) turbidites deposited by waning, surge-type turbidity currents; (iii) hybrid event

This article has been accepted for publication and undergone full peer review but has not been through the copyediting, typesetting, pagination and proofreading process which may lead to differences between this version and the Version of Record. Please cite this article as doi: 10.1111/sed.13105

beds deposited by transitional flows; and (iv) mass transport deposits emplaced during rare slope failures. The abundance of thick-bedded massive sandstones, frequent bed amalgamation, the distribution of hyperpycnites across the lobes and the abundance and systematic occurrence of plant-rich hybrid event beds and associated climbing ripple cross-laminated beds in the lobe fringes, suggest that hyperpycnal flow was the most important mechanism driving lobe progradation. Shelf-edge positioned fluvial channels linked to the basin floor lobe complexes via deeply incised, sandstone-filled slope channels, suggest that rivers fed directly onto the slopes where their dense, sand-laden discharges readily generated quasi-steady hyperpycnal flows that regularly reached the basin floor. The composite architecture and complex waxing–waning flow facies configuration of the hyperpycnites is consistent with sustained and concomitant suspension and traction deposition under fluctuating subcritical to supercritical conditions. Similar sandstone beds occur on the clinoform slopes, indicating that the hyperpycnal flows operated likewise on the slope. Plant-rich hybrid event beds indicate transformation of initially turbulent flows by relative enrichment of clay and plant material via progressive sand deposition to such an extent that it suppressed turbulence. The multi-faceted character of the hyperpycnites reported here, challenges traditional beliefs that hyperpycnites assumingly preserve the waxing–waning signal of single-peaked floods.

Keywords Clinoforms, hybrid event beds, quasi-steady hyperpycnal turbidity currents, sediment gravity flows, submarine lobes, Svalbard.

INTRODUCTION

Turbidity currents play a key role in the transportation of sediment to the deep sea, where their deposits, termed turbidites, represent the final sink for terrigenous sediment (e.g. Bouma, 1962, Middleton, 1993; Mulder & Alexander, 2001; Talling *et al*., 2012). Three principal triggering mechanisms have been proposed for turbidity currents: (i) submarine slope failure; (ii) oceanic processes (i.e. storms, tides and internal waves); and (iii) direct sourcing from flooding rivers producing dense, sediment-laden, bottom-hugging discharges, commonly referred to as hyperpycnal

flows (Bates, 1953; Mulder & Alexander, 2001; Mutti *et al*., 2003; Piper & Normark, 2009; Talling *et al*., 2013; Talling, 2014). These flood-generated flows are turbulent, quasi-steady sediment gravity flows which can be classified as long-lived (i.e. sustained) turbidity currents (e.g. Mulder & Syvitski, 1995; Mulder *et al*., 2003; Mutti *et al*., 2003). Hyperpycnal flows are known to transport large volumes of fine-grained sediment into the ocean and are an important process governing coastal sediment balance and evolution (Mulder & Syvitski, 1995; Mulder *et al*., 2003; Dadson *et al*., 2005; Mulder & Chapron, 2011; Khripounoff *et al*., 2012; Warrick *et al*., 2013; Warrick, 2020; Talling *et al*., 2022). An elevated density contrast of the incoming sediment-laden flood water compared to that of the ambient basinal water, is a prerequisite for the generation of hyperpycnal flows (Bates, 1953). Plunging may also occur if the incoming water has a lower temperature, and thus higher density, than that of the basinal ambient (Mulder *et al*., 2003). In marine basins, which usually have lower temperatures relative to the incoming riverine flood water, the high concentration of dissolved salt greatly reduces the potential for plunging and hyperpycnal flow initiation (cf. Mulder *et al*., 2003). As such, hyperpycnal flow conditions are achieved more readily in freshwater basins. The outburst of sub-glacial meltwater plumes, which typically exhibit very low temperatures and carry significant amounts of suspended sediments, represent another extreme case that can generate hyperpycnal flows (Mackiewicz *et al*., 1984; Piper & Normark, 2009). For these reasons, hyperpycnal flow deposits ('hyperpycnites') are commonly described from various lacustrine and glacio-deltaic successions, reflecting the favourable conditions for dense underflows to form in these environments (e.g. Nemec *et al*., 1999; Zavala *et al*., 2006; Girard *et al*., 2012; Yang *et al*., 2017; Cao *et al*., 2018; Bellwald *et al*., 2020; Chen *et al*., 2021). Despite recent developments in the surveillance of naturally occurring turbidity currents (Clare *et al*., 2016; Azpiroz-Zabala *et al*., 2017; Hage *et al*., 2019; Maier *et al*., 2019; Heijnen *et al*., 2020; Heerema *et al*., 2022; Pope *et al*., 2022; Talling *et al*., 2022), monitoring data of hyperpycnal flows in the marine realm is relatively sparse. Most of the reported cases are related to flash floods in arid regions and show that these hyperpycnal flows are dilute, mud-rich bottom plumes, which is readily influenced by waves, storm-induced currents or tidal currents (e.g. Wright *et*

al., 1988; Sommerfield & Nittrouer, 1999; Warrick & Milliman, 2003; Warrick *et al*., 2008; Talling, 2014; Kantz *et al*., 2015; Shanmugam, 2018). Monitoring data from multiple freshwater reservoirs and dams also document the dilute, low-density, muddy nature of hyperpycnal flows (e.g. Olariu *et al*., 2011; Lai & Capart, 2009; Talling *et al*., 2013; Talling, 2014), further substantiated by core data from modern flood-generated shelf deposits, which mostly reveal mud-grade sediments (e.g. Wheatcroft *et al*., 1996; Sommerfield & Nittrouer, 1999). Regardless of these observations, hyperpycnal flows are commonly cited as an important process for transferring sand onto the shelf, and hyperpycnites are interpreted to be an important constituent of many ancient prodelta to delta front and shelf successions, as well as shelf–slope clinoform systems (Wright *et al*., 1988; Mulder & Syvitski, 1995; Mutti *et al*., 1999, 2003; Mellere *et al*., 2002; Plink-Björklund & Steel, 2004; Petter & Steel, 2006; Tinterri, 2007, 2011; Bhattacharya & MacEachern, 2009; Olariu *et al*., 2010; Paim *et al*., 2011; Liu *et al*., 2012; Warrick *et al*., 2013; Steel *et al*., 2016, 2018; Boulesteix *et al*., 2019; Grundvåg *et al*., 2020; Warrick, 2020). In addition, there is a growing body of literature describing hyperpycnites in ancient and modern submarine lobes, suggesting that hyperpycnal flows may transfer sand into deep-water environments (e.g. Mutti et al., 2003; Bourget *et al*., 2010; ; Zavala *et al*., 2012; Warrick *et al*., 2013; Chen *et al*., 2021). This is enigmatic, because it has been shown that hyperpycnal flows entering marine basins typically deposit their sandy load near the river mouth (e.g. Wright *et al*., 1990), presumably due to buoyancy reversal via a process referred to as lofting (e.g. Sparks *et al*., 1993; Zavala *et al*., 2011; Steel *et al*., 2017). As such, the role of hyperpycnal flows in transferring sand into deep-water basins remain ambiguous (e.g. Wright *et al*., 1990; Mulder *et al*., 2003; Talling, 2014; Shanmugam, 2018, 2019; van Loon *et al*., 2019; Heerema *et al*., 2022).

In this paper, the facies architecture and vertical to lateral distribution of various sandstone-dominated sediment gravity flow deposits in a series of exhumed basin floor lobe complexes in the Eocene succession of Spitsbergen, Arctic Norway, are presented (see Fig. 1A and B for location). The stratigraphic context and the palaeogeography of the basin are well-known (e.g. Steel *et al*., 1981; Steel & Olsen, 2002; Fig. 1B to D) and were recently summarized by Helland-Hansen & Grundvåg

(2021). The shelf-edge to slope segment of the clinoforms hosting the lobe complexes, reportedly contain flood-related hyperpycnites, which can be physically traced from shelf-edge positioned river channels into canyon heads or gullies on the uppermost slope (Fig. 2A to D; Mellere *et al*., 2002; Plink-Björklund & Steel, 2004; Petter & Steel, 2006; Henriksen *et al*., 2010). The hyperpycnites on the slope occur as composite sandstone beds which commonly exhibit complex vertical facies arrangements, suggesting deposition by sustained hyperpycnal flows (Fig. 2E; Plink-Björklund & Steel, 2004; Petter & Steel, 2006). However, few, if any, of the previous studies of the clinoforms and the associated lobe complexes convincingly demonstrate the presence of sandy hyperpycnites on the basin floor (Crabaugh & Steel, 2004; Johannessen & Steel, 2005; Grundvåg *et al*., 2014a; Spychala *et al*., 2021). Here, sedimentological data from core and outcrops are combined to interpret flow processes and down-slope flow transformations responsible for the documented bed type variability and distribution. This study particularly explores the role of hyperpycnal flows and. based on distinct sedimentological evidence, it is argued that hyperpycnal flows were the most important process in transferring sand beyond the slope and governing progradation of the basin floor lobe complexes in Svalbard.

TERMINOLOGY

In this paper, the term *sediment gravity flow* is used for any type of subaqueous, gravity-driven flow containing dispersed sediment (e.g. Lowe, 1982; Middleton, 1993). *Turbidity current* is used for sediment gravity flows where sediments are chiefly suspended by fluid turbulence (e.g. Lowe, 1982; Middleton, 1993; Mulder & Alexander, 2001; Talling *et al*., 2012). *Low-density turbidity current* is used for relatively dilute and fully turbulent flows which deposit their load predominantly by suspension settling and subordinately by traction sedimentation (e.g. Bouma, 1962; Lowe, 1982; Middleton, 1993). *High-density turbidity current* is used for flows of high sediment concentrations which consist of a lower, laminar flow layer (where dispersive pressure caused by grain collisions, hindered settling and buoyant lift provides grain support), overlain by a less dense, turbulent suspension (Lowe, 1982; Postma *et al*., 1988). Studies show that many low-density density turbidity

currents also compose a basal flow layer of high sediment concentration where turbulence is dampened and other sediment support mechanisms operate (Lowe, 1982; Mutti *et al*., 1999; Mulder & Alexander, 2001; Talling *et al*., 2012). However, in this study, *turbidite* is used to denote an event bed deposited by a turbidity current, whatever mechanisms that supported the particles within the parent flow (e.g. Mutti *et al*., 1999). *Surge-type turbidity current* refers to a single short-lived (minutes to hours), downslope decelerating turbidity current which gradually lose its capacity to carry sediment (i.e. the highly unsteady, depletive waning flows of Kneller, 1995). *Sustained turbidity current* is used to denote long-lived flow events (several hours to months). This term is used interchangeably with *quasi-steady flow*, according to the terminology of Kneller & Branney (1995). The term hyperpycnal flow has been used for a broad spectrum of land-derived gravity flows, ranging from coarse-grained flows, which upon entering marine or lacustrine basins, continue directly as dense underflows, to dilute, turbulent plumes, which given sufficient density, plunge to form underflows (e.g. Mulder *et al*., 2003; Shanmugam, 2018; Zavala, 2020). *Hyperpycnal flow* is used according to the original work of Bates (1953), referring to sediment-laden, flood-related river discharges having excess density in comparison to the ambient water of the receiving basin. As such, hyperpycnal flows should not be mistaken for subaerial river currents where air is the ambient fluid. When hyperpycnal flows enter steep slopes or plunge, they generate long-lived, bottom-hugging, turbulent underflows which can be equated to sustained turbidity currents (i.e. the quasi-steady hyperpycnal turbidity current of Mulder & Alexander, 2001). It should be stressed that although all hyperpycnal flows (in the sense that this study uses the term) are sustained and turbulent, not all sustained turbidity currents equate to hyperpycnal flows because they can be produced by many other processes (cf. Felletti *et al*., 2009; Jackson *et al*., 2009). The term *hyperpycnite* is used for sediments deposited by flood-related hyperpycnal flows (e.g. Mulder *et al*., 2003). The terms *transitional flow* and *hybrid flow* are used interchangeably, both referring to sediment gravity flows operating in a state intermediate between turbidity currents and debris flows, and which commonly have a bipartite nature with a lower turbulent flow layer and an upper cohesive layer with laminar

flow properties (e.g. Lowe & Guy, 2000; Haughton *et al*., 2009; Sumner *et al*., 2009). Their deposits are referred to as *hybrid event beds* (HEBs; Haughton *et al*., 2003, 2009). *Debris flow* is used for cohesive (laminar) flows in which matrix strength is the main sediment support mechanism, and from which deposition occurs *en masse* (e.g. Lowe, 1982; Mulder & Alexander, 2001; Talling *et al*., 2012). The term *debrite* is used for their deposits.

GEOLOGICAL SETTING

Tectonic framework

Spitsbergen is the largest island of the Svalbard archipelago which represents the emergent and exhumed north-west corner of the Barents Shelf (Fig. 1A). During the Palaeocene to Eocene, the progressive northward opening of the North Atlantic promoted dextral strike–slip movements along the De Geer Zone with Svalbard moving southward and eventually separating from Greenland in the earliest Oligocene (i.e. at Chron 13; Doré *et al*., 2015). Most of the dextral movement along this regional transform gave a largely transtensive response, particularly in the southern segment of the sheared margin (Kristensen *et al*. 2018). However, western Spitsbergen, which was located between a restraining and a releasing bend of the shear zone, experienced transpression along the Hornsund Fault Zone resulting in *ca* 20 to 40 km of crustal shortening (Braathen *et al*., 1995; Bergh *et al*., 1997; Fig. 1A and B).

In western Spitsbergen, the transpression led to extensive basement uplift and thin-skinned tectonics involving the upper Palaeozoic to Palaeogene sedimentary rock succession, ultimately resulting in the formation of the *ca* 300 km long NNW–SSE trending West Spitsbergen Fold-and-Thrust Belt (WSFTB; Fig. 1B; Braathen *et al*., 1995; Bergh *et al*., 1997). The development of the WSFTB has occasionally been linked to the Eurekan Fold Belt in North Greenland and Arctic Canada (e.g. Piepjohn *et al*., 2016), whereby compression peaked at 47 to 49 Ma (mid Eocene). Concomitant with the structural deformation, regional flexural subsidence associated with stacking of thrust sheets and tectonic loading, led to the development of an elongated, NNW–SSE-oriented and

asymmetrical syncline referred to as the Central Tertiary Basin (CTB; Fig. 1B and C; e.g. Steel *et al*., 1981).

The CTB covers large parts of southern and central Spitsbergen and represents the foreland basin to the WSFTB (Steel *et al*., 1981; Helland-Hansen, 1990; Helland-Hansen & Grundvåg, 2021). From the Oligocene onwards, Svalbard has experienced exhumation in the range of 2 to 3 km with at least (depending on position in the basin) 0.5 to 1.0 km of strata loss due to subsequent erosion (e.g. Marshall *et al*., 2015). Thermo-tectonic processes and rift-shoulder uplift, as well as isostatic rebound associated with recurrent late Neogene and Quaternary glaciations have all contributed to the regional exhumation (Dimakis *et al*., 1998; Lasabuda *et al*., 2018).

During the Eocene, the CTB had limited connection to the open sea and formed a large embayment which widened south towards the Barents Shelf (Steel *et al*., 1981, 1985; Helland-Hansen & Grundvåg, 2021). This, in combination with high rates of precipitation and terrestrial runoff, created ideal conditions for establishing a hyperpycnal flow-dominated sourcing regime in the basin (Mellere *et al*., 2002; Plink-Björklund & Steel, 2004; Helland-Hansen & Grundvåg, 2021).

Lithostratigraphy and age of the basin fill

The basin strata of the CTB comprises the up to 1.9 km thick Palaeogene Van Mijenfjorden Group whose upper part consists of an Eocene–Oligocene (?) succession (Steel *et al*., 1981; Helland-Hansen & Grundvåg, 2021). This succession has a preserved thickness of >1.5 km and represents the main infill of the CTB. A regional shift in provenance from northerly-derived sediments in the Palaeocene to westerly derived sediments in the Eocene reflects the sedimentary response to the evolving WSFTB (Helland-Hansen, 1990; Petersen *et al*., 2016; Helland-Hansen & Grundvåg, 2021).

The Eocene–Oligocene (?) basin fill succession records the eastward progradation of a fluvio-deltaic and modest shelf-margin system, and consists of three formations that are genetically linked:

the basin floor and slope deposits of the Frysjaodden Formation pass gradually upwards into shallow marine and deltaic deposits of the Battfjellet Formation and continental strata of the Aspelintoppen Formation (Fig. 1D; Steel *et al*., 1981, 1985; Helland-Hansen, 1990; Steel & Olsen, 2002; Grundvåg *et al*., 2014b). The overall regressive nature of the basin fill manifests the evolution from an underfilled deep marine to an overfilled continental foreland basin, mostly during the Eocene (Johannessen & Steel, 2005; Helland-Hansen & Grundvåg, 2021).

Shelf-margin clinoforms and basin floor fans

The Eocene part of the succession has previously received considerable attention in the literature because of its seismic-scale (1 km x 10 km) outcrops (particularly along the northern shores of Van Keulenfjorden; Fig. 1C) displaying shelf-prism type clinforms which constitutes a characteristic and spectacular motif of the basin filling (Fig. 2A; Helland-Hansen, 1990; Plink-Björklund *et al*., 2001; Steel & Olsen, 2002). The investigated lobe complexes belong to the Bjørnsonfjellet Member of the Frysjaodden Formation and occur as a series of kilometre-scale, basinward thickening–thinning sandstone wedges sandwiched between thick mudstone units of basin floor and slope origin (Fig. 1D; Steel *et al*., 1981; Steel & Olsen, 2002; Grundvåg *et al*., 2014a). Because the lobe complexes occur in the basin floor segment of the clinoforms, they are commonly referred to as basin floor fans (e.g. Steel & Olsen, 2002; Crabaugh & Steel, 2004; Johannessen & Steel, 2005). Previous investigations have established the presence of three separate and independent basin floor fan systems in the Van Keulenfjorden area, each containing several lobe complexes (Steel & Olsen, 2002; Crabaugh & Steel, 2004; Johannessen *et al*., 2011; Grundvåg *et al*., 2014a). In this paper, they are referred to as (from west to east) the Pallfjellet, the Sysselmannbreen and the Hyrnestabben lobe complexes, respectively (Fig. 1D).

Sandstone-dominated shelf-edge delta deposits of the Battfjellet Formation occur up-dip of the lobe complexes (Figs 1D and 2; Plink-Björklund *et al*., 2001; Mellere *et al*., 2002; Steel & Olsen, 2002; Johannessen & Steel, 2005; Petter & Steel, 2006; Grundvåg *et al*., 2014a). Occasionally, these

deposits can be traced down-dip via sandstone-rich slope wedges, which extend up to 5 km into the basin with reliefs in the order of 150 to 300 m at angles of 3° to 5°, into the basin floor-positioned lobe complexes (Fig. 2; Mellere *et al*., 2002; Johannessen & Steel, 2005; Petter & Steel, 2006; Helland-Hansen & Grundvåg, 2021). Palaeo-water depths of the basin have previously been estimated to be generally <20 m on the shelf (based on the thickness of shoreface-shelf parasequences; Helland-Hansen, 2010), deepening to 200 to 400 m across the shelf edge (based on the height of the clinoforms; Mellere *et al*., 2002; Johannessen & Steel, 2005). The preserved basin fill succession thins eastwards from >700 m in the west to *ca* 300 m in the east in concert with a loss of both sandstone-dominated slope wedges and basin floor fans (Helland-Hansen & Grundvåg, 2021). Collectively, this indicates a gradual shallowing of the basin, as well as contemporary decreasing slope relief and gradients to the east, presumably reflecting the rising forebulge of the CTB (Helland-Hansen, 1990; 2010; Bruhn & Steel, 2003; Helland-Hansen & Grundvåg, 2021).

STRATIGRAPHIC SIGNIFICANCE AND DEPOSITIONAL ARCHITECTURE OF THE LOBE COMPLEXES

The three basin floor fan systems in the Van Keulenfjorden area comprise four lobe complexes each (Crabaugh & Steel, 2004; Johannessen & Steel, 2005; Grundvåg *et al*., 2014a). Thus, for convenience, the lobe complexes are numbered in a continuous fashion: the Pallfjellet lobe complexes are referred to as LC 1 to LC 4 (Fig. 3), the Sysselmannbreen lobe complexes as LC 5 to LC 8 (Figs 4 and 5) and the Hyrnestabben lobe complexes as LC 9 to LC 12 (Fig. 6). This numbering convention must not be confused with the clinoform numbering established by Steel & Olsen (2002), despite LC 1 to LC 4 coincidentally corresponding to clinoforms 1 to 4 (Figs 1D and 3). In fact, it was the Pallfjellet lobe complexes that originally formed the basis for the clinoform numbering in the westernmost part of the basin. Because of basin margin uplift, there are no Eocene shelf–slope strata preserved west of Pallfjellet. Thus, based on the presence of the four lobe complexes at Pallfjellet, as well as the shelf-slope-basin floor facies tracts documented elsewhere in the basin, Steel & Olsen (2002) inferred the

presence of at least four older shelf-breaks (and related clinoform units) outside the preserved outcrop window. To avoid confusion and for clarification, this study only refers to the clinoform numbers whenever needed. Stratigraphically, the Pallfjellet lobe complexes are the oldest of the three investigated systems, and the Hyrnestabben lobe complexes the youngest (Fig. 1D). This relationship is not constrained by any biostratigraphic data but is based on their respective location in the basin (relative to the western basin margin) and the assumption that each lobe complex stratigraphically represents the basin floor segment of individual, progradationally stacked shelf-margin clinoforms (Fig. 1C and D). The successive shelf-edges of these clinoforms have been mapped by previous studies (Plink-Björklund *et al*., 2001; Mellere *et al*., 2002; Steel & Olsen, 2002; Grundvåg *et al*., 2014b). The depositional architecture, internal organization and the established hierarchy of the lobe complexes builds largely on previous studies (Steel & Olsen, 2002; Crabaugh & Steel, 2004; Johannessen & Steel, 2005; Petter & Steel, 2006; Grundvåg *et al*., 2014a; Spychala *et al*., 2021). Thus, to provide stratigraphic context for the recognized bed types described later, a summary is given here.

Pallfjellet lobe complexes

The Pallfjellet lobe complexes (LC 1 to LC 4) occur in the westernmost part of the study area as a series of four 10 to 50 m thick, progradationally stacked lobe complexes (Fig. 3A and B; Steel & Olsen, 2002; Johannessen & Steel, 2005; Grundvåg *et al*., 2014a). Palaeocurrent data, mostly based on current ripple cross-lamination, indicate generally eastward-directed sediment transport into the basin (Figs 1C and 3B; Grundvåg *et al*., 2014a). Neither the proximal part of the three lowermost lobe complexes (LC 1 to LC 3) nor the shelf-slope segment of the clinoforms which host them are preserved. However, based on the lower slope position of LC 4, the overall progradational stacking pattern, and the presence of an overlying *ca* 150 m thick slope shale succession containing slope channel fills, it is reasonable to suggest that each of the Pallfjellet lobe complexes represents the

basin-floor segment of separate shelf-margin clinoforms that successively prograded into the basin (Figs 1D and 3; Steel & Olsen, 2002; Johannessen & Steel, 2005). In a down-dip, basinward direction, the lobe complexes pinch out at the neighbouring mountain (i.e. the western ridge of Brogniartfjella), giving a minimum pinch-out distance of *ca* 8 to 9 km (Fig. 3B; Grundvåg *et al*., 2014a). Internally each lobe complex consists of a variable number of shingled to aggradationally stacked lobes and lobe elements (Fig. 3C and D; Grundvåg *et al*., 2014a). The successive, basinward offset stacking trend at lobe complex scale and the upward increase in bed thickness and degree of amalgamation observed in many of the lobes, indicates an overall progradational system (Fig. 3B).

Sysselmannbreen lobe complexes

The Sysselmannbreen lobe complexes (LC 5 to LC 8) are penetrated by a fully cored research well, BH 10-2008 'Sysselmannbreen', which is located near the axis of the CTB and visualized from (onshore) two-dimensional reflection seismic data (Figs 4 and 5; Johannessen *et al*., 2011; Grundvåg *et al*., 2014a). The seismic investigations demonstrate that the Sysselmannbreen lobe complexes occur as a series of high amplitude anomalies exhibiting offset-stacking to the east/north-east (Fig. 5A; Johannessen *et al*., 2011; Grundvåg *et al*., 2014a). Each of the anomalies extend basinward for at least 3 to 4 km before abruptly terminating (most likely due to seismic resolution). The seismic data is generally of too low resolution and quality to further delineate the internal architecture of the lobe complexes. The core and gamma-ray data, however, document and confirm that the seismic anomalies represent sandstone-dominated gravity flow deposits (Fig. 4; Johannessen *et al*., 2011; Grundvåg *et al*., 2014a). Four 15 to 40 m thick lobe complexes have been recognized in the well (Fig. 4; Grundvåg *et al*., 2014a). Internally, the lobe complexes contain various gravity flow deposits and display upward bed thickening (Grundvåg *et al*., 2014a). Up to six stacked lobes are recognized in LC 6. The uppermost Sysselmannbreen lobe complex (LC 8) exhibits a high degree of bed amalgamation and erosive scouring, possibly indicating position at the base-of-slope or within the channel-lobe

transition zone (Fig. 4). A *ca* 150 m thick slope shale succession, which in the seismic data displays eastward dipping clinoform geometries, cap the lobe complexes (Fig. 5; Johannessen *et al*., 2011; Grundvåg *et al*., 2014a). Collectively, this demonstrates the progradational nature of the lobe complexes and the associated clinoform system (Johannessen *et al*., 2011; Grundvåg *et al*., 2014a).

Hyrnestabben lobe complexes

The Hyrnestabben lobe complexes (LC 9 to LC 12) occur as a series of four 5 to 45 m thick vertically and compensationally stacked lobe complexes located *ca* 10 km east of the CTB axis (Figs 1D and 6; Steel & Olsen, 2002; Crabaugh & Steel, 2004; Johannessen and Steel, 2005). Based on their location within the basin, these lobe complexes represent the youngest of the three systems discussed in this paper (Fig. 1C and D). The lowermost lobe complex (LC 9) has its up-dip pinch-out to the north-west of Hyrnestabben on the neighbouring mountain of Storvola (i.e. Clinoform 12 of Steel & Olsen, 2002), thus extending basinward for a minimum distance of *ca* 6.5 km (Figs 2A and 6; Crabaugh & Steel, 2004; Petter & Steel, 2006; Spychala *et al*., 2021). The most up-dip segment of the two succeeding lobe complexes 10 and 11 are exposed in a north-west/south-east-oriented outcrop section on Storvola which can be traced further across to Hyrnestabben where the outcrop transect gradually turns to the north-east (Fig. 1C; Crabaugh & Steel, 2004). This enables tracing of facies tracts from shelf to base-of-slope environments on Storvola near parallel to the inferred eastward depositional dip direction of the lobe complexes (Figs 2A and 6) across to Hyrnestabben and further to the north-east (along near strike) to where they laterally to distally pinch out over a total distance of *ca* 6 km. The two middle lobe complexes are evidently compensationally stacked on Hyrnestabben (Fig. 6; Crabaugh and Steel, 2004; Johannessen & Steel, 2005), but also exhibit a progradational component as observed from their up-dip relationship to the shingled sandstone-dominated slope wedges on Storvola (i.e. attributed to clinoforms 14A and 14C of Steel & Olsen, 2002; Petter & Steel, 2006). Large-scale folding and soft-sediment deformation occur frequently in the upper parts of several lobe

complexes, and particularly the uppermost part of the youngest lobe complex is pervasively deformed (LC 12, the 'pink fan' of Crabaugh & Steel, 2004, attributed to clinoform 15 of Steel & Olsen, 2002). Apparent slope channels with internal lateral accretion packages have been reported on the north-eastern side of Hyrnestabben, occurring in the same stratigraphic interval as the lobe complexes (Henriksen *et al*., 2011). However, detailed investigations and lateral tracing of these features suggest that they instead represent the soft-sediment deformed channel-lobe transition zone of LC 11 (this study).

METHODOLOGY AND DATA SET

The data set investigated in this study includes multiple sedimentary logs from two outcrop sections along the so-called 'Van Keulenfjorden transect' (Fig. 1C and D; Steel & Olsen, 2002). The WNW–ESE-oriented Pallfjellet–Brogniartfjella outcrop section (10 logs on Pallfjellet, two on the western ridge of Brogniartfjella; Figs 1C and 3) is parallel to the regional depositional dip and exposes the Pallfjellet lobe complexes. The Storvola-Hyrnestabben outcrop section (22 logs on Hyrnestabben and eight on Storvola; Figs 1C and 6) comprises a north-west/south-east-oriented and a south-west/north-east-oriented segment and exposes the Hyrnestabben lobe complexes at near dip parallel to near strike parallel directions. The data set also includes core and accompanying gamma ray data from well BH 10-2008 (Fig. 4; Johannessen *et al*., 2011; Grundvåg *et al*., 2014a). In addition, the well is tied to a 2D reflection seismic line which intersects the well site in a west–east direction (Fig. 5; Johannessen *et al*., 2011). All of the sedimentary logs were measured bed-by-bed (with a resolution of a few centimetres and typically drawn at scale 1:20) and include descriptions of lithology, grain-size, sorting, sedimentary structures and trace fossils, as well as palaeocurrent data from the outcrop sections (mainly from current ripple cross-lamination, tool marks and flute casts). Where possible, lateral facies transitions and stratal geometries were determined by walking out beds and key surfaces in the outcrops (usually at only a few hundred metres), and from visual tracing on

photograph-mosaics. Bed type proportions were calculated and plotted using Microsoft Excel. Bed amalgamation is very common at a variety of scales and hampers sub-division into bed types, which naturally influences bed type statistics. It may involve two or multiple beds, eventually forming amalgamated units ranging from a few centimetres to several metres in thickness. Amalgamated units were defined (and thus plotted separately) as sandstone packages bounded at their base and top by mudstone beds, which internally exhibits multiple sand-on-sand contacts (demarcated by abrupt grain-size breaks) and/or discontinuous mudstone interbeds.

FACIES AND BED TYPES OF THE LOBE COMPLEXES

From the analysis of outcrop and core data, 13 recurrent sedimentary lithofacies are recognized within the lobe complexes (Table 1). Bed types are distinguished by their constituent lithofacies and the relative proportion of these, and are further classified into four main groups reflecting the inferred behaviour of the flows from which they originated: (i) hyperpycnites (HPs) deposited by hyperpycnal flows; (ii) turbidites (TBs) primarily deposited by surge-type turbidity currents; (iii) hybrid event beds (HEBs) deposited by transitional flows; and (iv) mass-transport deposits (MTDs; Fig. 7) deposited by slumps, slides and debris flows. A description of the recognized types of gravity flow event beds are given below.

Hyperpycnite beds (HPs)

AHP – amalgamated sandstone units

Description. Up to 5 m thick amalgamated sandstone (AHP) units characterized by a massive, thick-bedded appearance preserving few sedimentary structures (facies T_A, S_1 and S_2; Table 1). Amalgamation surfaces are demarcated by horizons of aligned intraformational mudstone clasts, or low-relief scour surfaces with thin lags of coarse-grained to very coarse-grained sandstone (i.e. abrupt grain-size breaks). In addition, thin (<0.1 m thick), discontinuous mudstone interbeds and floating solitary mudstone clasts occur locally. Dewatering structures are variably present, whereas

thin (some few centimetres) and poorly developed intervals of plane parallel lamination occur within or at the tops of the AHP units. Two laterally related sub-categories are recognized. The first type, which represents deposition in confined settings (AHP-C; Fig. 7A), is the major constituent of the *slope channel fill bed type association*. The AHP-C units consist of medium-grained to coarse-grained sandstone with ungraded lower parts and slightly finer-grained upper parts, which contain abundant horizons of imbricated to randomly oriented mudstone clasts. The second type, which represents deposition in largely unconfined settings (AHP-U; Fig. 7A), is the major constituent of the *lobe axis bed type association* and represent the down-dip continuation of the AHP-C units. The AHP-U units consist of fine-grained sandstone with no clear grain-size trends. Thin, discontinuous mudstone interbeds are present, whereas mudstone clast horizons are very rare.

Interpretation. The abundance of amalgamation features indicates that the AHP units has a composite origin. However, based on their thick-bedded and structureless appearance, the AHP units are interpreted to be deposited by progressive aggradation beneath sustained, high-density turbidity flows (e.g. Kneller & Branney, 1995), or by rapid deposition following the collapse of voluminous, surge-type, high-density turbidity currents (Lowe, 1982). Event beds deposited by surge-type currents are commonly draped by mud of hemipelagic or hemi-turbiditic origin, implying that a stack of such event beds in most circumstances will be separated by intervening mud deposits. As such, the sparsity and the thinness of interbedded mudstones in the AHP units, suggest that mud generally bypassed, did not have time to settle between successive flows (or flow pulses), or was readily eroded relatively soon after deposition by overriding currents (Walker, 1966). In sustained flows, temporal waning promotes sudden flow collapse and rapid dumping of sand, whereas waxing flow pulses may cause localized erosion, collectively resulting in thick, massive sand deposits of composite nature (e.g. Stow & Johansson, 2000; Mattern, 2002; Hodgson, 2009). Scour surfaces with lags of aligned mudstone rip-up clasts in the AHP-C units indicate recurrent erosion of transient mud accumulations followed by bed load traction. In high-density turbidity current deposits, the preservation of floating mudstone clasts has been attributed to intra-flow transport along the

rheological boundary between the basal laminar inertia layer (i.e. the sandy debris flow of Shanmugam, 1996) and the overriding, faster-moving turbulent layer of the flow, followed by *en masse* freezing and clast trapping in the middle of the deposit as the boundary progressively changes upward during waning flow (Postma *et al*., 1988; Stow & Johansson, 2000). Thus, in the AHP units where there is no profound evidence of internal scouring, multiple levels of floating mudstone clasts suggest progressive sediment aggradation underneath a sustained flow characterized by simultaneous bed load (traction) and suspended load deposition (Zavala & Pan, 2018). Although sustained turbidity currents can be initiated by many processes (as discussed later), a hyperpycnal flow origin for the AHP units is favoured, based on the lateral connectivity between shelf-edge positioned fluvial distributary channels, slope channels and basin floor fans, as documented by previous workers (Fig. 2; Johannessen & Steel, 2005; Petter & Steel, 2006; Helland-Hansen & Grundvåg, 2021).

HP1 – composite sandstone beds with internal truncations

Description. This bed type consists of 0.02 to 0.7 m thick, subtly-graded to non-graded or locally inversely–normally graded, medium-grained to very fine-grained sandstone beds characterized by multiple internal truncation surfaces and grain-size breaks, floating rip-up mudstone clasts (in the middle of the bed), intra-bed horizons of plane parallel to sub-parallel or low-angle wavy lamination, and small-scale (5 to 10 cm deep, up to 20 cm wavelength) scour-and-fill features separated by mound-like structures (HP1A; Figs 7A and 8A). The fill of the scours typically consists of medium-grained to coarse-grained, coarse-tail normally graded, massive sandstone (Fig. 8A). On some occasions, laminae, which thicken towards the centre of the scours, partly drape and partly onlap the scour surfaces (Fig. 8A). Water-escape structures are variably present. In places, strongly asymmetrical load casts with associated flame structures (shaped like Kelvin-Helmholtz waves) form laterally persistent horizons (or trains) within entirely sandstone-dominated beds (HP1B; Figs 7A and

8B). The load casts are typically coarser grained than the underlying and overlying sandstones. Some of the thicker HP1A and HP1B beds include a thin (some few centimetres) silty division on top consisting of horizontally aligned to imbricated and randomly oriented plant material and centimetre-sized coal clasts embedded in a silty sandstone matrix (Figs 7A and 8B). A lateral link to the plant-rich HEB1 and HEB2 bed types may thus be the case. Other beds exhibit a lower structured division (e.g. plane parallel lamination, current-ripple cross-lamination, etc.), sharply overlain by a coarser-grained, structureless, subtly graded division, which generally constitutes more than half of the bed thickness (HP1C; Figs 7A and 8C to E). A thin-bedded (bed thickness typically <0.05 m; Fig. 8D) variety of this bed type commonly co-occurs with the thin-bedded turbidites of TB3.

Interpretation. The general structureless, subtle to non-graded character of most HP1 beds suggests deposition by aggradation of sand from sustained, quasi-steady turbulent flows (Kneller & Branney, 1995). Their sharp, scoured bases indicate initial erosion by powerful turbulent flows. The many intra-bed truncation surfaces and scour-and-fill features indicate frequent velocity fluctuations (i.e. flow unsteadiness) with short-lived pulses of waxing flow conditions resulting in localized erosion, immediately followed by rapid suspension fallout during intervening waning flow. The plane parallel to sub-parallel and low-angle wavy lamination in some beds (HP1A; Fig. 8A) indicates bedload transport under upper flow regime (supercritical) conditions (Postma *et al*., 2009; Jobe *et al*., 2012; Cartigny *et al*., 2014). The intra-bed occurrence of strongly asymmetrical load and flame structures (for example, Fig. 8B) indicates concomitant deposition and shearing by internal flow pulses of contrasting densities (e.g. Butler *et al*., 2016). The lower structured division of the HP1C beds (Figs 7A and 8C to E) indicates sustained bed load traction under fluctuating subcritical to supercritical velocities. The sharp transition to the upper structureless division of these beds records erosion by a waxing (supercritical), turbulent flow, whereas the structureless nature of the upper division indicates rapid dumping of sand when the sustained, turbulent flow eventually collapsed and came to a complete halt (Plink-Björklund & Steel, 2004; Petter & Steel, 2006). Because abundant plant remains and similar composite bed architectures have been attributed to hyperpycnal flows

elsewhere (e.g. Paim *et al*., 2011; Zavala *et al*., 2011), a hyperpycnal flow origin for the HP1 bed type is favoured. The thin, inversely-to-normally graded sandstone beds with a lower laminated and an upper massive division (e.g., Fig 8D), which record deposition under waxing to waning velocities, may thus represent the depositional product of distal hyperpycnal flows (e.g. Mulder *et al*., 2003; Nakajima, 2006).

Sustained or pulsed turbidity currents triggered by other processes than hyperpycnal flows (for example, retrogressive slumping or earthquakes; Felletti *et al*., 2009; Jackson *et al*., 2009; Ho *et al*., 2018) and fully ponded or partially reflected turbidity currents in structurally confined basins (e.g. Tinterri *et al*., 2022), all of which may result in facies sequences similar to those of the HP1 beds, are discussed later.

HP2 – composite sandstone beds with complex facies arrangements

Description. This bed type consists of 0.2 to 0.8 m thick subtly-graded to non-graded, medium-grained to very-fine-grained sandstone beds characterized by complex facies arrangements (HP2; Figs 7A and 8F). The lower part of most beds is sharp based and structureless, whereas the upper part exhibits alternating divisions of plane parallel lamination, subcritical climbing current ripple cross-lamination, and subordinate structureless divisions (HP2A and HP2B; Fig. 7A). Locally, particularly in the lobe fringes, some beds, typically <0.4 m thick, are completely dominated by climbing current ripple cross-lamination, which occasionally displays transitions from subcritical via supercritical climbing current ripple cross-lamination into wavy lamination (HP2C and HP2D; Fig. 7A). Subtle grain-size variations occur within and between the various bed divisions. Bed tops are commonly sharp, but in some cases, an upper siltstone division may occur, grading upward into the overlying mudstone.

Interpretation. Based on the sharp-base, subtle normal grading and the complex facies arrangement with alternations of plane parallel laminated, climbing current ripple cross-laminated and thin

structureless divisions, these beds are interpreted to be deposited by semi-continuous bed load traction beneath sustained quasi-steady turbidity currents characterized by high amounts of suspended sand and recurrent waxing and waning pulses (e.g. Petter & Steel, 2006; Felletti *et al*., 2009; Jackson & Johnson, 2009). The lower structureless division indicates rapid aggradation and fallout from the initial turbulent flow. Plane parallel lamination indicate bed load transport under upper flow regime (supercritical) conditions, whereas current ripple cross-lamination points to deposition under slightly lowered, subcritical flow velocities promoting the development and migration of bed forms (Jobe *et al*., 2012; Baas *et al*., 2016). The common occurrence of climbing current ripple cross-lamination to wavy lamination suggest repeated episodes of rapid loss of flow momentum with high rates of suspension fallout and bed form aggradation being the result (Zavala *et al*., 2006, 2011; Jobe *et al*., 2012). The subordinate, intervening massive bed divisions presumably record rapid dumping of suspended sand during short-lived pulses of flow collapse. Sandstone beds with very similar complex vertical facies sequences as the HP2 beds, which previously has been attributed to deposition by sustained, fluctuating hyperpycnal flows, occur frequently on the upper slope segment of the clinoforms hosting the investigated lobe complexes (Fig. 2; Plink-Björklund & Steel, 2004; Petter & Steel, 2006). As such, the HP2 beds are interpreted to be hyperpycnites representing a less energetic, deposition-dominated variety of the closely related HP1 beds.

Turbidite beds (TB)

TB1 – thick-bedded turbidite sandstones

Description. Massive, non-graded to subtly graded, medium-grained to very-fine-grained sandstone beds typically 0.4 to 1.0 m thick with tabular geometries (Figs 7B and 9A). Most beds have a thin (some few centimetres), poorly developed upper division exhibiting plane parallel stratification (Fig. 9A). The thickest beds occasionally show signs of amalgamation (such as solitary, floating mudstone clasts in the middle of a bed, subtle grain-size changes and truncated dewatering structures; TB1A) or

pervasive soft-sediment deformation (mostly dewatering structures such as convolute bedding and dish structures; TB1B). The bed bases are typically sharp and flat, occasionally accompanied by load casts and associated flames. Some beds have scoured bases which cut some few centimetres to decimetres into the underlying deposits. Rip-up mudstone clasts are occasionally aligned above the scoured bases, forming discontinuous basal lags. Many TB1 beds thin and transition down-dip into TB2 beds.

Interpretation. There are many depositional models for massive sandstone beds in submarine lobes, including: (i) progressive aggradation of sand beneath quasi-steady high-density turbidity currents (e.g. Kneller & Branney, 1995); (ii) rapid deposition of sand from collapsing, voluminous, surge-type (unsteady), high-density turbidity currents (e.g. Lowe, 1982); (iii) rapid sand deposition by hyperpycnal flows following buoyancy reversal and lofting processes (Gladstone & Pritchard, 2010; Stevenson & Peakall, 2010; Steel *et al*., 2016); and (iv) *en masse* freezing of the laminar flow layer at the base of high density turbidity currents (i.e. the sandy debris flow of Shanmugam, 1996). All of these processes could equally have contributed to the deposition of the TB1 beds, although the latter alternative is the least favourable since few features consistent with such processes were observed (for example, bed tops with mudstone clasts, inverse grading, irregular upper contacts, etc.; see Shanmugam, 1996). Nonetheless, the scoured bases, which occasionally are accompanied by basal lags of mudstone clasts, indicate initial erosion by powerful, fully turbulent flows prior to deposition (e.g. Crabaugh & Steel, 2004). The TB1A beds were probably deposited by quasi-steady high-density turbidity currents, in which the subtle grain-size breaks and internal truncations reflect temporal velocity fluctuations (Kneller & Branney, 1995). The dewatered character of the TB1B beds indicate rapid suspension deposition of sand followed by liquefaction processes, whereas subtle grading and the traction-generated structures in the upper part of most beds record waning flow conditions (Lowe, 1982). The down-dip thinning of beds and the concomitant transition into TB2 beds, indicate that most of the flows depositing TB1 beds decelerated and gradually lost their transport capacity as they travelled basinward, which is typical for surge-type turbidity currents. As such, a turbidite

affinity for the TB1 beds is preferred, although it is acknowledged that some TB1A beds are transitional to the AHP-U deposits and may thus reflect deposits of hyperpycnal flows (Fig. 7).

TB2 – thin to medium-bedded turbidite sandstones

Description. Subtly graded, to less commonly normally graded, sharp-based, fine-grained to very-fine-grained, sheet-like sandstone beds, typically 0.05 to 0.4 m thick (Figs 7B and 9B). The TB2 beds are typically structureless throughout, yet many beds include a slightly finer-grained, upper division exhibiting plane parallel stratification and/or current ripple cross-lamination (commonly subcritical climbing sets; Figs 7B, 9B and 9C). Stacked beds are typically separated by thin mudstone units. However, scoured bases and bed amalgamation occur frequently in places.

Interpretation. Based on the normal to subtle grading, sharp bases and the presence of sedimentary structures attributed to traction, TB2 beds are interpreted as turbidites deposited by surge-type (unsteady), low-density turbidity currents (e.g. Kneller, 1995). The grading and vertical facies arrangement further indicates deposition under waning flow conditions, typical for basinward decelerating turbidity currents (e.g. Bouma, 1962; Kneller, 1995).

TB3 – very thin-bedded turbidite sandstones and siltstones

Description. Normally to subtly graded, sharp-based, very-fine-grained sandstone to siltstone beds, typically <0.1 m thick, (TB3A and TB3B; Figs 7B and 9D). Most of the thin sandstone and siltstone beds are tabular and structureless but may locally exhibit plane parallel laminated bed tops. Lenticular beds with current ripple cross-lamination occur in some few places (TB3C; Fig. 7B). On many occasions, the sandstone or siltstone beds alternate with equally thin-bedded mudstones, forming couplets which stack into decimetre to several metres thick heterolithic sheet-like packages (TB3D; Fig. 7B), which represent an important constituent of the distal lobe fringe bed type association (e.g. Spychala *et al*., 2021). Many TB3 beds appear to transition up-dip into TB2 beds, thus being part of a lateral continuum of bed type configurations.

Interpretation. Based on their limited thickness, fine-grained character, normal to subtle grading and the occasional presence of traction-generated structures, the TB3 beds are interpreted to be deposited by distally waning, surge-type, low-density turbidity currents of limited volumes (*sensu* Lowe, 1982). Based on the apparent lateral and genetic relation to the TB2 beds, it seems likely that the currents depositing the TB3 beds represent the residual, fine-grained, distal continuation of higher density flows which deposited their coarser-grained sediment load further up-dip.

TB4 – siltstone to mudstone turbidites

Description. Structureless, normally to subtly graded and non-graded, sharp-based, siltstone to mudstone beds, generally <0.1 m thick, but occasionally reaching thicknesses up to 0.4 m (Fig. 7B). TB4 beds usually have tabular geometries and occur in close association with TB3 beds, typically being important constituents of the lobe fringe to distal lobe fringe bed type associations. Faint parallel lamination to discontinuous wavy lamination, millimetre-scale silt streaks and mudstone-filled scours, aligned or randomly oriented plant debris and bioturbation are variably present. Some of these beds are transitional to the background mudstone deposits (Fig. 7B).

Interpretation. Based on their siltstone to mudstone-dominated character, occasional normal grading and sharp bases, the TB4 beds are attributed to deposition by dilute, low-density, mud-rich turbidity currents (e.g. Stow & Shanmugam, 1980; Bhattacharya & MacEachern, 2009; Boulesteix *et al*., 2019). The mudstone-filled scours indicate erosion by waxing, turbulent flows followed by rapid mud deposition during flow collapse. High fallout rates of mud from hypopycnal plumes are known to initiate small, muddy turbidity currents that can erode the seafloor far off the coastline and concomitantly promote regional mud deposition (Parsons *et al*., 2001; Piper & Normark, 2009).

Hybrid event beds (HEBs)

HEB1 – bipartite to tripartite sandstone beds rich in plant debris

Description. These beds consist of 0.1 to 0.9 m thick bipartite beds with a lower, sharp-based, subtly graded to non-graded, fine to very-fine-grained structureless sandstone division, and an upper, poorly sorted, finer-grained (silty sandstone to sandy siltstone) division rich in fossilized plant detritus (Figs 7C and 10A to C). Some few beds, which typically exhibit signs of amalgamation or water-escape related deformation, exceed 1.5 m in thickness (HEB1A; Fig. 7C). The contact between the lower and upper division of the HEB1 beds is gradational and less commonly sharp (non-erosive) or loaded. In the latter case, flame structures protrude from the sandstone into the overlying fine-grained division. The thickness proportion between the two divisions may vary greatly laterally within a bed or between stacked beds (compare Fig. 10A to 10C). In the thickest beds, the basal sandstone division is usually thicker than the upper (only some few exceptions recorded; Fig. 10A and B), whereas the opposite is usually the case in thinner bed varieties (those <0.2 m thick; Fig. 10C and D). The plant detritus is typically randomly distributed within the overall sandy matrix of the upper division, although clast alignment and imbrication, as well as coarse-tail inverse grading occur in places (Fig. 10C and D). Thin, silty sandstone beds may cap the plant-rich division, locally resulting in a tripartite bed architecture (HEB1C; Figs 7C, 10C and 10D).

Interpretation. The distinct bipartite character of these beds suggests deposition by hybrid sediment gravity flows (Haughton *et al*., 2003, 2009). Based on the sharp base, structureless and subtly graded character, the lower sandstone division is interpreted as a high-density turbidity current deposit (e.g. Haughton *et al*., 2003, 2009; Amy & Talling, 2006; Hodgson, 2009). The poor sorting and random distribution of plant material in the upper division suggests *en masse* deposition by a cohesive debris flow (Amy & Talling, 2006; Hodgson, 2009). When a turbulent flow expands across a basin floor and decelerates, sand-grade sediment is rapidly deposited in the off-axis region of a lobe, whereas finer-grade sediment and plant material may become concentrated in the flow tail or upper part of the

flow. Concentration of these components can suppress turbulence, causing transformation into laminar flow and the generation of a cohesive debris flow which partly overrides the underlying turbidite deposit (e.g. Hodgson, 2009; Kane & Pontén, 2012; Kane *et al*., 2017; Southern *et al*., 2017; Hussain *et al*., 2021). The bed thickness variation and the varying thickness proportion between the two divisions reflect a proximal/axial to distal/off-axis continuum. Thick sandstone beds with a thin upper division reflect deposition in proximal and axial lobe settings, whereas thinner beds with a thick upper division relative to the basal division are interpreted to represent deposition in the distal and off-axis areas, as reported in many other ancient submarine lobe systems (e.g. Hodgson, 2009; Kane & Pontén, 2012; Kane *et al*., 2017; Spychala *et al*., 2017a). The thin bedded sandstone which occurs in the uppermost part of the tripartite beds, indicates deposition by low-density turbidity currents related to the passage of the dilute, fine-grained flow tail.

HEB2 – banded sandstones rich in plant debris

Description. This bed type consists of 0.05 to 0.3 m thick, sharp-based, subtly to non-graded beds with a fine-grained to very-fine-grained basal sandstone division, and an upper banded division consisting of mud-poor very fine-grained sandstone layers alternating with mud-rich sandstone to siltstone layers rich in fossil plant detritus (Figs 7C and 10E to I). The contact between the divisions is typically gradational with poorly developed layers (pseudo banding) with aligned and occasionally imbricated plant detritus (Facies B_1, Table 1) transitioning upward into well-developed bands rich in plant detritus (Facies B_2, Table 1; HEB2A, Fig. 10E to G). In some beds, there is a sharp contact between the sandstone division and the overlying banded division (HEB2B; Figs 7C, 10H and I). This bed type is closely associated and commonly co-occurs and alternates with HEB1 beds.

Interpretation. The gradational transition from structureless to banded sandstone implies that the two divisions are co-genetic and were deposited by the same hybrid flow. The basal division was deposited by aggradation underneath a non-cohesive, high-density turbidity current (e.g. Haughton

et al., 2009), whereas the upper, banded division is attributed to deposition under quasi-laminar (transitional/slurry) flow conditions, indicating that the flow changed from turbulent to laminar without fully transforming into a cohesive debris flow (e.g. Lowe & Guy, 2000; Sumner *et al*., 2009; Kane & Pontén, 2012; Southern *et al*., 2017). Turbulence suppression caused by entrainment of mud, concentration of residual material (such as plant detritus) in the flow tail and upper flow layer, or flow deceleration during flow spreading (e.g. Kane *et al*., 2017; Southern *et al*., 2017) may all promote flow transformation.

HEB3 – bipartite sandstone beds rich in mudstone clasts

Description. This bed type is 0.3 to 1.2 m thick and exhibits a distinct two-folded bed division (Fig. 7C). The lower bed division typically consists of fine-grained to very-fine grained, structureless to faintly stratified, subtly graded to non-graded sandstone (Fig. 10J to M). Bed bases are sharp, but load casts and associated flame structures occur in places. The contact to the upper division is either gradational or sharp with occasional loading. Where loaded, flame structures are commonly present. The upper division is poorly sorted and consists of a normally to subtly graded, muddy sandstone to siltstone rich in floating (intraformational) mudstone clasts, sandstone pseudo nodules and sub-ordinate fossil plant detritus (D_1 to D_3, Table 1). Locally, a thin (<2 cm thick) siltstone to very-fine-grained, normally graded sandstone layer may occur embedded within the upper and most fine-grained part of the bed. The mudstone clasts are generally randomly distributed, but in rare cases, they may be aligned parallel (or sub-parallel) to the bedding. Some of the mudstone clasts are bioturbated. Convolute bedding and overturned to recumbent folding occur in some beds (e.g. HEB3B; Figs 7C and 10L). The bed tops are sharp, but gradual transitions into overlying mudstones occur.

Interpretation. The bipartite (to tripartite) bed character with a lower sandstone division and an upper poorly sorted division containing mudstone clasts, indicates deposition by a bipartite flow

which underwent transformation from turbulent to laminar before final deposition (Haughton *et al*., 2003, 2009; Hodgson, 2009). Thus, the massive appearance of the lower division suggests rapid deposition and progressive aggradation beneath a high-density turbidity current. The poorly sorted, distorted and chaotic fabric with randomly distributed mudstone clasts and sandstone pseudo nodules point to *en masse* deposition from a laminar (debris) flow for the upper bed division (Amy & Talling, 2006). The clasts are intra-basinal and represent semi-consolidated erosional products that were entrained into the flow (e.g. Fonnesu *et al*. 2018). It has previously been argued that the entrainment and disintegration of mud clasts may be responsible for the transformation of turbulent flows into laminar cohesive flows (e.g. Haughton *et al*., 2003; Hodgson, 2009; Pierce *et al*., 2018). Deceleration during flow spreading may also reduce the suspension capacity of a flow, promoting flow collapse and laminar transformation of the upper part of the flow along its full length (Kane *et al*., 2017). Alternatively, beds exhibiting an upper division with convolute bedding or overturned folding, as well as sandstone pseudo nodules, particularly the beds occurring in the lobe fringes, may record deposition and deformation by reversed flow pulses reflected by the forebulge slope (Muzzi Magalhaes & Tinterri, 2010; Tinterri *et al*., 2022). The thin, normally graded sandstone to siltstone bed that occurs locally within the upper fine-grained portion of some beds reflects deposition by the low-density turbulent tail of the current (Haughton *et al*., 2009; Hodgson, 2009). HEBs like those documented here are typically reported from lobe off-axis to lobe fringe environments elsewhere (Haughton *et al*., 2009; Hodgson, 2009; Kane *et al*., 2017; Fonnesu *et al*., 2018). They are also increasingly being recognized in base-of-slope to proximal lobe environments where they presumably record deposition following up-dip erosion and channel incision events (e.g. Haughton *et al*., 2009; Pierce *et al*., 2018; Brooks *et al*., 2022). As such, it is inferred that there is a link between HEB3 beds in proximal lobe axis settings and mudstone rip-up clast-bearing AHP-C deposits occurring in the up-dip slope channel fills (Fig. 6C). Some of the HEB3 beds may also be transitional to the slump deposits of MTD3 (Fig. 7C and D; e.g. Muzzi Magalhaes & Tinterri, 2010).

Mass transport deposits (MTDs)

Description. Several types of mass transport deposits (MTDs) occur in the investigated lobe complexes (Fig. 7D). MTD1 beds occur as up to 5 m thick, asymmetrically folded (basinward-oriented fold axis), heterolithic, thin-bedded units in LC 1 (at Pallfjellet) and LC 9 (i.e. clinoform 12 at Storvola; Figs 7D and 11A). Within both of these lobe complexes, the MTD1 units involve folded lobe fringe deposits consisting mostly of TB2 and TB3 beds and thin mudstone interbeds.

MTD2 occurs as up to 1 m thick heterolithic, thin-bedded units (consisting of TB3 and TB4 beds and alternating mudstone interbeds) displaying pervasive folding with no preferred fold-axis orientations (Figs 7D and 11B). MTD2 occurs in the distal and uppermost part of LC 9 (at Hyrnestabben). Here, these deposits are located on top of thicker, undeformed, gently dipping turbidite sandstone beds (Fig. 11B). They also occur in the channel-lobe transition zone of LC 10 at eastern Storvola (not dealt with here).

MTD3 occurs within the base-of-slope segment of LC 10 and is the dominant bed type of LC 12 (belonging to clinoforms 14B and 15 of Steel & Olsen, 2002; respectively). At Hyrnestabben, the MTD3 deposits within LC 12 can be traced across the entire outcrop for more than 3.5 km. Here, these deposits are recorded as a 1 to 5 m thick heterolithic sandstone unit, which exhibits a distorted and chaotic character with overturned to recumbent slump folds (involving several beds or the entire unit; Fig. 11C), convolute bedding (folding within a single bed), dish structures, boudinage-like features and syn-sedimentary micro-faults (Fig. 11D), none of which display a preferred vergence. In places less affected by pervasive soft-sediment deformation, sandstone (5 to 30 cm thick) and interbedded mudstone beds may form coherent heterolithic bed-sets, which gradually become partly rotated, folded and distorted laterally. Poorly sorted sandstone units rich in organic detritus (mostly plant remains), deformed mudstone to sandstone intra-clasts of various sizes (up to 10 cm in diameter) occur laterally of the distorted bed sets (Fig. 11E).

Interpretation. Based on their general distorted to chaotic character, these bed types are interpreted to represent slide and slump deposits. Based on the low degree of deformation, the thin-bedded and heterolithic character and their restricted stratigraphic occurrence in lobe fringe deposits, the MTD1 beds are interpreted as small, gravity-triggered slides of limited lateral translation and deformation with finite liquefaction and sediment mixing. The preferred fold axis orientation, suggests that the sliding took place on gently inclined, basinward-dipping surfaces inherited from underlying seafloor topography.

Based on its limited thickness, slump folded fabric (with no vergence) and the position on top of undeformed turbidite sandstone beds, the MTD2 beds are recognized as the result of minor slumps with short run-out distances, and which experienced moderate degrees of liquefaction and shear-related deformation. Their position within lobe fringes and channel-lobe-transition zones, indicates that the sloping nature of the underlying deposit to some degree promoted the instability.

The chaotic and highly variable character of the MTD3 beds indicate deposition by slumping and debris flows. The presence of poorly sorted sandstone units suggests that the slumps transformed into cohesive debris flows. Mudstone and sandstone intra-clasts indicate that some of the sediments was semi-consolidated prior to slumping. The occurrence of coherent to folded bed-sets suggests that these sections only partly underwent deformation, sliding down the slope as larger, semi-consolidated blocks. The large amount of dispersed plant remains suggests a deltaic origin for these slump-emplaced sediments. The collapse of over-steepened mouth bars located near the shelf-edge are known to be an important sediment source for many accreting slope systems. Rotated slump blocks overlain by slope lobes and slope channels containing hyperpycnal flow deposits have been documented on the associated slope segment of clinoform 15 on Storvola (Pontén & Plink-Björklund, 2009).

BED TYPE ASSOCIATIONS

Based on the stratigraphic distribution, relative proportion and abundance of bed types, as well as degree of bed amalgamation and overall sandstone content, four bed type associations are recognized, representing: (i) *lobe axis*; (ii) *lobe off-axis*; (iii) *lobe fringe;* and (iv) *distal lobe fringe* depositional sub-environments (Fig. 12; see also Grundvåg *et al*., 2014a and Spychala *et al*., 2021). The four bed type associations stack to form recurrent thickening-upward and sandying-upward units, referred to as *lobes*, in accordance with previous studies (Figs 13 and 14; Crabaugh & Steel, 2004; Grundvåg *et al*., 2014a; Spychala *et al*., 2021). In the vertical domain, a lobe is characterized by distal lobe to lobe fringe deposits being conformably overlain by lobe off-axis, which is capped by erosively based lobe axis deposits (Figs 13 and 14; Grundvåg *et al*., 2014a; Spychala *et al*., 2021). There are no definite boundaries between the bed type associations in the lateral domain. Lobe axis deposits can for example be traced for significant distances along an outcrop, eventually transitioning (on some occasions rather abruptly) into off-axis and lobe fringe deposits (see more details in Spychala *et al*., 2021). As such, the recorded distribution and stacking of bed type associations, at lobe scale, are very similar to that reported in submarine lobes elsewhere (e.g. Hodgson *et al*., 2006; Prélat *et al*., 2009; Macdonald *et al*., 2011; Kane *et al*., 2017; Spychala *et al*., 2017b, 2021; Hansen *et al*., 2019). Because each lobe complex comprises several stacked lobes, the four bed type associations occur at multiple levels within a single lobe complex (Figs 3D, 4B, 13 and 14).

Based on the lateral and vertical distribution and the relative proportion of bed type associations, it is possible to interpret *proximal*, *medial* and *distal* zones at lobe complex scale (i.e. relative to the base-of-slope, *sensu* Hodgson, 2009; see also Grundvåg *et al*., 2014a; Figs 12, 16 and 17). For example, lobes of the medial zone record markedly reduced amounts of scouring and amalgamation in comparison to lobes of the proximal zone. Instead, they are dominated by off axis to lobe fringe deposits and exhibit a diverse bed type variability in comparison to those of the proximal zone, which is dominated by lobe axis deposits (Figs 13B, 16 and 17). Intercalations of thin-

bedded lobe fringe and fine-grained distal fringe deposits characterize lobes of the distal zone (Figs 12 and 13C, see lobes 1 and 2 of LC 5 in Fig. 17).

Various mudstone-dominated and sandstone-rich slope deposits occur stratigraphically above and up-dip of the lobe complexes (Figs 2 and 15A to D). These have been documented thoroughly in the past (e.g. Plink-Björklund *et al*., 2001; Mellere *et al*., 2002; Plink-Björklund & Steel, 2004; Johannessen & Steel, 2005; Petter & Steel, 2006; Grundvåg *et al*., 2014a). However, erosively based, lenticular-shaped sandstone bodies, previously interpreted as slope channels, occur on the slope of some clinforms, and appear to link up with basin floor lobe complexes further down dip (Fig. 2; Plink-Björklund *et al*., 2001; Steel & Olsen, 2002; Johannessen & Steel, 2005; Petter & Steel, 2006). Although briefly described in previous publications, these features need to be assessed in more detail because they may give hints on sourcing mechanisms and flow behaviour. As such, *slope channel* deposits are described separately.

Lobe axis deposits

Lobe axis deposits are characterized by 1 to 5 m thick amalgamated sandstone units (AHP-U, Figs 7, 14A and 14B). In the proximal lobe complex zone, the amalgamated units can reach thicknesses up to *ca* 13 m, thus hampering division into individual lobes (e.g. Figs 12B and 13A; see specifically sections 3 and 6 in Fig. 16A, and LC 8 and lobes 4 and 5 of LC 5 in Fig. 17A). The amalgamated lobe axis deposits in the proximal zone are thus very similar to channel mouth deposits reported in submarine lobes elsewhere (e.g. Hofstra *et al*., 2018; Hodgson *et al*., 2022). When traced laterally, the amalgamated units of the proximal zone tend to thicken and split into several 2 to 10 m thick aggradationally to progradationally stacked lobes, each exhibiting pronounced to more subtle upward coarsening and thickening trends, and many having amalgamated tops (Figs 14A and 16A). Recognition of bed types is problematic within the amalgamated units, especially in the narrow core,

although various thick-bedded to medium-bedded, commonly top-truncated hyperpycnite (for example, HP1A, HP2A and HP2B; Fig. 7A) and turbidite (TB1 and TB2; Fig. 7B) beds may be distinguished on some occasions (Figs 13A, 16 and 17). The amalgamation naturally biases the bed inventory statistics, particularly masking the presence of individual hyperpycnites, giving the impression that these deposits are less abundant in the lobe axis deposits than what is actually the case (Figs 13, 16 and 17). Soft-sediment deformed or structureless intervals, caused by extensive water escape, occur locally (also noted by Crabaugh frequently & Steel, 2004). Erosion occurs on the base of the thickest beds and particularly at the base of the amalgamated units which occasionally scours several decimetres into underlying deposits (for example, TB1A and AHP-U; Figs 7, 13 and 14). Internal low-angle truncation surfaces and horizons of rip-up mudstone clasts occur in places. Fine tail deposits like interbedded siltstones and mudstones are rare. The uppermost finer grained division of the thickest sandstone beds (TB1; Fig. 7B) may occasionally transition laterally into plant detritus-rich divisions (HEB1A; Fig. 7C). Mudstone clast-bearing HEBs (HEB3; Fig. 7C) may constitute a significant portion of some proximal lobe axis deposits (up to 13%, see section 3 of LC 11, Fig. 16).

Deposits of the lobe axis are mostly tabular but can also show low relief pinching and swelling due to minor compensational stacking of beds. The commonly observed erosive relationship between the lobe axis deposits and the underlying off-axis deposits presumably indicates the presence of shallow distributary channels across the lobes (e.g. Crabaugh & Steel, 2004; Grundvåg *et al*., 2014a; Figs 12A, 14C to E). In some lobes, these thick-bedded, amalgamated lobe axis deposits are incised by up to 1 m thick packages consisting of thin (<5 cm) and irregular bedded, fine-grained to medium-grained sandstones (for example, Fig. 14D). Upon closer inspection, the thin-bedded appearance of these units is caused by the presence of multiple bypass surfaces, each overlain by a thin, top-truncated sandstone, thus resembling the *tractional lag* deposits of Porten *et al*. (2016).

Lobe off-axis deposits

Lobe off-axis deposits form laterally extensive, tabular packages which are dominated by medium-bedded structureless to structured sandstone beds (TB1C and TB2), beds exhibiting internal truncations and complex facies arrangements (HP1B and HP1C), thick beds displaying planar lamination (HP2A), as well as units of thin-bedded sandstones, which commonly exhibit current ripple cross-lamination (HP2C and TB2C; Figs 7, 13B, 16 and 17). Bipartite hyperpycnite beds and HEBs having upper divisions rich in plant debris (HP1A, HEB1B and HEB2) commonly alternate with the thin-bedded turbidite sandstones, occasionally forming significant accumulations (for example, Fig. 13B). Interbedded siltstone beds are common, and typically separate individual beds and bed-sets. Mudstone clast-bearing HEBs (HEB3; Fig. 7C) may constitute a significant portion of some lobe off-axis deposits in the proximal lobe complex zone (up to 22%, see lobe 6 of LC 6, Fig. 17), but are very rare in the off-axis deposits of lobes positioned in the medial lobe complex zone.

Lobe fringe deposits

Lobe fringe deposits comprise a wide range of bed types, and from all the lobe sub-environments the lobe fringe is the most variable in facies and bed thicknesses (Figs 13C, 16 and 17). Typically, the lobe fringe deposits occur as heterolithic sandstone packages dominated by thin to medium-bedded structureless to structured sandstones (TB2 beds), as well as beds exhibiting internal truncations (HP1B and HP1C; Fig. 7A) and thin beds (typically <0.2 m) frequently exhibiting climbing current ripple cross-lamination (HP2C and HP2D). Thicker sandstone beds are sporadically interbedded within these deposits (TB1B and TB1C). Thin-bedded, heterolithic packages (TB3 and subordinate TB2A beds; Fig. 7B) containing thin plant-rich HEBs (HEB1C and HEB2 beds; Fig. 7C) and siltstone beds (TB4A) are common. Some lobe fringe deposits of lobes representing the distal zone contain significant amounts (up to 43%, see lobe 2 of LC 5 in Fig. 17) of plant-rich HEBs (i.e. HEB1 and HEB2; Fig. 7C). Mudstone and sandstone clast-bearing HEBs are very rare in the lobe fringes but may form locally important accumulations (for example, 20% of lobe 2 of LC 5 in Fig. 17). Distorted and

asymmetrically folded bed successions and bed sets may occur locally (MTD1 and MTD2 units, Figs 7D and 11A).

Distal lobe fringe deposits

This bed type association is generally weathered and scree-covered in the outcrops and is therefore best observed in the Sysselmannbreen core (Fig. 4B). The distal lobe fringe deposits form up to 5 m thick heterolithic siltstone to mudstone-dominated packages in the lower part of some lobe complexes where they commonly intercalate with lobe fringe deposits (for example, see LC5 in Figs 4B and 17A). The transition from lobe fringe to distal lobe fringe is marked through the change from packages with variable bed thickness to thin-bedded packages with very low sandstone percentages (<20%). Interbeds of normally graded, structureless to planar laminated, very thin-bedded, very-fine grained sandstone beds are variably present (TB3; Fig. 7B). Sharp-based, normally to non-graded siltstone to mudstone beds occur locally (TB4; Fig .7B).

Slope channel deposits

Description. Lenticular-shaped sandstone bodies with erosional, concave-up bases occur locally in the slope segment of the clinoforms (Fig. 15A). They typically cut several metres into the surrounding (slope) mudstones but may also occur within the sandstone-rich slope wedges of some clinoforms (for example, clinoforms 12 and 14 of Steel & Olsen, 2002; Fig. 2). The lenticular bodies may be some few tens to a couple of hundred metres wide and may, on some occasions, be traced down-dip into the basin floor lobe complexes (Figs 1D, 2, 6B and 15E). The scoured base exhibits flute casts, abundant rip-up mudstone clasts and subordinate lithic conglomerates (Fig. 15F and G), whereas their tops are most typically sharp and flat. Internally, the lenticular bodies consist of highly amalgamated sandstones with a thick-bedded and structureless to dewatered appearance (AHP-C; Figs 7A and 15E), which appears to onlap the basal erosive surface. Locally, the upper part of the

channelized sandstone bodies is characterized by up to 2 m thick heterolithic units consisting of thin-bedded turbidite sandstones (TB3).and interbedded mudstones, as well as subordinate hyperpycnites (HP1) and hybrid event beds (HEB1).

Interpretation. Based on their stratigraphic position, lenticular geometries, concave-up and erosive bases incising into surrounding slope deposits, these sandstone bodies are interpreted to represent the fill of low-sinuosity slope channels (e.g. Plink-Björklund *et al*., 2001; Steel & Olsen, 2002; Johannessen & Steel, 2005; Petter & Steel, 2006; Helland-Hansen & Grundvåg, 2021). Flute casts and rip-up mudstone clasts at the base indicate channel formation through initial erosion by powerful, fully turbulent flows. The thick-bedded and amalgamated nature of the channel fills and the locally dewatered appearance points to rapid deposition by the collapse of voluminous, quasi-steady, high-density turbidity flows. Horizons of aligned mudstone clasts may indicate progressive sand aggradation accompanied by bed load transport of clasts beneath sustained turbidity flows (e.g. Kneller & Branney, 1995). Albeit many flows deposited their load in the channels, the high degree of bed amalgamation (see above description of the AHP-C beds; Fig. 7A) and the down-dip relationship to the basin floor lobe complexes, indicate that the channels where relatively long-lived conduits for flows bypassing the slope. The sharp tops indicate abrupt channel abandonment caused by sudden decrease in sediment flux (for example, via channel avulsion or other processes affecting the fluvio-deltaic feeder system). Accordingly, the heterolithics in the top of some channel fills suggest decreasing sedimentation rates and gradual abandonment, or lateral migration.

In modern submarine channels, scour fills containing massive sand, and up-slope dipping beds, which successively onlap (in an up-dip direction) the underlying erosive surface, have been linked to upstream-migrating supercritical bedforms (i.e. cyclic steps, see Cartigny *et al*., 2014) caused by flow instabilities (Hage *et al*., 2018). Given the steepness of the clinoform slopes in the present case (3 to 5°; e.g., Johannessen & Steel, 2005), the lenticular appearance of the channel bodies and the onlapping nature of the channel fill sandstones, channel back-filling by supercritical turbidity currents

may offer an alternative interpretation (e.g. Postma & Cartigny, 2014; Hage *et al*., 2018). Under such conditions, high sediment concentrations and hindered settling at the base of individual flows may have suppressed turbulence, thus forcing deposition of massive sand beds in the channel (e.g. Postma *et al*., 2009).

DISCUSSION

Criteria for recognizing basin floor lobes fed by hyperpycnal flows

Several criteria have previously been proposed for the recognition of hyperpycnal flow-dominated turbidite systems, including: (i) physical connection between shelf-edge positioned fluvial channels and slope channels; (ii) systematically accreted turbidite slope wedges; (iii) an abundance of massive thick-bedded turbidite sands; (iv) abundant composite beds (for example, exhibiting inverse–normal grading and intra-bed cut-and-fill features); (v) abundant climbing current-ripple cross-lamination (particularly in frontal lobe regions); (vii) abrupt down-dip pinch-out of thick turbidite beds (caused by lofting processes); (viii) abundance of plant fragments; (ix) low abundance of mass transport deposits; and (x) an overall sand-prone turbidite system (Mulder *et al*., 2003; Mutti *et al*., 2003; Plink-Björklund & Steel, 2004; Zavala *et al*., 2006, 2011; Paim *et al*., 2011; Steel *et al*., 2016). In addition, hyperpycnal flows appear to result in lobate deposits with a high length to width ratio, presumably recording prolonged flood discharge and quasi-steady flow behaviour in combination with lofting processes followed by rapid deposition (e.g. Zavala *et al*., 2006; Steel *et al*., 2017; Yang *et al*., 2017; Chen *et al*., 2021).

If reviewed individually, none of these criteria are unique to systems fed by hyperpycnal flows (e.g. Talling, 2014; Shanmugam, 2018). Thick and massive deep-water sandstones, for example, may be produced by a wide range of processes (e.g. Lowe, 1982; Kneller & Branney, 1995; Shanmugam, 1996; Gladstone & Pritchard, 2010; Stevenson & Peakall, 2010; Steel *et al*., 2016), bed amalgamation likewise (e.g. Walker, 1966; Mattern, 2002), and climbing ripple cross-lamination may reflect deposition from surge-type flows experiencing deceleration and expansion due to loss of

confinement or decrease in slope angle (Jobe *et al*., 2012). In fact, the architecture of the lobe complexes documented here, which is characterized by an overall proximal to distal reduction in amalgamation, sandstone content and bed thicknesses, as well as the abundance of HEBs in the lobe fringes (see Figs 3, 4, 6, 12, 13, 16 and 17), is very similar to that reported in sandy lobe complexes fed by surge-type turbidity currents and hybrid flows elsewhere (e.g. Walker, 1978; Piper & Normark, 2001; Mattern, 2002; Hodgson *et al*., 2006; Prélat *et al*., 2009; Bourget *et al*., 2010; Macdonald *et al*., 2011). Moreover, it seems that many small-sized to moderate-sized turbidite systems occurring along tectonically active margins are sand dominated (e.g. Walker, 1978; Piper & Normark, 2001; Mutti *et al*., 2003). However, the fact that most of the above-mentioned recognition criteria are widely identified in the present case cannot be escaped, including the physical connection between shelf-edge positioned fluvial channels and slope channels (for example, Figs 2, 6 and 15), which strongly suggests that the basin floor lobes were dominantly fed by hyperpycnal flows (see also review by Plink-Björklund & Steel, 2004).

At bed scale, some of the most striking evidence includes frequent bed amalgamation, an abundance of thick, massive sandstone beds (for example, the AHP units and TB1 beds; Fig. 7), an abundance of plant remains (forming separate divisions in many beds, particularly in the HEB1 and HEB2 bed types as discussed separately below; see Figs 7, 8B and 10) and, more importantly, an abundance of composite beds across the full length of the lobes, from proximal to distal (Figs 13, 14, 16 and 17), which exhibit internal truncations and complex facies arrangements attributable to deposition by quasi-steady hyperpycnal flows of fluctuating velocities and densities (HP1 and HP2; Figs 7A, 8 and 18; e.g. Mutti *et al*., 2003; Zavala *et al*., 2006, 2011; Tinterri, 2007, 2011). The majority of the hyperpycnite beds documented here exhibit facies sequences deviating from the classical hyperpycnite facies model (see Figs 7A and 8), which is portrayed by a thin inversely–normally graded bed recording deposition during the waxing to waning stages of a single-peaked flood (Mulder *et al*., 2003; Lamb *et al*., 2010). The exception is the thin-bedded, inversely-to-normally

graded varieties of the HP1 beds (for example, Fig. 8D) which, based on their occurrence in the lobe fringes, may reflect distal hyperpycnal flow deposits. Interestingly, it has been debated whether it is possible to preserve even the simplest flood signal in sandy, deep-water hyperpycnites (e.g. Nakajima, 2006; Lamb *et al*., 2010; Shanmugam, 2018). Conversely, it has been suggested that flood signals have a higher preservation potential in mud-grade sediments, since muddy (low-density) hyperpycnal plumes are less influenced by plunge point dynamics (e.g. Lamb *et al*., 2010). Nonetheless, it is suggested here that the repeated waxing–waning configuration in the HP1 and HP2 beds was caused by the dynamic interplay between hyperpycnal flood waters and multiple other processes, including: (i) plunge-point translations (Lamb *et al*., 2010); (ii) hydraulic jumps at the river mouth, within the slope channels and particularly at the base of slope (as discussed in the final paragraph); (iii) internal waves developing at the interface between contrasting density layers (or pulses) within the flow (Pomar *et al*. 2012); as well as (iv) tidal modulation of the dense river effluent and superimposed storm wave activity during coupled storm-flood events (e.g. Mutti *et al*., 2003; Tinterri, 2007, 2011). Collectively, this promoted spatiotemporal instabilities and velocity pulsing within the flow, which further caused fluctuations between subcritical and supercritical conditions (e.g. Kostaschuk *et al*., 2018; Salinas *et al*., 2020).

It is, however, important to emphasize that the interpreted hyperpycnites coexist with turbidites (high-density and low-density types), hybrid event beds and subordinate mass transport deposits (Figs 7, 16 and 17), which conspicuously demonstrates that there was no unequivocal flow process, which alone was responsible for the transfer of sand onto the basin floor (Fig. 18). Multi-pulsed and sustained (steady or quasi-steady) turbidity currents initiated by processes other than hyperpycnal flood discharge can result in deposits of very similar characteristics to the interpreted hyperpycnites of this study (e.g. Kneller & Branney, 1995; Mulder *et al*., 2003; Talling, 2014; Ho *et al*., 2018; Heerema *et al*., 2022). Supercritical flows may also deposit composite beds due to flow instabilities and velocity fluctuations (e.g. Postma *et al*., 2009; Hofstra *et al*., 2018; Cornard &

Pickering, 2019), and fully ponded or partially reflected turbidity currents can result in so-called *contained-reflected beds* exhibiting complex facies sequences (e.g. Muzzi Magalhaes & Tinterri, 2010; Tinterri *et al*., 2022). Therefore, other potential triggering mechanisms and flow processes are carefully evaluated below. In addition, the physiography of the basin is thoroughly discussed to highlight various factors which promoted the establishment of the inferred hyperpycnal flow-dominated sourcing regime.

Alternative triggering mechanisms and processes promoting sustained turbidity currents

Sustained turbidity currents may originate or transform from several types of land-derived, dense flows such as debris flows, jökulhlaups, flash floods and lahars (Mulder *et al*., 2003; Shanmugam, 2018; Zavala, 2020). However, most of these flow types are related to specific climatic or physiographic settings and were virtually unlikely to occur in the CTB. Plink-Björklund & Steel (2004) evaluated alternative triggering mechanisms for sustained turbidity currents in the CTB, including instability and sediment remobilization related to volcanism, seismically triggered subaerial sliding in the drainage basin, storm surges, retrogressive slope failure and breaching, as well as downslope transformation from debris flows, and found all of these mechanisms unlikely. Instead, Plink-Björklund *et al*. (2004) favoured the combination of relative sea-level falls, which drove deltas across the shelf and promoted fluvial incision when sea level dropped below the shelf break and hyperpycnal river discharge directly onto the slope. A close relationship between sea-level lowstand and hyperpycnal flow deposition have also been invoked for clinoform systems elsewhere (e.g. Mutti *et al*., 2003; Paim *et al*., 2011). However, it is also known that hyperpycnally fed turbidite systems operate likewise during sea-level highstands (e.g. Henriksen *et al*., 2011; Steel *et al*., 2016).

Retrogressive slope failure, particularly involving over-steepened delta fronts, or due to tectonically induced seismic shocking, are some of the most widely cited mechanisms for generating sustained turbidity currents (e.g. Felletti *et al*., 2009; Jackson & Johnson, 2009). In submarine

canyons, retrogressive slumping in combination with breaching and knickpoint migration, can do the same (Van den Berg *et al*., 2002; Heijnen *et al*., 2020). However, if slumping were to be an important process in the present case, slump scar infills should be readily recognized on the slope of the clinoforms. This is clearly not the case. Hitherto, only one potential slump scar (on the slope of clinoform 13 on Storvola) has been observed and there are generally few other reports of such features despite numerous investigations of the clinoform slopes (e.g. Plink-Björklund *et al*., 2001; Mellere *et al*., 2002; Plink-Björklund & Steel, 2004; Johannessen & Steel, 2005; Petter & Steel, 2006; Helland-Hansen & Grundvåg, 2021). A notable exception is a proposed slump-generated canyon at the shelf-edge to upper slope segment of Clinoform 8 (Steel *et al*., 2000; Mellere *et al*., 2003; Plink-Björklund & Steel, 2004). Johannessen & Steel (2005) interpreted the same feature to represent a channelized, shelf-edge-positioned mouth bar.

The low abundance of mass transport deposits on the basin floor supports the notion of a system where slope failures rarely occurred. In this regard, the mass transport-dominated LC 12 (MTD3; Fig. 7D) appears to be an oddity. Pontén & Plink-Björklund (2009) documented rotated slump blocks on the associated up-dip slope segment (clinoform 15 of Steel & Olsen, 2002) as well as shelf-edge delta wedges and slope channels, all containing abundant and locally pervasively soft sediment deformed sustained flow turbidites. Ergo, in the case of LC 12, it seems that slope instability and catastrophic failure was caused by high sedimentation rates on the shelf edge, although a seismic trigger cannot be excluded.

In the Cellino Basin, Italy, Felletti *et al*. (2009) attributed a series of thick (up to 23 m) composite sandstone beds to sustained turbidity currents generated by seismically triggered slope failures along the basin margin. Despite having a similar composite nature as the interpreted hyperpycnites of the present study, the Cellino beds are much thicker, exhibit a sheet-like architecture and lack a systematic stacking trend. Earthquakes may also influence the sediment flux in a basin indirectly by contributing to increased sedimentation rates and subsequent slope

instability. Dadson *et al*. (2005), for instance, reported an increase in the frequency of hyperpycnal flows as well as the concentration of suspended load in several rivers following an earthquake in Taiwan, and related this to seismically triggered landslides in the catchment area.

Monitoring data from the Squamish Delta, Canada, shows that turbidity current activity occurs frequently sometime after river floods (Clare *et al*., 2016). It has been postulated that the combination of elevated river discharge and increased sedimentation rates results in rapid delta front progradation, sediment loading and increased pore pressure, which eventually provoke post-flood delta front failures (Clare *et al*., 2016). A very similar sequence of events has been proposed for fluvially-derived slope to basin floor turbidites in the Jurassic Los Molles Formation in the Neuquén Basin, Argentina (Paim *et al*., 2011). Moreover, in a recent monitoring study of the Congo Submarine Canyon, Talling *et al*. (2022) demonstrate that river floods, in combination with spring tides and rapid sediment accumulation at the river mouth, can generate violent canyon flushing turbidity flows. In this respect, it is intriguing to see that another recent deep-water surveillance program in Bute Inlet, Canada, has documented river/delta front-derived turbidity currents with thin, yet very dense heads which are capable of transporting sand beyond the delta front and bypass it into deep-water (Pope *et al*., 2020). Sustained underflow may also develop from fine-grained, dilute river plumes originating from tidally modulated river mouths (Parsons *et al*., 2001; Clare *et al*., 2016; Hage *et al*., 2019) and may likewise be achieved inherently by short-lived turbidity currents due to a phenomenon referred to as flow stretching (e.g. Azpiroz-Zabala *et al*., 2017). However, these processes are typical of mud-rich systems.

Basin palaeo-physiography

There appears to be no available monitoring data or published accounts of flood-derived sandy hyperpycnal flows in the modern record, which naturally questions their existence and relevance as deep-water transport agents (e.g. Talling, 2014; Shanmugam, 2018). However, most deep-water

systems currently being monitored are in completely different settings than the case presented here. The Homathko/Southgate and Squamish deltas in western Canada, for example, are in the inner part of fjords and are fed by glacial meltwater (e.g. Clare *et al*., 2016; Hage *et al*., 2019; Heijnen *et al*., 2020; Pope *et al*., 2022). Other examples such as the Congo, Gaoping, Monterey and Var are all coupled river-submarine canyon systems variably influenced, by amongst others, the Present eustatic highstand, tidal forcing, typhoons and anthropogenic forcing (e.g. Liu *et al*., 2012; Talling, 2014; Maier *et al*., 2019; Heerema et al., 2022; Talling *et al*., 2022).

It is well-known that hyperpycnal flows form more readily in freshwater than in saltwater (e.g. Bates, 1953; Mulder *et al*., 2003; Zavala *et al*., 2006; Olariu *et al*., 2011). Greenhouse climatic conditions prevailed in the Eocene, and multiple palaeo-climatic proxies indicate increased precipitation rates and warmer temperatures for the entire Arctic, Svalbard being no exception (e.g. Greenwood *et al*., 2010; Harding *et al*., 2011). The increased rates of precipitation and terrestrial runoff combined with the CTB's limited connection to the open sea, inhibited water mass circulation and concomitantly promoted brackish water conditions (Fig. 18A; Steel *et al*., 1981, 1985; Mellere *et al*., 2002; Helland-Hansen & Grundvåg, 2021). The lowered density of the ambient brackish basinal water therefore significantly reduced the sediment concentrations required for river outflows to generate dense, bottom-hugging underflows. In addition, the asymmetrical foreland basin geometry of the CTB, with deep water and short, steep slopes in the west (clinoform geometries indicate water depths of *ca* 250 to 400 m, and slope lengths of 3 to 5 km with dip-angles up to 5°; for example, Fig. 2A; Plink-Björklund *et al*., 2001; Mellere *et al*., 2002; Plink-Björklund & Steel, 2004; Johannessen & Steel, 2005; Petter & Steel, 2006) created an ideal setting for dense, sediment-laden effluents to continue directly onto the slope, igniting sustained hyperpycnal flows. The latter is manifested by the connection between fluvial channels positioned at the shelf edge, which can be traced down-dip, via deeply incised slope channels, into basin floor lobes (Figs 2 and 6; Plink-Björklund & Steel, 2004; Johannessen & Steel, 2005; Petter & Steel, 2006). Several studies have also pointed out other important factors such as the short distance between the tectonically active, mountainous

provenance area of the WSFTB and deep-water depocentres (only some few tens of kilometres; e.g. Steel *et al*., 2000; Mellere *et al*., 2002; Steel & Olsen, 2002; Fig. 18A), the narrow width of the sedimentary shelf prism, implying short transit distances for prograding deltas (some few kilometres; Helland-Hansen, 2010) and the high-supply character of the fluvial system (as evidenced by the elongated and lobate geometry of the deltas, the common soft sediment deformation features, and the poor sorting of the sediments at multiple levels in the progradational package; Helland-Hansen & Grundvåg, 2021).

Based on length estimates derived from the exposed, sandstone-dominated parts of the lobe complexes, it seems that many of the flows managed to transport significant amounts of sand at least 9 km into the basin (Figs 3B and 6B). The actual run-out distances of individual flows must have been much longer since estimates do not include slope lengths and do not consider the lateral extent of the heterolithic lobe complex fringes (which are poorly exposed and impossible to estimate). However, this indicates that the Spitsbergen lobe complexes are an order of magnitude smaller than other known examples of hyperpycnal-fed submarine lobes (cf. Piper & Normark, 2001; Bourget *et al*., 2010).

Turbidity currents operating in narrow, structurally confined basins, or bathymetrically complex basins, may be reflected and produce reversed flow pulses which interact with the parental flow, eventually depositing composite beds with complex facies arrangements. These deposits, commonly referred to as contained-reflected turbidite beds (e.g. Muzzi Magalhaes & Tinterri, 2010; Tinterri *et al*., 2022), may, in part, resemble the hyperpycnites presented here. They show bipartite to tripartite architectures, typically having a lower structureless division succeeded by structured divisions showing signs of flow reversals and interaction of flow pulses (Tinterri *et al*., 2022). Thus, could the composite architecture of the hyperpycnites of this study result from flows being reflected against the rising forebulge of the CTB? It is of course a possibility that some voluminous flows managed to transverse the entire basin and run up the forebulge slope before being reversed.

However, the actual position of the forebulge of the CTB is debated, but there is consensus that the basin must have extended several tens of kilometres further east of the preserved basin (e.g. Bruhn & Steel, 2003; Helland-Hansen & Grundvåg, 2021). This study found little compelling evidence of flow reversals in the beds described here (Fig. 7), albeit that the HEB3B beds occurring in some lobe fringes may represent potential candidates (for example, Fig. 10L, see also the topmost bed of lobe 2 in Fig. 13C). Combined with the palaeogeographic uncertainties and the limited pinch-out distance of the lobe complexes (typically <10 km; for example, Figs 3, 5 and 6), which indicate that most flows had relatively short run-outs, flow reflection related to structural confinement seems unlikely, although some influence cannot be ruled out. Finally, the similarity between the basin floor hyperpycnites and those occurring on the upper slope segment of the clinoforms (for example, Fig. 2D and E; Petter & Steel, 2006), which surely could not have been influenced by flow reflection or deflection, points to a common process, such as hyperpycnal flows, which operated likewise on the upper slope as on the basin floor.

Another previously neglected factor that must have influenced the Spitsbergen lobe complexes is the global intensification of weathering rates during the Eocene 'hothouse' (e.g. Dypvik *et al*., 2011). Several studies demonstrate re-organization of river systems and a significant increase in the amount of dissolved and suspended load delivered into the ocean during this period (e.g. Foreman *et al*., 2012). In the CTB, the nearby source area, in this case the evolving WSFTB (Fig. 18A), comprised stacked thrust sheets consisting of shale and sandstone-bearing Palaeozoic to Mesozoic strata. Weathering of these terranes provided massive amounts of sand readily available for erosion and transport and choked the rivers with suspended fines and dissolved load. It has been shown that the sediment concentration needed for generating dense river-derived underflows may be as low as 1 to 5 kg/m^3, and in extreme cases 0.1 to 1.0 kg/m^3 (Parsons *et al*., 2001; Mulder *et al*., 2003). It may thus be that the lowered density of the ambient water and the elevated bulk density of the inflowing riverine water, primed by favourable climatic conditions and active tectonism, formed a potent

combination for generating a persistent, hyperpycnal flow-dominated supply regime, which eventually gave birth to the investigated series of sandy basin floor lobe complexes (Fig. 18).

The Al Batha turbidite system off the Oman margin, which reportedly is fed by sandy hyperpycnal flows (Bourget *et al*., 2010), shares many similarities with the Spitsbergen lobe complexes, despite being in an arid climatic zone where flashfloods are the most important triggering mechanism for hyperpycnal flows. The Al Batha turbidite system is characterized by having a mountainous hinterland containing easily erodible material, which is drained by a network of small, steep gradient 'dirty' rivers (*sensu* Milliman & Syvitski, 1992), a narrow shelf intercepted by slope channel/canyon heads, and steep to moderate slope gradients (Bourget *et al*., 2010). As such, the Spitsbergen turbidite system showcases several important factors which appear to be essential and possibly universal prerequisites for hyperpycnal turbidite systems to develop, including coupled fluvial-slope feeder channel systems, steep slopes of sufficient relief, a narrow shelf combined with high sediment supply, as well as a mountainous, tectonically active hinterland drained by small to medium-sized 'dirty' rivers. Based on the stratigraphic occurrence and the age of the Spitsbergen lobe complexes, it may be speculated that hyperpycnal turbidite systems develop readily during periods of extreme climatic forcing, such as during the Eocene and the Cretaceous when greenhouse conditions prevailed.

The origin and distribution of plant-rich hybrid event beds

Traditionally, the abundance of plant material has been used as a diagnostic criterion for interpreting hyperpycnally sourced turbidites, and particularly for interpreting fallout deposits related to lofting processes (Mutti *et al*., 2003; Plink-Björklund & Steel, 2004; Pritchard & Gladstone, 2009; Paim *et al*., 2011; Zavala *et al*., 2011, 2012; Steel *et al*., 2016). However, tidal currents and longshore currents are both capable of transporting plant material away from fluvial entry points to sites more prone to turbidity current initiation such as canyon heads (Talling, 2014; Shanmugam, 2018), and low-density

turbidity currents may deposit plant-rich, deep-water turbidites (Saller *et al*., 2006). Thus, inferring hyperpycnal sourcing based solely on the occurrence of plant remains should be avoided.

In this study, however, the abundance of plant-rich HEBs and the physiography of the basin, make a strong case for hyperpycnal sourcing (Fig. 18). The concentration of plant-rich HEBs in the lobe off-axis to lobe fringe deposits (see for example section 22 in Fig. 16 and lobes 1 and 2 of LC 5 in Fig. 17) is particularly intriguing because it mimics the spatial distribution of mudstone clast-rich HEBs reported in many other submarine lobes (e.g. Haughton *et al*., 2009; Porten *et al*., 2016; Kane *et al*., 2017; Southern *et al*., 2017; Pierce *et al*., 2018). In mudstone clast rich HEBs, flow transformation is proposedly driven by clay enrichment via turbulent erosion and entrainment of mud clasts in combination with flow deceleration in low gradient settings, such as the lobe fringe (e.g. Haughton *et al*., 2003; Hodgson, 2009; Southern *et al*., 2017; Pierce *et al*., 2018). Hodgson (2009) attributed the occurrence of plant-rich HEBs in the basin floor lobes of the Karoo Basin, South Africa, to hybrid flows triggered by the collapse of shelf-edge deltas rich in terrestrial material. That study found it unlikely that dilute river floods could transform into dense, cohesive debris flows, which usually requires significant seafloor erosion and clay entrainment. However, it has later been postulated that decelerating, clay-rich, turbidity currents may experience sudden loss of turbulence, even at low concentrations, whereby reduction in bed-shear stress and suspension capacity result in the formation of a low yield strength basal layer which inhibits vertical mixing within the flow (Eggenhuisen *et al*., 2017; Kane *et al*., 2017). The result is rapid deposition from the laminarized basal flow and concomitant clay concentration in the upper flow layer, which promote *en masse* transformation.

A similar scenario for hyperpycnal flows (see also Hussain *et al*., 2021) is suggested here. When a hyperpycnal flow, which carries significant volumes of suspended sand, fines and plant remains, experience rapid deceleration (for example, caused by flow expansion and thinning),

temporarily waning (for example caused by variations in the flood hydrograph, plunge point translations, or internal flow instabilities; e.g. Mulder *et al*., 2003; Tinterri, 2007; Lamb *et al*., 2010; Zavala *et al*., 2011), or finally comes to rest (i.e. losing all its capacity), large quanta of sand can be deposited rather abruptly through progressive aggradation as the flow collapses (Fig. 18B). The remaining flow becomes enriched in residual material, including plant debris, to such an extent that it suppresses turbulence and stimulates *en masse* transformation to laminar flow behaviour, which eventually results in the deposition of a co-genetic turbidite–debrite bed (HEB1; Figs 7C and 18B). Lofting plumes can theoretically enhance this process by removing significant amounts of clay and silt from the upper part of the flow (to be carried away and deposited through suspension fallout elsewhere), resulting in a relative enrichment of plant material in the remaining bottom-hugging flow, ultimately forcing transformation into a quasi-laminar, hyperconcentrated flow (*sensu* Mulder & Alexander, 2001; Pritchard & Gladstone, 2009).

In the lobe fringe deposits investigated in this study, HEBs with a linked debrite division typically co-occur with HEBs having an upper banded division (HEB1 versus HEB2; Fig. 7C) and beds exhibiting climbing ripple cross-lamination (HP2C, HP2D; Fig. 7A). Traditionally, banding has been attributed to the cyclic deposition and freezing of sand and mud layers on top of a cohesive viscous, near-bed sublayer (Lowe & Guy, 2000), as well as cyclic fallout deposition from lofting plumes coming off hyperpycnal flows (Zavala *et al*., 2006, 2011, 2012). However, it is suggested that the banding indicates transitional regimes in the upper layer of some hybrid flows (turbulent and laminarized fluctuations) and that the two HEB types represent various stages of turbulence-suppressed flow transformation.

HEBs with banding have been described from various deep-water settings elsewhere but appear to be more common in slope-positioned lobes and channels, base-of-slope channel mouths and proximal lobe regions than in distal, lobe fringe regions (Kane & Pontén, 2012; Southern *et al*.,

2017; Spychala *et al*., 2017b; Hofstra *et al*., 2018; Stevenson *et al*., 2020). In addition, thin and poorly developed banded units seem to be diagnostic of full-length confined deep-water systems (Haughthon *et al*., 2009; Southern *et al*., 2017; Tinterri *et al*., 2022). Interestingly, Stevenson *et al*. (2020), suggested that banding is a result of sustained traction and bedform aggradation underneath quasi-steady flows in *proximal settings* (see also Baas *et al*., 2016). The same authors argue that the unsteady behaviour, rapid deceleration and catastrophic collapse of flows in distal settings suppress traction and inhibit banding-related bedforms to develop, eventually favouring *en masse* flow transformation and linked-debrite deposition (i.e. deposits similar to HEB1/HEB3 beds in the present study; Fig. 7C). As such, the occurrence of banded HEBs in the fringes and distal fringes of the Spitsbergen lobes is enthralling, because if they represent banding-related bed forms, they may indicate that quasi-steady flows operated in the distal regions of the lobe where they promoted sustained traction deposition (Fig. 18B). The occurrence of beds exhibiting climbing ripple cross-lamination (HP2C and HP2D; Fig. 7A), which commonly alternate with both types of plant-rich HEBs in the lobe fringe deposits, also indicate sustained traction and temporarily high fallout rates from quasi-steady flows that reached the distal/frontal lobe regions. Climbing current-ripple cross-lamination appears to be very common in frontal lobes fed by quasi-steady hyperpycnal flows (Zavala *et al*., 2006, 2011), and less common in lateral and frontal lobes fed by surge-type turbidity currents (Spychala *et al*., 2017b; Hansen *et al*., 2019). It is therefore suggested that the combination of systematically occurring plant-rich HEBs, including banded varieties, and climbing ripple cross-laminated beds in the fringes of basin floor lobes, provide a strong criterion for interpreting deposition by hyperpycnal flows.

Supercritical turbidity currents versus hyperpycnal flows

Plane parallel to sub-horizontal stratification, wavy lamination, coarse-tail normal grading, and intra-bed scour-and-fill features, which were observed in many of the HP1 beds, have all been attributed to deposition by supercritical turbidity currents (i.e. rapid/unstable flow, Postma *et al*., 2009;

Cartigny *et al*., 2014; Cornard & Pickering, 2019). Supercritical, surge-type turbidity currents running down slope channels may transform into subcritical flow via a hydraulic jump in areas where there is a marked reduction in gradient and the incoming high-velocity flow undergoes abrupt deceleration, such as at the base-of-slope, or where a confined flow experiences sudden lateral expansion, such as in the channel-lobe-transition zone (e.g. Postma & Cartigny, 2014; Hodgson *et al*., 2022). A turbidity current may also experience repeated hydraulic jumps on its way down the feeder channel when it passes over in-channel bed forms, such as cyclic steps or crescentic sediment waves (e.g. Postma & Cartigny, 2014; Hofstra *et al*., 2018), or when it leaves the base-of-slope channel mouth due to lateral switching of the high velocity flow core and the concomitant dynamic interplay between erosion, deposition and bedform development near the channel mouth (i.e. the 'hose' effect of Hofstra *et al*., 2018). All of these processes cause spatiotemporal flow instabilities and velocity pulsing which can produce turbidite beds with complex subcritical to supercritical facies expressions. In addition, experimental studies have shown that repeated transitions between subcritical and supercritical conditions may take place in transcritical flows, even in the absence of underlying bedforms (Salinas *et al*., 2020).

Although it seems possible that fluctuating velocities in supercritical, surge-type turbidity currents may produce turbidite beds with complicated facies architectures like the hyperpycnite beds presented here (i.e. the AHP, HP1 and HP2 bed types; Figs 7 and 18B), the many other signals consistent with deposition by quasi-steady hyperpycnal flows, as already discussed and summarized below, cannot be rejected (Fig. 18). Neither can the signs of deposition by supercritical flows in the proximal as well as the distal reaches of the lobes be neglected. Supercritical flow conditions can be maintained for long distances if a flow is confined (e.g. Hamilton *et al*., 2015; Postma *et al*., 2016). This is interesting considering the self-incisional nature of hyperpycnal flows, in which their fast-moving, turbulent body tends to erode shallow channels across the associated lobe (e.g. Mulder & Alexander, 2001; Zavala *et al*., 2006, 2011; Yang *et al*., 2017; Zavala & Pan, 2018). Therefore, rather than dismissing one or the other, it is suggested here that the quasi-steady nature of the hyperpycnal

flows, in combination with flow confinement in shallow distributary channels, periodically fostered supercritical flow conditions across the full length of the lobes (or generated supercritical flow pulses that propagated across the lobes), which ultimately resulted in the deposition of hyperpycnite beds dominated by facies consistent with supercritical flow (for example, HP1A and HP1B; Fig. 7A).

Finally, the combination of the following features indicate that hyperpycnal flows were the main deep-water sediment delivery mechanism in the CTB: (i) the lateral facies tract with shelf-edge positioned fluvial channels that link up with basin floor lobe complexes via deeply incised slope channels (Figs 1D, 2, 6 and 15E; Crabaugh & Steel, 2004; Plink-Björklund & Steel, 2004; Johannessen & Steel, 2005; Petter & Steel, 2006; Helland-Hansen & Grundvåg, 2021); (ii) the frequent occurrence of interpreted hyperpycnites on the slope segment of the clinoforms (e.g. Plink-Björklund *et al*., 2001; Petter & Steel, 2006; Fig. 2); (iii) the proximal to distal abundance of composite sandstone beds exhibiting internal truncations and complex facies arrangements (Figs 7A, 8, 13, 14, 16 and 17), which facies-wise resemble the previously reported slope hyperpycnites (Fig. 2E); and (iv) the systematic co-occurrence of plant-rich HEBs and climbing ripple cross-laminated beds in the lobe fringes (recording sustained traction and contemporary high rates of suspended load fallout). As such, this study provides additional recognition criteria for hyperpycnites, and illustrates the importance of river floods in transferring sand into deep waters via hyperpycnal flows.

CONCLUSION

Hyperpycnal flows generated by river floods are a widely cited triggering mechanism for sustained turbidity currents. However, their ability in transferring sand into deep-water basins is unclear. This study investigates the spatial and stratigraphic distribution, as well as the variability of various sediment gravity flow deposits in progradationally stacked basin floor lobe complexes in the Eocene succession of Spitsbergen, Arctic Norway. Four principal flow types interacted during progradation of the lobe complexes: (i) hyperpycnal flows depositing sandy hyperpycnites; (ii) surge-type turbidity

currents depositing turbidites; (iii) transitional flows depositing hybrid event beds; and (iv) rare slumps, slides and debris flows emplacing mass transport deposits.

Frequent bed amalgamation, an abundance of thick-bedded massive sandstones, the proximal to distal abundance of composite beds exhibiting internal truncations and complex facies arrangements consistent with deposition from sustained flows of fluctuating densities and velocities, and an abundance of plant remains, typically concentrated in the upper division of hybrid event beds, indicates that quasi-steady hyperpycnal flows were the most important process in transferring sand onto the basin floor. This is substantiated by the low abundance of mass transport deposits on the basin floor and the concomitant lack of slump scars on the slope (which could have indicated that slope failures triggered sustained turbidity currents), as well as the shelf-slope-basin floor facies tract where shelf-edge delta and fluvial distributary channel deposits can be traced down-dip into basin floor lobe complexes via deeply incised slope channels filled by thick-bedded hyperpycnite and turbidite sandstones. This suggests that sand-laden river effluents discharged directly on to the steep slopes, readily generating powerful, quasi-steady hyperpycnal flows. The hyperpycnal discharge regime was primed by favourable physiographic conditions, including brackish basinal waters that lowered the density threshold for hyperpycnal flow to initiate, an immense influx of sediments eroded from a tectonically active hinterland composed of older sedimentary strata, and increased weathering rates which choked the feeding rivers with suspended fines which elevated the bulk density of incoming riverine waters.

The frequent and systematic occurrence of bipartite plant-rich hybrid event beds, particularly in the lobe fringes, suggest transformation of fully turbulent currents rich in plant material, such as flood-generated hyperpycnal flows, into transitional or laminar flows. Rapid sand deposition during flow deceleration, either due to expansion or temporarily waning, forced turbulence suppression via concentration of fine-grained sediments and plant material. The relative enrichment of fines resulted in negative buoyancy and flow lofting, which further concentrated the amount of plant material

relative to the other components. This inhibited turbulent mixing in the remaining bottom-hugging flow and eventually forced *en masse* transformation.

The composite and complex facies architecture of the interpreted sandy hyperpycnites, which deviate from the classical facies model for hyperpycnites, presumably reflects the interaction between a wide range of processes, including plunge point translations and internal flow instabilities, clearly demonstrating that it is problematic to link composite deep-water deposits to simple, single peaked flood hydrographs. Finally, this study illustrates the complexity of deep-water sediment gravity flow deposits and highlights the need to carefully evaluate bed-scale facies variations in combination with analyses of entire facies tracts and basin physiography to confidently separate hyperpycnites from deposits of multi-pulsed or sustained turbidity currents triggered by other mechanisms (for example, retrogressive slope failure), reflected turbidity currents and supercritical, surge-type turbidity currents, which all produce beds with complex facies sequences.

AUTHOR CONTRIBUTIONS

SAG collected most of the data and wrote most of the manuscript. EB, JE, WHH, EPJ, FP and YS contributed to the data collection and analysis. All authors contributed to the discussion of the results.

FUNDING

The project received funding from the Research Council of Norway (grant number 228107). YS, JTE, and FP received funding from the Netherlands Organisation for Scientific Research (grant number 864.13.006).

ACKNOWLEDGEMENTS

We are grateful for the financial support from Equinor (former Statoil) during our fieldwork campaigns in 2009 and 2010. JE, FP and YS, are grateful for financial support from Equinor, Shell and ExxonMobil during our fieldwork in 2017. David Kosowski and Silje Smith-Johnsen are thanked for precious assistance during past fieldwork campaigns. Elliot Broze is acknowledged for great companionship in the field and for valuable contributions to this project during his thesis work at Hyrnestabben. We endorse Stig Henningsen for his safe boat operations and good evening company onboard. We are also grateful for the invaluable logistical support from Sara Cohen at UNIS. Finally, we are grateful for detailed journal reviews and constructive feedback by Ronald Steel, Mattia Matti and Roberto Tinterri.

DATA AVAILABILITY STATEMENT

The data that support the findings of this study are available from the corresponding author upon reasonable request.

REFERENCES

Amy, L.A. and **Talling, P.J.** (2006) Anatomy of turbidites and linked debrites based on long distance (120 x 30 km) bed correlation, Marnoso Arenacea Formation, Northern Apennines, Italy. *Sedimentology*, **53**, 161–212.

Azpiroz-Zabala, M., Cartigny, M. J. B., Talling, P. J., Parsons, D. R., Sumner, E. J., Clare, M. A., Simmons, S. M., Cooper, C. and **Pope, E. L.** (2017) Newly recognized turbidity current structure can explain prolonged flushing of submarine canyons. *Sci. Adv.*, **3**, e1700200.

Baas, J.H., Best, J.L. and **Peakall, J.** (2011) Depositional processes, bedform development and hybrid bed formation in rapidly decelerated cohesive (mud– sand) sediment flows. *Sedimentology*, **58**, 1953–1987.

Baas, J.H., Best, J.L. and **Peakall, J.** (2016) Predicting bedforms and primary current stratification in cohesive mixtures of mud and sand. *J. Geol. Soc.*, **173**, 12–45.

Bates, C.C. (1953) Rational theory of delta formation. *AAPG Bull.*, **37**, 2119–2162.

Bellwald, B., Planke, S., Becker, L.W.M. and **Myklebust, R.** (2020) Meltwater sediment transport as the dominating process in mid-latitude trough mouth fan formation. *Nature Com*., **11**, 4645.

Bergh, S.G., Braathen, A. and **Andresen, A.** (1997) Interaction of basement-involved and thin-skinned tectonism in the Tertiary fold-thrust belt of central Spitsbergen, Svalbard. *AAPG Bull*., **81**, 637-661.

Bhattacharya, J. and **MacEachern, J.** (2009) Hyperpycnal rivers and prodeltaic shelves in the Cretaceous seaway of North America. *J. Sed. Res.*, **79**, 184–209.

Boulesteix, K., Poyatos-Moré, M., Flint, S.S., Taylor, K.G., Hodgson, D.M. and **Hasiotis, S.T.** (2019) Transport and deposition of mud in deep-water environments: processes and stratigraphic implications. *Sedimentology*, **66**, 2894–2925.

Bouma, A.H. (1962) *Sedimentology of Some Flysch Deposits: A Graphic Approach to Facies Interpretation*. Elsevier, Amsterdam, 168 pp.

Bourget, J., Zaragosi, S., Mulder, T., Schneider, J.L., Garlan, T., Van Toer, A., Mas, V. and **Ellouz-Zimmermann, N.** (2010) Hyperpycnal-fed turbidite lobe architecture and recent sedimentary processes: a case study from the Al Batha turbidite system, Oman margin. *Sed. Geol.*, **229**, 144–159.

Braathen, A., Bergh, S.G. and **Maher, H.D.** (1995) Structural outline of a Tertiary basement-cored uplift/inversion structure in western Spitsbergen, Svalbard: kinematics and controlling factors. *Tectonics*, **14**, 95–119.

Brooks, H.L., Ito, M., Zuchuat, V., Peakall, J. and **Hodgson, D.M.** (2022) Channel-lobe transition zone development in tectonically active settings: Implications for hybrid bed development. *The Depositional Record*, **8**, 829–868.

Bruhn, R. and **Steel, R.** (2003) High-resolution sequence stratigraphy of a clastic foredeep succession (Paleocene, Spitsbergen): An example of peripheral-bulge-controlled depositional architecture. *J. Sed. Res.*, **73,** 745–755.

Butler, R. W., Eggenhuisen, J. T., Haughton, P. and **McCaffrey, W. D.** (2016). Interpreting syndepositional sediment remobilization and deformation beneath submarine gravity flows; a kinematic boundary layer approach. *J. Geol. Soc.*, **173**, 46–58.

Cao, Y., Wang, Y., Gluyas, J.G., Liu, H., Liu, H. and **Song, M.** (2018) Depositional model for lacustrine nearshore subaqueous fans in a rift basin: the Eocene Shahejie Formation, Dongying sag, Bohai Bay Basin, China. *Sedimentology*, **65**, 2117–2148.

Cartigny, M.J.B., Ventra, D., Postma, G. and **van Den Berg, J.H.** (2014) Morphodynamics and sedimentary structures of bedforms under supercritical-flow conditions: new insights from flume experiments. *Sedimentology*, **61**, 712–748.

Chen, P., Xian, B., Li, M., Liang, X., Wu, Q., Zhang, W., Wang, J., Wang, Z. and **Liu, J.** (2021) A giant lacustrine flood-related turbidite system in the Triassic Ordos Basin, China: sedimentary processes and depositional architecture. *Sedimentology*, **68**, 3279–3306.

Clare M.A., Hughes Clarke J.E., Talling P.J., Cartigny M.J.B. and **Pratomo D.G.** (2016) Preconditioning and triggering of offshore slope failures and turbidity currents revealed by most detailed monitoring yet at a fjordhead delta. *Earth Planet. Sci. Lett.*, **450**, 208–220.

Cornard, P.H. and **Pickering, K.T.** (2019) Supercritical-flow deposits and their distribution in a submarine channel system, Middle Eocene, Ainsa Basin, Spanish Pyrenees. *J. Sed. Res.*, 89, 576– 597.

Crabaugh, J.P. and **Steel, R.J.** (2004) Basin-floor fans of the Central Tertiary Basin, Spitsbergen: relationship of basinfloor sand-bodies to prograding clinoforms in a structurally active basin. In: *Confined Turbidite Systems* (eds S.A. Lomas and P. Joseph), *Geol. Soc. London Spec. Publ.*, **222**, 187–208.

Dadson, S., Hovius, N. Pegg, S., Dade, W. B., Horng, M. J. and **Chen, H.** (2005) Hyperpycnal river flows from an active mountain belt. *J. Geophys. Res.*, **110**, F04016.

Dimakis, P., Braathen, B.I., Faleide, J.I., Elverhøi, A. and **Gudlaugsson, S.T.** (1998) Cenozoic erosion and the preglacial uplift of the Svalbard-Barents Sea region. *Tectonophysics*, **300**, 311–327.

Doré, A.G., Lundin, E.R., Gibbons, A., Sømme, T.O. and **Tørudbakken, B.O.** (2015) Transform margins of the Arctic: a synthesis and re-evaluation. In: *Transform Margins: Development, Controls and Petroleum Systems* (eds. M. Nemcok, S. Rybar, S.T. Sinha, S.A. Hermeston and L. Ledvenyiova), *Geol. Soc. London Spec. Publ.*, 431, 63–94.

Dypvik H., Riber L., Burca F., Rüther D., Jargvoll D., Nagy J. and **Jochmann M.** (2011) The Paleocene–Eocene Thermal Maximum (PETM) in Svalbard—clay mineral and geochemical signals. *Palaeogeogr. Palaeoclimatol. Palaeoecol.*, **302**, 156–169.

Eggenhuisen, J.T., Cartigny, M.J.B. and **de Leeuw, J.** (2017) Physical theory for near-bed turbulent particle-suspension capacity. *Earth Surf. Dynam.*, **5**, 269–281.

Felletti, F., Carruba, S. and **Casnedi, R.** (2009) Sustained turbidity currents: evidence from the Pliocene Periadriatic foredeep (Cellino Basin, Central Italy). In: *External controls on deep-water depositional systems* (eds. B. Kneller, O.J. Martinsen and B. McCaffrey), *SEPM Spec. Publ.*, **92**, 325–346.

Fonnesu, M., Haughton, P., Felletti, F. and **McCaffrey, W.D.** (2015) Short length-scale variability of hybrid event beds and its applied significance. *Mar. Petrol. Geol*., **67,** 583–603.

Fonnesu, M., Felletti, F., Haughton, P.D.H., Patacci, M. and **McCaffrey, W.D.** (2018) Hybrid event bed character and distribution linked to turbidite system sub-environments: The North Apennine Gottero Sandstone (north-west Italy). *Sedimentology*, **65,** 151–190.

Foreman, B. Z., Heller, P. L. and **Clementz, M. T.** (2012) Fluvial response to abrupt global warming at the Palaeocene/Eocene boundary. *Nature*, **491**, 92–95.

Girard, F., Ghienne, J.-F. and **Rubino, J.-L.** (2012) Occurrence of hyperpycnal flows and hybrid event beds related to glacial outburst events in a Late Ordovician proglacial delta (Murzuq Basin, SW Libya). *J. Sed. Res.*, **82**, 688–708.

Gladstone, C. and **Pritchard, D.** (2010) Patterns of deposition from experimental turbidity currents with reversing buoyancy. *Sedimentology*, **57**, 53–84.

Gladstone, C., McClelland, H.L.O., Woodcock, N.H., Pritchard, D. and **Hunt, J.E.** (2018) The formation of convolute lamination in mud-rich turbidites. *Sedimentology*, **65**, 1800–1825.

Greenwood, D.R., Basinger, J.F. and **Smith, R.Y.** (2010) How wet was the Arctic Eocene rain forest? Estimates of precipitation from Paleogene Arctic macrofloras. *Geology*, **38**, 15–18.

Grundvåg, S.-.A., Johannessen, E.P., Helland-Hansen, W. and **Plink-Björklund, P.** (2014a) Depositional architecture and evolution of progradationally stacked lobe complexes in the Eocene Central Basin of Spitsbergen. *Sedimentology*, **61**, 535–569.

Grundvåg, S.-A., Helland-Hansen, W., Johannessen, E.P., Olsen, A.H. and **Stene, S.A.K.** (2014b) The depositional architecture and facies variability of shelf deltas in the Eocene Battfjellet Formation, Nathorst Land, Spitsbergen. *Sedimentology*, **61**, 2172–2204.

Grundvåg, S-A., Jelby, M. E., Olaussen, S. and **Śliwińska, K. K.** (2020) The role of shelf morphology on storm-bed variability and stratigraphic architecture, Lower Cretaceous, Svalbard. *Sedimentology*, **68**, 196–237.

Hage, S., Cartigny, M.J.B., Clare, M.A., Sumner, E.J., Vendettuoli, D., Hughes Clarke, J.E., Hubbard, S.M., Talling, P.J., Lintern, D.G., Stacey, C.D., Englert, R.G., Vardy, M.E., Hunt, J.E., Yokokawa, M., Parsons, D.R., Hizzett, J.L., Azpiroz-Zabala, M. and **Vellinga, A.J.** (2018) How to recognize crescentic bedforms formed by supercritical turbidity currents in the geologic record: insights from active submarine channels. *Geology*, **46**, 563–566.

Hage, S., Cartigny, M.J.B., Sumner, E.J., Clare, M.A., Hughes Clarke, J.E., Talling, P.J., Lintern, D.G., Simmons, S.M., Jacinto, R.S., Vellinga, A.J., Allin, J.R., Azpiroz-Zabala, M., Gales, J.A., Hizzett, J.L., Hunt, J.E., Mozzato, A., Parsons, D.R., Pope, E.L., Stacey, C.D., Symons, W.O., Vardy, M.E. and **Watts C.** (2019). Direct monitoring reveals initiation of turbidity currents from extremely dilute river plumes. *Geophys. Res. Lett.*, **46**, 11310–11320.

Hamilton, P.B., Strom, K.B. and **Hoyal, D.C.J.D.** (2015) Hydraulic and sediment transport properties of autogenic avulsion cycles on submarine fans with supercritical distributaries. *J. Geophys. Res. Earth Surf.*, **120**, 1369–1389.

Hansen, L.A.S., Hodgson, D.M., Pontén, A., Bell, D. and **Flint, S.** (2019) Quantification of basin-floor fan pinchouts: examples from the Karoo Basin, South Africa. *Front. Earth Sci.*, **7**, 00012.

Harding, I.C., Charles, A.J., Marshall, J.E.A., Pälike, H., Roberts, A.P., Wilson, P.A., Jarvis, E., Thorne, R., Morris, E., Moremon, R., Pearce, R.B. and **Akbari, S.** (2011) Sea-level and salinity fluctuations during the Paleocene–Eocene thermal maximum in Arctic Spitsbergen. *Earth Planet. Sci. Lett.*, **303**, 97–107.

Haughton, P., Davis, C., McCaffrey, W. D. and **Barker, S. P.** (2009). Hybrid sediment gravity flow deposits – Classification, origin and significance. *Mar. Pet. Geol.*, **26**, 1900–1918.

Haughton, P. D. W., Barker, S. P. and **McCaffrey, W. D.** (2003). 'Linked' debrites in sand-rich turbidite systems - origin and significance. *Sedimentology*, **50**, 459–482.

Heijnen, M.S., Clare, M.A., Cartigny, M.J.B., Talling, P.J., Hage, S., Gwyn Lintern, D., Stacey, C., Parsons, D.R., Simmons, S.M., Chen, Y., Sumner, E.J., Dix, J.K. and **Hughes Clarke, J.E.** (2020) Rapidly-migrating and internally-generated knickpoints can control submarine channel evolution. *Nat. Commun.*, **11**, 3129.

Helland-Hansen, W. (1990) Sedimentation in Paleogene foreland basin, Spitsbergen. *AAPG Bull.*, **74**, 260–272.

Helland-Hansen, W. (2010) Facies and stacking patterns of shelf-deltas within the Palaeogene Battfjellet Formation, Nordenskiöld Land, Svalbard: implications for subsurface reservoir prediction. *Sedimentology*, **57**, 190–208.

Helland-Hansen, W. and **Grundvåg, S.-A.** (2021). The Svalbard Eocene-Oligocene (?) Central Basin succession: Sedimentation patterns and controls. *Basin Res.*, **33**, 729–753.

Henriksen, S., Pontén, A., Janbu, N. and **Paasch, B.** (2011) The importance of sediment supply and sequence-stacking pattern in creating hyperpycnal flows. In: *Sediment transfer from shelf to deep water - Revisiting the delivery system* (eds R.M. Slatt and C. Zavala), *AAPG Stud. Geol.*, **61**, 1–24.

Heerema, C.J., Cartigny, M.J.B., Jacinto, R.S., Simmons, S.M., Apprioual, R. and **Talling, P.J.** (2022) How distinctive are flood-triggered turbidity currents? *J. Sed. Res.*, **92**, 1–11.

Ho, V.L., Dorrell, R.M., Keevil, G.M., Burns, A.D. and **McCaffrey, W.D.** (2018) Pulse propagation in turbidity currents. *Sedimentology*, **65**, 620–637.

Hodgson, D. (2009). Distribution and origin of hybrid beds in sand-rich submarine fans of the Tanqua depocentre, Karoo Basin, South Africa. *Mar. Pet. Geol.*, **26**, 1940–1956.

Hodgson, D., Flint, S., Hodgetts, D., Drinkwater, N., Johannessen, E. and **Luthi, S.** (2006). Stratigraphic evolution of fine-grained submarine fan systems, Tanqua Depocenter, Karoo Basin, South Africa. *J. Sed. Res.*, **76**, 20–40.

Hodgson, D.M., Peakall, J. and **Maier, K.L.** (2022) Submarine channel mouth settings: processes, geomorphology, and deposits. *Front. Earth Sci.*, **10**, 790320.

Hofstra, M., Peakall, J., Hodgson, D.M. and **Stevenson, C.J.** (2018) Architecture and morphodynamics of subcritical sediment waves in an ancient channel–lobe transition zone. *Sedimentology*, **65**, 2339–2367.

Hussain, A., Haughton, P., Shannon, P., Morris, E., Pierce, C. and **Omma, J.** (2021) Mud-forced turbulence dampening facilitates rapid burial and enhanced preservation of terrestrial organic matter in deep-sea environments. *Mar. Pet. Geol.*, **130**, 105101.

Jackson, C.A.-L. and **Johnson, H.D.** (2009) Sustained turbidity currents and their interaction with debrite-related topography; Labuan Island, offshore NW Borneo, Malaysia. *Sed. Geol.*, **219**, 77–96.

Jobe, Z. R., Lowe, D. and **Morris, W.** (2012). Climbing-ripple successions in turbidite systems: depositional environments, sedimentation rates and accumulation times. *Sedimentology*, **59**, 867–898.

Johannessen, E.P. and **Steel, R.J.** (2005) Shelf-margin clinoforms and prediction of deepwater sands. *Basin Res.*, **17**, 521–550.

Johannessen, E.P., Henningsen, T., Bakke, N.E., Johansen, T.A., Ruud, B.O. and **Riste, P.** (2011) Paleogene clinoform succession on Svalbard expressed in outcrops, seismic logs and cores. *First Break*, 29, 35–44.

Kane, I. and **Pontén, A.** (2012). Submarine transitional flow deposits in the Paleogene Gulf of Mexico. *Geology*, **40**, 1119–1122.

Kane, I., Pontén, A. S. M., Vangdal, B., Eggenhuisen, J., Hodgson, D. and **Spychala, Y. T.** (2017) The stratigraphic record and processes of turbidity current transformation across deep-marine lobes. *Sedimentology*, **64**, 1236–1273.

Katz, T., Ginat, H., Eyal, G., Steiner, Z., Braun, Y., Shalev, S. and **Goodman-Tchernov, B.N.** (2015) Desert flash floods form hyperpycnal flows in the coral-rich Gulf of Aqaba, Red Sea. *Earth Planet. Sci. Lett.*, **417**, 87–98.

Kneller, B. C. (1995) Beyond the turbidite paradigm: physical models for deposition of turbidites and their implications for reservoir prediction. In: *Characterization of Deep Marine Clastic Systems* (eds A.J. Hartley and D.J. Prosser), *Geol. Soc. London Spec. Publ.*, **94**, 31–49.

Kneller, B. and **Branney, M.** (1995) Sustained high-density turbidity currents and the deposition of thick massive sands. *Sedimentology*, **42**, 607–616.

Kostaschuk, R., Nasr-Azadani, M. M., Meiburg E., Wei, T., Chen, Z., Negretti, M. E., Best, J., Peakall, J. and **Parsons, D.R.** (2018). On the causes of pulsing in continuous turbidity currents. *J. Geophys. Res.*, **123**, 2827–2843.

Kristensen, T.B., Rotevatn, A., Marvik, M., Henstra, G.A., Gawthorpe, R.L. and **Ravnås, R.** (2018) Structural evolution of sheared margin basins: the role of strain partitioning. Sørvestsnaget Basin, Norwegian Barents Sea. *Basin Res.*, **30**, 279-301.

Lai, S.Y.J. and **Capart, H.** (2009) Reservoir infill by hyperpycnal deltas over bedrock. *Geophys. Res. Lett.*, **36**, L08402.

Lamb, M.P., McElroy, B., Kopriva, B., Shaw, J. and **Mohrig, D.,** (2010) Linking river-flood dynamics to hyperpycnal-plume deposits: experiments, theory, and geological implications. *Geol. Soc. Am. Bull.*, **122**, 1389–1400.

Lasabuda, A.P.E., Laberg, J.S., Knutsen, S.-M. and **Safronova, P.** (2018) Cenozoic tectonostratigraphy and pre-glacial erosion: A mass-balance study of the northwestern Barents Sea margin. *J. Geodynamics*, **119**, 149–166.

Liu, J.T., Wang, Y.-H., Yang, R.T., Hsu, R.T., Kao, S.-J., Lin, H.-L. and **Kuo, F.H.** (2012) Cyclone induced hyperpycnal turbidity currents in a submarine canyon. *J. Geophys. Res.*, **117**, C04033.

Lowe, D.R. (1982) Sediment gravity flows: II. Depositional models with special reference to the deposits of high-density turbidity currents. *J. Sed. Petrol.*, **52**, 279–297.

Lowe, D.R. and **Guy, M.** (2000) Slurry-flow deposits in the Britannia Formation (Lower Cretaceous), North Sea: a new perspective on the turbidity current and debris flow problem. *Sedimentology*, **47**, 31–70.

Macdonald, H.A., Peakall, J., Wignall, P.B. and **Best, J.** (2011) Sedimentation in deep-sea lobe-elements: implications for the origin of thickening-upward sequences. *J. Geol. Soc.*, **168**, 319–331.

Mackiewicz, N.E., Powell, R.D., Carlson, P.R. and **Molnia, B.F.** (1984) Interlaminated iceproximal glacimarine sediments in Muir Inlet, Alaska. *Mar. Geol.*, **57**, 113–147.

Maier, K.L., Gales, J.A., Paull, C.K., Rosenberger, K., Talling, P.J., Simmons, S.M., Gwiazda, R., McGann, M., Cartigny, M.J.B., Lundsten, E., Anderson, K., Clare, M.A., Xu, J., Parsons, D., Barry, J.P., Wolfson-Schwehr, M., Nieminski, N.M. and **Sumner, E.J.** (2019) Linking direct measurements of turbidity currents to submarine canyon-floor deposits. *Front. Earth Sci.*, **7**, 00144.

Marshall, C., Uguna, J., Large, D.J., Meredith, W., Jochmann, M., Friis, B., Vane, C., Spiro, B.F., Snape, C.E. and **Orheim, A.** (2015) Geochemistry and petrology of Palaeocene coals from

Spitzbergen—Part 2: Maturity variations and implications for local and regional burial models. *Int. J. Coal Geol.*, **143**, 1–10.

Mattern, F. (2002) Amalgamation surfaces, bed thicknesses, and dish structures in sand-rich submarine fans: numeric differences in channelized and unchannelized deposits and their diagnostic value. *Sed. Geol.*, **150**, 203–228.

Mellere, D., Plink-Björklund, P. and **Steel, R.J.** (2002) Anatomy of shelf deltas at the edge of a prograding Eocene shelf margin, Spitsbergen. *Sedimentology*, **49**, 1181–1206

Mellere, D., Breda, A. and **Steel, R.J.** (2003) Fluvial incised shelf-edge deltas and linkage upper-slope channels (Central Tertiary Basin, Spitsbergen). In: *Shelf-Margin Deltas and Linked Downslope Petroleum Systems: Global Significance and Future Exploration Potential* (eds H.H. Roberts, N.C. Rosen, R.H. Fillon and J.B. Anderson), *SEPM Soc. Sed. Geol.,* **23**, 231–266.

Middleton, G.V. (1993) Sediment deposition from turbidity currents. *Annu. Rev. Earth Planet. Sci.*, 21, 89–114.

Milliman, J.D. and **Syvitski, J.P.M.** (1992) Geomorphic/tectonic control of sediment discharge to the ocean; the importance of small mountainous rivers. *J. Geol.*, **100,** 525–544.

Mulder, T. and **Alexander, J.** (2001) The physical character of subaqueous sedimentary density flows and their deposits. *Sedimentology*, **48**, 269–299.

Mulder, T. and **Chapron, E.** (2011) Flood deposits in continental and marine environments: character and significance. In: *Sediment Transfer from Shelf to Deep Water-Revisiting the Delivery System* (eds R.M. Slatt and C. Zavala), *AAPG Stud. Geol.*, **61**, 1–30.

Mulder, T. and **Syvitski, J.P.** (1995) Turbidity currents generated at river mouths during exceptional discharges to the world oceans. *J. Geol.*, **103**, 285–299.

Mulder, T., Syvitski, J.P.M., Migeon, S., Faugéres, J.C. and **Savoye, B.** (2003) Marine hyperpycnal flows: initiation, behavior and related deposits. A review. *Mar. Petrol. Geol.*, **20**, 861–882.

Mutti, E., Tinterri, R., Remacha, E., Mavilla, N., Angella, S. and **Fava, L.** (1999) An Introduction to the Analysis of ancient turbidite basins from an outcrop perspective. *AAPG Course Notes*, **39,** 93 pp.

Mutti, E., Tinterri, R., Benevelli, G., Di Biase, D. and **Cavanna, G.** (2003) Deltaic, mixed and turbidite sedimentation of ancient foreland basins. *Mar. Petrol. Geol.*, **20**, 733–755.

Muzzi Magalhaes, P. and **Tinterri, R.** (2010). Stratigraphy and Depositional Setting of Slurry and Contained (Reflected) Beds in the Marnoso-Arenacea Formation (Langhian-Serravallian) Northern Apennines, Italy. *Sedimentology*, **57,** 1685–1720.

Nakajima, T. (2006) Hyperpycnites deposited 700 km away from river mouths in the Central Japan Sea. *J. Sed. Res.*, **76**, 60–73.

Nemec, W., Lønne, I. and **Blikra, L.H.** (1999) The Kregnes moraine in Gauldalen, west-central Norway: anatomy of a Younger Dryas proglacial delta in a palaeofjord basin. *Boreas*, **28**, 454–476.

Olariu, C., Steel, R.J. and **Petter, A.L.** (2010) Delta-front hyperpycnal bed geometry and implications for reservoir modeling: cretaceous Panther Tongue delta, Book Cliffs, Utah. *AAPG Bull.*, **94**, 819–845.

Olariu, C., Bhattacharya, J.P., Leybournes, M.I., Boss, S.K. and **Stern, R.J.** (2011) Interplay between river discharge and topography of the basin floor in a hyperpycnal lacustrine delta. *Sedimentology*, **59**, 704–728.

Paim, P.S.G., Lavina, E.L.C., Faccini, U.F., da Silveira, A.S., Leanza, H. and **d'Avila, R.S.F.** (2011) Fluvial-derived turbidites in the Los Molles Formation (Jurassic of the Neuquén Basin): Initiation, transport, and deposition. In: *Sediment Transfer from Shelf to Deep Water-Revisiting the Delivery System* (eds R.M. Slatt and C. Zavala), *AAPG Stud. Geol.*, **61**, 95–116.

Parsons, J.D., Bush, J.W.M. and **Syvitski, J.P.M.** (2001) Hyperpycnal plume formation from riverine outflows with small sediment concentrations. *Sedimentology*, **48**, 465–478.

Petersen, T.G., Thomsen, T., Olaussen, S. and **Stemmerik, L.** (2016) Provenance shifts in an evolving Eurekan foreland basin: the Tertiary Central Basin, Spitsbergen. *J. Geol. Soc*., **173**, 634–648.

Petter, A.L. and **Steel, R.J.** (2006) Hyperpycnal flow variability and slope organization on an Eocene shelf margin, Central Basin, Spitsbergen. *AAPG Bull.*, **90**, 1451–1472.

Piepjohn, K., von Gosen, W. and **Tessensohn, F.** (2016) The Eurekan deformation in the Arctic: an outline. *J. Geol. Soc.*, **173**, 1007–1024.

Pierce, C. S., Haughton, P. and **Shannon, P. M.** (2018). Variable character and diverse origin of hybrid event beds in a sandy submarine fan system, Pennsylvanian Ross Sandstone Formation, western Ireland. *Sedimentology*, **65**, 952–992.

Piper, D.J.W. and **Normark, W.R.** (2001) Sandy fans – from Amazon to Hueneme and beyond. *AAPG Bull.*, **85**, 1407–1438.

Piper, D.J.W. and **Normark, W.R.** (2009) Processes that initiate turbidity currents and their Influence on turbidites: a marine geology perspective. *J. Sed. Res.*, **79**, 347–362.

Plink-Björklund, P. and **Steel, R.J.** (2004) Initiation of turbidity currents: outcrop evidence for Eocene hyperpycnal flow turbidites. *Sed. Geol.*, **165**, 29–52.

Plink-Björklund, P., Mellere, D. and **Steel, R.J.** (2001) Turbidite variability and architecture of sand-prone, deepwater slopes: Eocene clinoforms in the Central Basin, Spitsbergen*. J. Sed. Res.*, **71**, 895–912.

Pomar, L., Morsilli, M., Hallock, P. and **Bádenas, B.** (2012). Internal waves, an under-explored source of turbulence events in the sedimentary record. *Earth Sci. Rev.*, **111,** 56–81.

Pontén, A. and **Plink-Björklund, P.** (2009) Process regime changes across a regressive to transgressive turnaround in a shelf-slope basin, Eocene Central Basin of Spitsbergen. *J. Sed. Res.*, **79**, 2–23.

Pope, E.L., Cartigny, M.J.; Clare, M.A.; Talling, P.J.; Lintern, D.G.; Vellinga, A.; Hage, S.; Acikalin, S.; Bailey, L.; Chapplow, N., Chen, Y., Eggenhuisen, J., Hendry, A., Heerema, C.J., Heijnen, M.S., Hubbard, S.M., Hunt, J.E., McGhee, C., Parsons, D.R., Simmons, S.M., Stacey, C.D. and **Vendettuoli, D.** (2022) First source-to-sink monitoring shows dense head controls sediment flux and runout in turbidity currents. *Sci. Adv.*, **8**, eabj3220.

Porten, K.W., Kane, I.A., Warchoł, M.J. and **Southern, S.J.** (2016) A sedimentological process-based approach to depositional reservoir quality of deep-marine sandstones: an example from the Springar Formation, Northwestern Vøring Basin, Norwegian Sea. J. *Sediment. Res.*, **86**, 1269e1286.

Postma, G., Nemec, W. and **Kleinspehn, K. L.** (1988). Large floating clasts in turbidites: a mechanism for their emplacement. *Sed. Geol.*, **58**, 47–61.

Postma, G. and **Cartigny, M.J.B.** (2014) Supercritical and subcritical turbidity currents and their deposits - A synthesis. *Geology*, **42**, 987–990.

Postma, G., Cartigny, M.J.B. and **Kleverlaan, K.** (2009) Structureless, coarse-tail graded Bouma Ta formed by internal hydraulic jump of the turbidity current? *Sed. Geol.*, **219**, 1–6.

Postma, G., Hoyal, D.C.J.D., Abreu, V., Cartigny, M., Demko, T., Fedele, J., Kleverlaan, K. and **Pederson, K.H.** (2016) Morphodynamics of supercritical turbidity currents in the channel-lobe transition zone. In: *Submarine Mass Movements and Their Consequences* (eds G. Lamarche and J. Mountjoy), pp. 469–478. Springer, Dordrecht.

Prélat, A., Hodgson, D. and **Flint, S.** (2009) Evolution, architecture and hierarchy of distributary deep-water deposits: a high-resolution outcrop investigation from the Permian Karoo Basin, South Africa. *Sedimentology*, **56**, 2132–2154.

Pritchard, D. and **Gladstone, C.** (2009) Reversing buoyancy in turbidity currents: Developing a hypothesis for flow transformation and for deposit facies and architecture. *Mar. Petrol. Geol.*, **26,** 1997–2010.

Salinas, J., Balachandar, S., Shringaroure, M., Fedele, J., Hoyal, D. and **Cantero, M.** (2020). Soft transition between subcritical and supercritical currents through intermittent cascading interfacial instabilities. *Proc. Natl. Acad. Sci. USA.*, **117**, 18278–18284.

Saller, A.H., Dunham, J. and **Lin, R.** (2006) Leaves in turbidite sands: the main source of oil and gas in the deep-water Kutei Basin, Indonesia. *AAPG Bull.*, **90**, 1585–1608.

Shanmugam, G. (1996) High-density turbidity currents: are they sandy debris flows? *J. Sed. Res.*, **66**, 2–10.

Shanmugam, G. (2018) The hyperpycnite problem. *J. Palaeogeogr.*, **7**, 6. https://doi.org/10.1186/s42501-018-0001-7.

Shanmugam, G. (2019) Climatic and tectonic controls of lacustrine hyperpycnite origination in the late Triassic Ordos Basin, Central China: Implications for unconventional petroleum development: Discussion. *AAPG Bull.*, **103**, 505–510.

Sommerfield, C.K. and **Nittrouer, C.A.** (1999) Modern accumulation rates and a sediment budget for the Eel shelf: a flood-dominated depositional environment. *Mar. Geol.*, **154,** 227–241.

Southern, S.J., Kane, I.A., Warchoł, M.J., Porten, K.W. and **McCaffrey, W.D.** (2017) Hybrid event beds dominated by transitional-flow facies: character, distribution and significance in the Maastrichtian Springar Formation, north-west Vøring Basin, Norwegian Sea. *Sedimentology*, **64**, 747–776.

Sparks, R.S.J., Bonnecaze, R.T., Huppert, H.E., Lister, J.R., Hallworth, M.A., Mader, H. and **Phillips, J.** (1993) Sediment-laden gravity currents with reversing buoyancy. *Earth Planet. Sci. Lett.*, **114,** 243–257.

Spychala, Y. T., Hodgson, D. and **Lee, D. R.** (2017a) Autogenic controls on hybrid bed distribution in submarine lobe complexes. *Mar. Pet. Geol.*, **88**, 1078–1093.

Spychala, Y. T., Hodgson, D., Prélat, A., Kane, I., Flint, S. and **Mountney, N.** (2017b). Frontal and lateral submarine lobe fringes: comparing sedimentary facies, architecture and flow processes. *J. Sed. Res.*, **87**, 75–96.

Spychala, Y.T., Eggenhuisen, J.T., Tilston, M. and **Pohl, F.** (2020) The influence of basin setting and turbidity current properties on the dimensions of submarine lobe elements. *Sedimentology*, **67**, 3471–3491.

Spychala, Y.T., Ramaaker, T.A.B., Eggenhuisen, J.T., Grundvåg, S.-A., Pohl, F. and **Wróblewska, S.** 2021. Proximal to distal grain-size distribution of basin-floor lobes: A study from the Battfjellet Formation, Central Tertiary Basin, Svalbard. *The Depositional Record*, **8**, 436–456.

Steel, R.J. and **Olsen, T.** (2002) Clinoforms, clinoform trajectories and deepwater sands. In: *Sequence Stratigraphic Models for Exploration and Production: Evolving Methodology, Emerging Models and Application Histories* (eds J.M. Armentrout and N.C. Rosen), *SEPM Soc. Sed. Geol.*, **22**, 367–381.

Steel, R., Dalland, A., Kalgraff, K. and **Larsen, V.** (1981) The Central Tertiary Basin of Spitsbergen: sedimentary development of a Sheared-Margin Basin. In: *Geology of the North Atlantic Borderland* (eds J.W. Kerr and A.J. Ferguson), *Can. Soc. Petrol. Geol. Mem*., **7**, 647–664.

Steel, R. J., Mellere, D., Plink-Björklund, P., Crabaugh, J., Deibert, J., Loeseth, T. and **Schellpeper, M.** (2000) Deltas vs rivers on the shelf edge: their relative contributions to the growth of shelf-margins and basin-floor fans (Barremian & Eocene, Spitsbergen). In: *Deep-Water Reservoirs of the World* (eds P. Weimer, R.M. Slatt, J. Coleman, N. C. Rosen, H. Nelson, A.H. Bouma, M.J. Styzen and D.T. Lawrence), *SEPM Soc. Sed. Geol.*, **20**, 981–1009.

Steel, R., Gjelberg, J., Helland-Hansen, W., Kleinspehn, K., Nøttvedt, A. and **Rye-Larsen, M.** (1985) The Tertiary strike-slip basins and orogenic belt of Spitsbergen. *SEPM Spec. Publ.*, **37**, 339–359.

Steel, E., Simms, A.R., Steel, R. and **Olariu, C.** (2018) Hyperpycnal delivery of sand to the continental shelf: insights from the Jurassic Lajas Formation, Neuquén Basin, Argentina. *Sedimentology*, **65**, 2149–2170.

Steel, E., Simms, A.R., Warrick, J. and **Yokoyama, Y.** (2016) Highstand shelf fans: the role of buoyancy reversal in the deposition of a new type of shelf sand body. *Geol. Soc. Am. Bull.*, **128**, 1717–1724.

Steel, E., Buttles, J., Simms, A., Mohrig, D. and **Meiburg, E.** (2017) The role of buoyancy reversal in turbidite deposition and submarine fan geometry. *Geology*, **45**, 35–38.

Stevenson, C.J. and **Peakall, J.** (2010) Effects of topography on lofting gravity flows: Implications for the deposition of deep-water massive sands. *Mar. Petrol. Geol.*, **27**, 1366–1378.

Stevenson, C.J., Peakall, J., Hodgson, D., Bell, D. and **Privat, A.** (2020) TB or not TB: banding in turbidite sandstones. *J. Sed. Res.*, **90**, 821–842.

Stow, D.A. and **Shanmugam, G.** (1980) Sequence of structures in fine-grained turbidites: Comparison of recent deep-sea and ancient flysch sediments. *Sed. Geol.*, **25**, 23–42.

Stow, D.A. and **Johansson, M.** (2000) Deep-water massive sands: nature, origin and hydrocarbon implications. *Petrol. Geol.*, **17**, 145–174.

Sumner, E.J., Talling, P.J. and **Amy, L.A.** (2009) Deposits of flows transitional between turbidity current and debris flow. *Geology*, **37**, 991–994.

Talling, P. (2014) On the triggers, resulting flow types and frequencies of subaqueous sediment density flows in different settings. *Mar. Geol.*, **352**, 155–182.

Talling, P.J., Paull, C.K. and **Piper, D.J.W.** (2013) How are subaqueous sediment density flows triggered, what is their internal structure and how does it evolve? Direct observations from monitoring of active flows. *Earth Sci. Rev.*, 125, 244–287.

Talling, P.J., Masson, D.G., Sumner, E.J. and **Malgesini, G.** (2012) Subaqueous sediment density flows: depositional processes and deposit types. *Sedimentology*, **59,** 1937–2003.

Talling, P.J., Baker, M.L., Pope, E.L., Ruffel, S.C., Jacinto, R.S., Heijnen, M.S., Hage, S., Simmons, S.M., Hasenhündl, M., Heerema, C.J., McGhee, C., Apprioual, R., Ferrant, A., Cartigny, M.J.B., Parsons, D.R., Clare, M.A., Tshimanga, R.M., Trigg, M.A., Cula, C.A., Faria, R., Gaillot, A., Bola, G., Wallance, D., Griffiths, A., Nunny, R., Urlaub, M., Pierce, C., Burnett, R., Neasham, J. and **Hilton, R.J.** (2022) Longest sediment flows yet measured show how major rivers connect efficiently to deep sea. *Nat. Commun.*, **13**, 4193.

Tinterri, R. (2007). The lower Eocene Roda Sandstone (south-central Pyrenees): an example of a flood-dominated river delta system in a tectonically controlled basin. *Riv. It. Paleo. Strat.*, **113,** 223–255.

Tinterri, R. (2011) Combined flow sedimentary structures and the genetic link between sigmoidal and hummocky cross stratification. *Geol. Acta*, **10,** 43–85.

Tinterri, R., Mazza, T. and **Muzzi Magalhaes, P.** (2022) Contained-reflected megaturbidites of the Marnoso-arenacea Formation (Contessa Key Bed) and Helminthoid Flysches (Northern Apennines, Italy) and Hecho Group (South-Western Pyrenees). *Front. Earth Sci.*, **10:817012**. doi: 10.3389/feart.2022.817012.

van Loon, A.T., Hüneke, H. and **Mulder, T.** (2019) The hyperpycnite problem: comment. *J. Palaeogeogr.*, **8**, p. 24.

Van den Berg, J., Van Gelder, A. and **Mastbergen, D.R.** (2002) The importance of breaching as a mechanism of subaqueous slope failure in fine sand. *Sedimentology*, **49**, 81–95.

Walker, R.G. (1966) Shale grit and Grindslow shales: transition from turbidite to shallow water sediments in the upper Carboniferous of northern England. *J. Sed. Res.*, **36**, 90–114.

Walker, R.G. (1978) Deep-water sandstone facies and ancient submarine fans: model for exploration for stratigraphic traps. *AAPG Bull.*, **62**, 932–966.

Warrick, J.A. and **Milliman, J.D.** (2003) Hyperpycnal sediment discharge from semi-arid southern California rivers-implications for coastal sediment budgets. *Geology*, **31**, 781–784.

Warrick, J.A., Xu, J.P., Noble, M.A. and **Lee, H.J.** (2008) Rapid formation of hyperpycnal sediment gravity currents offshore of a semi-arid California river. *Cont. Shelf Res.*, **28**, 991–1009.

Warrick, J.A., Simms, A.R., Ritchie, A., Steel, E., Dartnell, P., Conrad, J.E. and **Finlayson D.P.** (2013) Hyperpycnal plume-derived fans in the Santa Barbara Channel, California. *Geophys. Res. Lett.*, **40**, 2081–2086.

Warrick, J.A. (2020) Littoral sediment from rivers: patterns, rates and processes of river mouth morphodynamics. *Front. Earth Sci.*, **8**, 00355.

Wheatcroft, R.A., Borgeld,J. C., Born, R. S., Drake, D. E., Leithold, E. L., Nittrouer, C. A. and **Sommerfield, C. K.** (1996) The anatomy of an oceanic flood deposit. *Oceanography*, **9,** 158–162.

Wright, L., Wiseman, W., Yang, Z.-S., Bornhold, B., Keller, G.H., Prior, D.B. and **Suhayda, J.N.** (1990) Processes of marine dispersal and deposition of suspended silts off the modern mouth of the Huanghe (Yellow River). *Cont. Shelf. Res.*, **10,** 1–40.

Wright, L., Wiseman, W., Bornhold, B., Prior, D.B., Suhayda, J.N., Keller, G.H., Yang, Z.-S. and **Fan, Y.B.** (1988) Marine dispersal and deposition of Yellow River silts by gravity-driven underflows. *Nature*, **332**, 629–632.

Yang, R., Jin, Z., van Loon, A. J., Han, Z. and **Fan, A.** (2017) Climatic and tectonic controls of lacustrine hyperpycnite origination in the Late Triassic Ordos Basin, central China: Implications for unconventional petroleum development. *AAPG Bull.*, **101**, 95–117.

Zavala, C. (2020) Hyperpycnal (over density) flows and deposits. *J. Palaeogeogr.*, **9**, 17. https://doi.org/10.1186/s42501-020-00065-x.

Zavala, C. and **Pan, S.** (2018) Hyperpycnal flows and hyperpycnites: origin and distinctive characteristics. *Lithol. Reserv.*, **30**, 1–27.

Zavala, C., Arcuri, M. and **Blanco Valiente, L.** (2012) The importance of plant remains as diagnostic criteria for the recognition of ancient hyperpycnites. *Rev. Paléobiol.*, **11**, 457–469.

Zavala, C., Arcuri, M., Di Meglio, M., Gamero Diaz, H. and **Contreras, C.** (2011) A genetic facies tract for the analysis of sustained hyperpycnal flow deposits. In: *Sediment Transfer from Shelf to Deep Water-Revisiting the Delivery System* (eds R.M. Slatt and C. Zavala), *AAPG Stud. Geol.*, **61**, 31–51.

Zavala, C., Ponce, J., Drittanti, D., Arcuri, M., Freije, H. and **Asensio, M.** (2006) Ancient lacustrine hyperpycnites: a depositional model from a case study in the Rayoso Formation (Cretaceous) of west-central Argentina. *J. Sed. Res.*, **76**, 41–59.

FIGURE and TABLE CAPTIONS

Fig. 1. (**A**) Location map of Svalbard, which represents the uplifted and exposed north-western corner of the Barents Shelf. The transform De Geer Zone runs parallel to the western margin of Svalbard. HFZ: Hornsund Fault Zone, SFZ: Senja Fracture Zone. (**B**) Map showing location of the West Spitsbergen fold and thrust belt (WSFTB) and the associated Central Tertiary Basin (CTB). The study area is marked by a white square. (**C**) Aerial photograph of the study area showing the location of the investigated sections along the northern shores of Van Keulenfjorden. The data set also includes a fully cored research borehole (Fig. 4) and a two-dimensional (2D) reflection-seismic line (Fig. 5) crossing the well at Sysselmannbreen. Aerial photograph from https://toposvalbard.npolar.no/. (**D**) Stratigraphy of the exposed upper Palaeocene to Eocene and Oligocene(?) part of the CTB fill along the '*Van Keulenfjorden transect*'. This study pertains to a series of basin floor fans referred to as the Pallfjellet, Sysselmannbreen and Hyrnestabben lobe complexes. Clinoform 14 (following the clinoform numbering convention of Steel & Olsen, 2002) is highlighted because of its importance for understanding the lateral facies tract from shelf to basin floor (see Fig. 2 for more details). The transect is modified and redrawn from Steel & Olsen (2002).

Fig. 2. Illustration of the typical shelf-slope-basin floor facies tract of the clinoforms hosting the basin floor lobe complexes. (**A**) Clinoform 14 (with base and top marked by white stippled lines) is by far the most studied clinoform unit of the CTB and is excellently exposed at the mountains of Storvola and Hyrnestabben. Here, it is possible to trace shelf and shelf-edge delta deposits basinward across the shelf-edge, down the slope and further onto the basin floor where several lobe complexes occur (LC 9 to LC 12). (**B**) Fluvial distributary channels occur near the shelf-edge and cut into its associated delta front deposits. (**C**) The deltaic sandstone-dominated deposits transitions laterally (basinward) into heterolithic sandstone-rich units, interpreted as slope lobes and shallow slope channels. Log redrawn from Petter & Steel (2006). Both the log examples are from clinoform 14A (see Fig. 6B and

Petter & Steel, 2006, for internal sub-division of the clinoform). (**D**) Example of a sandstone-rich slope-lobe unit on the upper slope segment of Clinoform 14A. Note the overall thickening-upward trend. (**E**) Internally, the slope lobes contain composite beds, on some occasions being up to several metres thick, with complex vertical facies sequences, suggesting deposition by long-lived hyperpycnal flows characterized by fluctuating velocities (e.g. Plink-Björklund & Steel, 2004; Petter & Steel, 2006). Measuring stick for scale (20 cm). (**F**) The middle slope segment of Clinoform 14 appears to be a zone of extensive bypass, as evident by the presence of erosively-based, lenticular-shaped sandstone units, interpreted as slope channel fills. Internally, they typically exhibit several truncation surfaces. (**G**) In the lower slope-to-basin floor segment, the slope channel bodies are gradually replaced by sheet-like, basinward-thickening sandstone units. These units are typically erosively based, and consists of thick bedded, amalgamated sandstones (i.e. the AHP deposits of Fig. 7A), which is interpreted to represent the channel-lobe transition zone of the basin-floor lobe complexes.

Fig. 3. Overview of the Pallfjellet lobe complexes. (**A**) Overview photograph of Pallfjellet showing the four lobe complexes (LC 1 to LC 4). The lobe complexes overlie a *ca* 300 m thick succession of basin floor shale and is capped by a 150 m thick unit of slope shale. A slope channel is well-exposed on the western ridge of the mountain. (**B**) Correlation panel documenting the internal architecture and the progradational stacking pattern of the lobe complexes. Colour coding shown in Fig. 1D. Modified from Grundvåg *et al*. (2014a). Palaeocurrent data derived from current ripple cross-lamination indicate an overall eastward sediment flux into the basin. The top surface of LC 2 was used as a flattening datum for the correlation panel. Note that LC 3 and LC 4 pinch out further west at Brogniartfjella. (**C**) Photograph showing a stack of lobes within LC 2, note the upward thickening of beds within each lobe. (**D**) Photograph and a measured section of LC 3, illustrating the amalgamation of lobes in proximal axial parts of the lobe complexes.

Fig. 4. Overview of the stratigraphy recorded in fully cored Well BH 10-2008 at Sysselmannbreen. The four investigated lobe complexes (LC 5 to LC 8) are embedded within the shales of the Frysjaodden Formation and show a clear progradational stacking trend (see Grundvåg *et al*., 2014a for more details).

Fig. 5. Two-dimensional reflection seismic data from Sysselmannbreen. The line crosses Well BH 10-2008. See Fig. 1C for location. (**A**) Uninterpreted seismic line tied to the gamma-ray log of Well BH 10-2008. Note the presence of high-amplitude reflection anomalies exhibiting an offset stacking pattern towards the ENE (i.e. basinward), and how these anomalies correlate to an interval of serrated and blocky gamma ray signatures in the well (details shown in Fig. 4B). (**B**) Interpreted seismic line, showing a basinward-prograding slope succession, which partly connects with and overlie the progradationally-stacked series of lobe complexes. The interpretation is modified from Grundvåg *et al*. (2014a), based on Johannessen *et al*. (2011). The seismic data is from Johansen *et al*. (2011).

Fig. 6. Overview of the Hyrnestabben lobe complexes. **(A)** Photograph showing the relation between clinoforms at Storvola (CF 12 to CF 17, following nomenclature of Steel & Olsen, 2002) and the Hyrnestabben lobe complexes exposed at eastern Storvola and Hyrnestabben (LC 9 to LC 12). Note that the clinoform numbering does not correspond to that of the lobe complexes. See main text for explanation. (**B**) Diagram based on outcrop observations illustrating the stratigraphic relationship between shelf-edge delta deposits and their associated slope wedges and basin floor lobe complexes. Note the progradational and compensational stacking of the lobe complexes. The location of measured sections used in this study are marked on the panel. Colour coding shown in Fig. 1D. (**C**) Overview photograph of the main outcrop at Hyrnestabben. Parts of the outcrop have been involved in a landslide, so care must be taken when investigating the lobe complexes at this

location (i.e. some sections are partly repeated). Note the lateral thickening of LC 11. (**D**) Sedimentary log spanning LC 9 to LC 12. Position of the section is marked in (**C**).

Fig. 7. Schematic summary of the different bed types recognized in the investigated lobe complexes. Facies characteristics are given in Table 1.

Fig. 8. Representative pictures of inferred hyperpycnite beds (HPs). (**A**) Details of a HP1A bed exhibiting an undulating internal scour surface and low-angle stratification, typical of deposition by sustained flow of fluctuating velocities. (**B**) A bed displaying an internally asymmetrically loaded sand-on-sand contact, indicating deposition by successive pulses within the same flow event (bed type HP1B). (**C**) A bed exhibiting a lower plane parallel laminated division (T_B) truncated by a coarser-grained massive division (T_A; bed type HP1C), suggestion deposition under waxing to waning flow conditions. (**D**) A stack of thin-bedded hyperpycnites, each displaying a lower laminated division and an upper structureless division. Thin-bedded hyperpycnites commonly co-occur with thin-bedded turbidites in the lobe fringes, suggesting that many hyperpycnal flows reached far into the basin. (**E**) Details of a HP1C bed exhibiting a clear waxing–waning configuration with a lower structured division ($T_{B\text{-}C}$) sharply overlain by a coarser-grained structureless division (T_A). (**F**) A HP2B bed exhibiting a complex facies arrangement with alternations of various traction-generated structures ($T_{B/C}$), collectively suggesting deposition under fluctuating sub-critical velocity conditions. All photographs are from the Hyrnestabben lobe complexes. Bed type details are given in Fig. 7A.

Fig. 9. Representative pictures of turbidite beds (TBs) exhibiting classical Bouma-type facies arrangements pointing to deposition under waning flow conditions. (**A**) A thick-bedded sandstone bed dominated by a massive lower division overlain by a thin, laminated upper division (bed type

TB1C). (**B**) A medium-bedded sandstone exhibiting normal grading and a clear two-fold division with a plane parallel stratified upper division overlying a massive division (bed type TB2B). (**C**) A thin-bedded sandstone characterized by a poorly developed massive division, successively overlain by a plane parallel and a current-ripple cross-laminated division (bed type TB2C). (**D**) A heterolithic unit composed of interbedded mudstones and very thin sandstones beds exhibiting normal grading and occasionally plane parallel lamination to current-ripple cross-lamination (bed type TB3D). All photographs are from the Hyrnestabben lobe complexes. Bed type details are given in Fig. 7B.

Fig. 10. Representative pictures of hybrid event beds (HEBs). Outcrop (**A**) and core (**B**) expression of HEBs exhibiting a lower massive division overlain by a, commonly, soft sediment deformed division rich in partly aligned plant detritus (bed type HEB1B). Outcrop (**C**) and core (**D**) expression of HEBs displaying a tripartite architecture with a thin and poorly developed lower sandstone division, a middle division dominated by imbricated plant detritus and an upper thin-bedded, laminated siltstone to sandstone division (bed type HEB1C). Outcrop (**E**) and core (**F**) and (**G**) expressions of HEBs characterized by a thin, lower massive sandstone division, a middle division containing aligned plant detritus and an upper, plant detritus-rich division exhibiting distinct banding (bed type HEB2A). Outcrop (**H**) and core (I) expression of HEBs showing a two-folded architecture with an upper, banded division (bed type HEB2B). Outcrop (**J**) and core (**K**) expression of HEBs characterized by a lower massive sandstone division overlain by a mudstone clast-rich, upper division (facies D_2). The mudstone clasts may be randomly oriented or exhibit imbrication (bed type HEB3A). (**L**) Outcrop expression of a HEB exhibiting an upper soft-sediment deformed division overlying a massive sandstone division of variable thickness (bed type HEB3B). (**M**) Core example of a HEB with a complex internal facies arrangement, possibly indicating a flow being transitional to a slump (HEB3C). The outcrop examples are from Hyrnestabben, apart from (**L**), which is located on the western ridge of Brogniartfjella (i.e. within the distal part of the Pallfjellet fan series). All core examples are from the

Sysselmannbreen well. Core width on all core photographs: 5 cm. Bed type details are given in Fig. 7C.

Fig. 11. Representative pictures of mass transport deposits (MTDs). (**A**) Typical expression of several metre-scale basinward-directed folds within thin-bedded heterolithic lobe fringe deposits of LC 9 at Storvola (MTD1). These mass transport deposits represent local slide events, which apparently did not evolve into a full-scale slump. (**B**) Decimetre-scale slump folds occur locally within thin-bedded heterolithic fringe and distal fringe deposits, and in proximity to channel margins (MTD2). These deposits record minor slides and slumps (of very limited run-out) associated with instability promoted by local relief. The example is from the channel-lobe transition zone of LC 10 at Storvola. (**C**) to (**E**) Examples of a laterally complex and chaotic MTD within LC 12 at Hyrnestabben. This particular MTD exhibit multiple lateral transitions between segments that record sliding with limited deformation (mostly folding; **C**), via units that contain abundant disintegrated and faulted strata due to increased shear-related deformation (**D**) to fully disintegrated debris-flow deposits (**E**). Bed type details are given in Fig. 7D.

Fig. 12. Schematic illustration of a lobe complex. (**A**) Plan-view architecture of a lobe complex showing the aerial distribution of lobe axis, lobe off-axis, lobe fringe and lobe distal fringe deposits. Scouring is most evident in the lobe axis. (**B**) Cross-sections showing the internal distribution of bed type associations from proximal to distal within a lobe complex consisting of a series of progradationally stacked lobes. The relative position of the logs shown in Figs 13 and 15 are indicated.

Fig. 13. Representative sedimentary logs illustrating the stratigraphic distribution of various beds and bed type associations which define lobes within the lobe complexes. (**A**) Example of a section dominated by amalgamated, thick-bedded deposits, indicating a proximal axial lobe domain. Location: lower part of LC 10 at Hyrnestabben, see Fig. 6D for stratigraphic position. (**B**) Section characterized by a series of (five) stacked lobes dominated by off-axis deposits, indicating a medial to distal lobe complex setting. Location: LC 11 at Hyrnestabben. See Fig. 6B for stratigraphic position. (**C**) Section through the distal/frontal part of LC 3 at the western ridge of Brogniartfjella. See Fig. 3B for stratigraphic position. The lower part of the section (lobe 2 of Grundvåg *et al*., 2014a) is dominated by fringe and distal fringe deposits, which record distal lobe progradation. Despite being in a distal part of the system, the stacked lobes in the upper part (lobes 3 and 4 of Grundvåg *et al*., 2014a) of the section display an upward increase in erosively based lobe axis deposits reflecting the prograding nature of the lobe complex and the possible presence of distributary channels across the lobes.

Fig. 14. Selected photographs showing the internal architecture of LC 11 at Hyrnestabben. (**A**) Laterally, stacked lobes (L1 to L5), which are typically separated by fringe or distal fringe deposits, may gradually merge to form thick, amalgamated sandstone units (AMU). The cliff is *ca* 20 m tall. Position of the outcrop segment is indicated in Fig. 6C. (**B**) Although LC 11 thins to less than <13 m further to the north-east along the outcrop belt, a series of five lobes may be recognized. The cliff is *ca* 10 m tall (lobe 1 is not shown on the photograph). (**C**) to (**E**) Detailed photographs showing the internal architecture of lobes 2, 4 and 5 of LC 11. Note the general vertical distribution of bed type associations with lobe fringe deposits overlain by lobe off-axis and lobe axis deposits. Amalgamation and internal scour surfaces, which indicate frequent erosion and bypass, is characteristic for the lobe axis deposits. Some lobe axis deposits (see example in **D**) contain amalgamated to thin-bedded turbidites that may represent tractional lags (*sensu* Porten *et al*., 2016) and erosive remnants in shallow distributary channels which acted as bypass zones during lobe progradation.

Fig. 15. Representative pictures of various slope deposits occurring up-dip and stratigraphically above the basin-floor lobe complexes (for example, Figs 2 and 6). (**A**) The slope succession is dominated by mudstones that frequently exhibit soft-sediment deformation structures and small-scale faults. Thinly bedded, normally graded sandstones and siltstones with sharp, erosive bases (**B**) and scour surfaces (**C**) are common features within the fine-grained slope succession. All core photographs from the Sysselmannbreen well. (**D**) Locally, heterolithic sandstone-rich successions form wedges that protrude from the shelf edge onto the upper slope to interfinger with the slope mudstones. These wedges record deposition from shelf-edge deltas, and previous studies have indicated that hyperpycnal flows were an important process for the overall accretion of the slope (e.g. Plink-Björklund & Steel, 2004; Petter & Steel, 2006). From clinoform 14B, central part of Storvola (see Fig. 6B for clinoform sub-division). (**E**) Up to 10 m thick, lenticular sandstone bodies with concave-up bases occur occasionally within the slope mudstone succession. These represent slope channels. Internally, the slope channel fill is characterized by a high degree of amalgamation and thick-bedded sandstones containing abundant rip-up mudstone clasts (Fig. 3A for location). (**F**) Frequent flute casts occur at the channel base. From the southern aspect of Pallfjellet. (**G**) A thick-bedded sandstone unit in the channel-lobe transition zone of LC10, exhibiting a scoured base and a mudstone clast-rich division interpreted as traction carpet deposits (facies S_2, Table 1). From the eastern ridge of Storvola.

Fig. 16. (**A**) Panel of six vertical logs along LC 11 at Hyrnestabben documenting the lateral distribution of bed types and bed type associations in a lobe complex. Note how the amalgamated units in the proximal segment of the lobe complex split laterally into multiple vertically stacked lobes. Tentative correlation with the top of the lobe complex used as datum. See Figs 1 and 6 for stratigraphic

context. CLTZ: channel lobe transition zone. (**B**) Charts showing the accumulative abundancy of the various bed types in each of the sections shown in (**A**).

Fig. 17. The Sysselmannbreen well penetrates a series of progradationally stacked lobe complexes (LC 5 to LC 8) recording successively more slope-proximal settings upwards in the succession (Figs 4 and 5). Thus, when the lobe complexes and their corresponding lobes are displayed in the lateral domain from proximal to distal (**A**), it is possible to get a first-hand impression of the spatial distribution of bed types and bed type associations. (**B**) Charts showing the abundancy of the various bed types in each of the lobes shown in (**A**). The amalgamated character of LC 8 makes a sub-division into lobes a redundant task.

Fig. 18. (**A**) Palaeogeographic reconstruction highlighting the most important allogenic forcing factors that facilitated the establishment of a hyperpycnal flow-dominated supply system. Collectively, favourable climatic conditions (leading to high rates of sediment supply), shelf-edge positioned river mouths, brackish water conditions in the basin and steep slopes promoted transfer of sand onto the deep-water basin floor, foremost via river-derived hyperpycnal flows. Turbidity currents triggered by other mechanisms, such as delta front failure, as well as slope instability-related slumping, played subordinate roles. WSFTB: West Spitsbergen fold-and-thrust belt. (**B**) Conceptual model showing the main components of a river-derived hyperpycnal flow and the composite character of its depositional product. See main text for explanation and Fig. 7 for more details on the different bed types. (**C**) Main components of a surge-type, waning turbidity current. These currents deposit 'classical' Bouma-type turbidites (i.e. TB1 to TB3, Fig. 7). (**D**) The main characteristics of a slump-derived cohesive debris flow and the resultant deposit (MTD3; Fig. 7). Deposition occurs via *en masse* freezing of the flow plug. Abbreviations: c – concentration, d – discharge, t – time, u – velocity.

Table 1. Summary of the sedimentary facies that constitute the various bed types shown in Fig. 7.

TABLE 1 Summary of the sedimentary facies that constitute the various bed types shown in Fig. 7.

Facies	Lithology and grain size	Description	Process interpretation	References
S_1	Coarse to medium-grained sandstone with subordinate mudstone clasts	Massive to weakly stratified, ungraded sandstone occasionally containing (layer-parallel) aligned rip-up mudstone clasts	Traction deposition beneath a high-density turbidity flow	Lowe (1982)
S_2	Coarse-grained to predominantly medium-grained sandstone with mudstone clasts	Bed division characterized by abundant aligned and locally imbricated mudstone clasts embedded in a sandstone matrix. The clasts exhibit coarse-tail inverse grading, transitioning upward into facies S_3	Traction carpet deposition beneath a high-density turbidity flow	Lowe (1982
S_3	Coarse-grained to predominantly medium to fine-grained sandstone	Massive, normally to weakly graded sandstone division exhibiting dewatering structures and containing randomly oriented mudstone clasts, the abundance of which tend to decrease upward. Restricted to AMC deposits (Fig. 6)	Deposition by a fully turbulent, high-density flow. Dewatering structures indicate rapid deposition	Lowe (1982)
T_A	Medium to very fine-grained sandstone	Sharp-based, massive/structureless, ungraded to poorly graded sandstone division. In places, the base is loaded or exhibit flute casts. Lithic pebbles or mudstone clasts occur sporadically at the base	Rapid suspension fall-out and sand aggradation from a high-density turbidity current	Bouma (1962)
T_B	Fine to very fine-grained sandstone	Plane parallel-laminated, ungraded to normally graded sandstone division	Traction deposition under upper flow regime conditions. Waning, low-density turbidity current	Bouma (1962)
T_C	Fine to very-fine-grained sandstone	Sandstones exhibiting current-ripple cross-lamination. Climbing sets are common.	Ripple development and migration under lower flow regime conditions. Climbing	Bouma (1962)

			sets indicate high sedimentation rates	
T_D	Very fine-grained sandstone to predominantly siltstone	Used for denoting undifferentiated, structured, normally graded siltstone units where outcrop quality hinders proper description. In core, multiple varieties are recognized (see T_1 to T_5 below)	Shear-sorting of grains and flocs carried by the rare part of the flow	Bouma (1962)
T_E	Siltstone to mudstone	Used for denoting undifferentiated mudstone units in outcrops where proper description is problematic. Correspond to T_6 to T_8	Suspension settling of sediments from the diluted, low-density tail of the flow	Bouma (1962)
$T_{1–8}$	Mudstone to siltstone and subordinate sandstone	Fine-grained facies variations (only detectable in core) including mudstones exhibiting convolute (T_1), irregular to lenticular (T_2), regular parallel (T_3), indistinct (T_4), to wispy (T_5) siltstone lamination, and normally graded to ungraded mudstone (T_6/T_7) and bioturbated mudstone (T_8)	Suspension settling of sediments from the diluted, low-density tail of the flow, as well as settling of 'background' mud	Stow & Shanmugam (1980)
B_1	Fine to very fine-grained sandstone and petrified plant detritus	Sandstone with abundant aligned and pseudo-layered plant detritus. In units of abnormally high concentration of plant material, imbrication commonly occurs. Transitional to facies B_2 and D_1	Deposition by transitional (quasi-laminar) flow. Flow transformation promoted by concentration of plant material	Similar to H2 of Haughton *et al*. (2009)
B_2	Fine to very fine-grained sandstone to siltstone with petrified plant detritus	Sandstone to siltstone division containing (layer-parallel) aligned plant detritus forming pronounced banding (individual band thickness: <2 cm)	Deposition by transitional (slurry) flow with fluctuating near-bed sediment concentrations and turbulence	Similar to M_2 of Lowe & Guy (2000) and H2 of Haughton *et al*. (2009). Baas *et al.* (2011)
D_1	Mud-rich, fine to very fine-grained sandstone and siltstone	Argillaceous sandstone to siltstone division containing abundant randomly oriented plant detritus. Soft-sediment deformation structures occur frequently	Deposition by debris flow originating from *en masse* transformation from turbulent to laminar flow	Lowe (1982). See also H3 of Haughton *et al.* (2009)
D_2	Fine-grained sandstone to siltstone rich in mudstone clasts	Aligned to randomly oriented rip-up mudstone clasts embedded in a muddy sand matrix	Substrate erosion and mud clast entrainment by a fully turbulent flow that transformed into a (laminar) debris flow	Similar to H3 of Haughton *et al.* (2009)

D_3	Mud-rich, very fine-grained sandstone to siltstone	0.1 to 0.3 m thick asymmetrically folded and convolute laminated division with occasional sandstone clasts and pseudo-nodules	Deposition by debris flow. Convoluted bedding may record: (i) unstable density gradients and buoyancy-driven fold growth; or (ii) liquefaction induced by decelerating reversed flow pulses, or cyclic stress caused by the passage of internal waves	Similar to H3 of Haughton *et al.* (2009): (i) Gladstone *et al.* (2018); (ii) Tinterri et al. (2022)

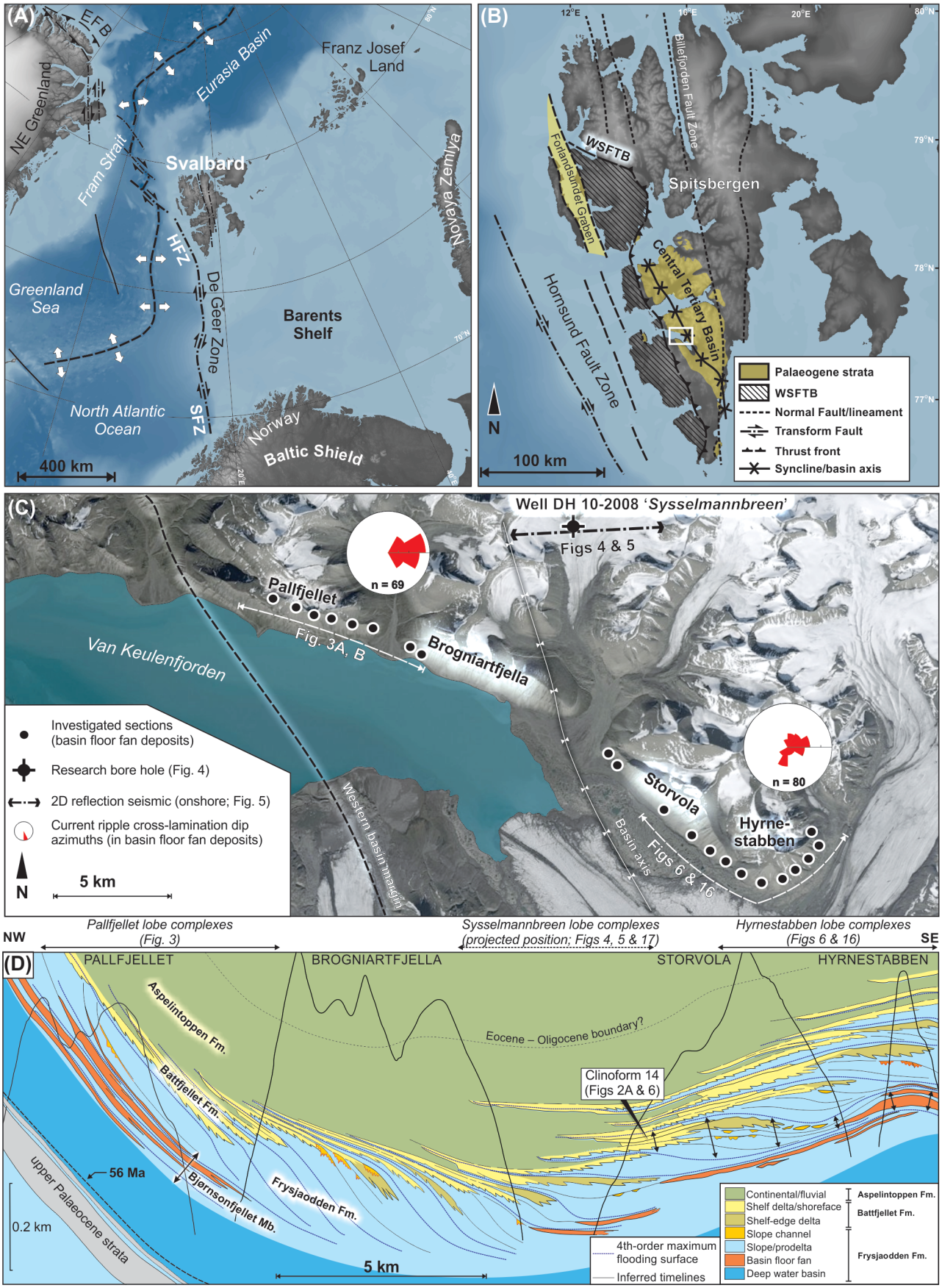

Figure 1_REVISED.tif

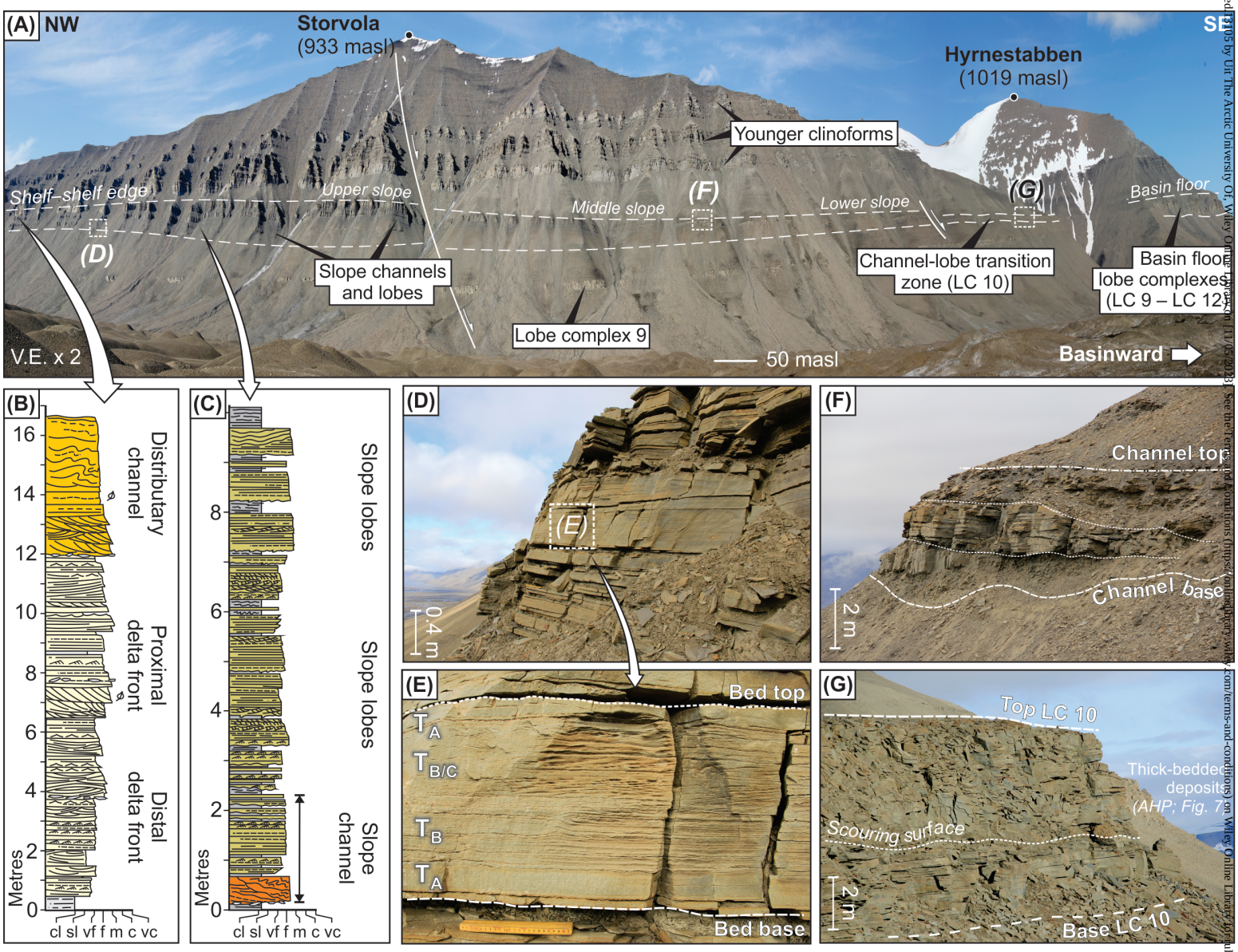

Figure 2_New.tif

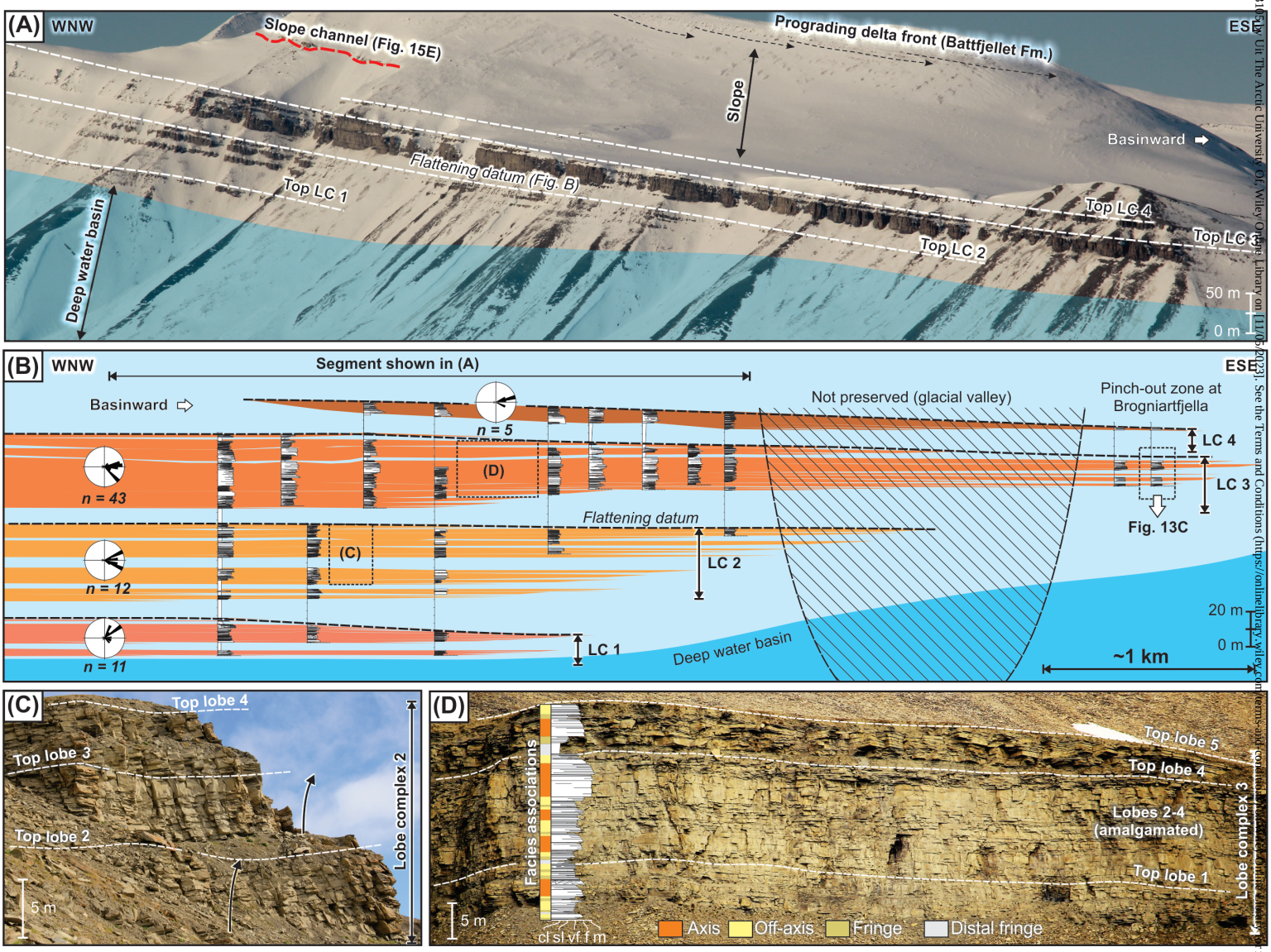

Figure 3_NEW.tif

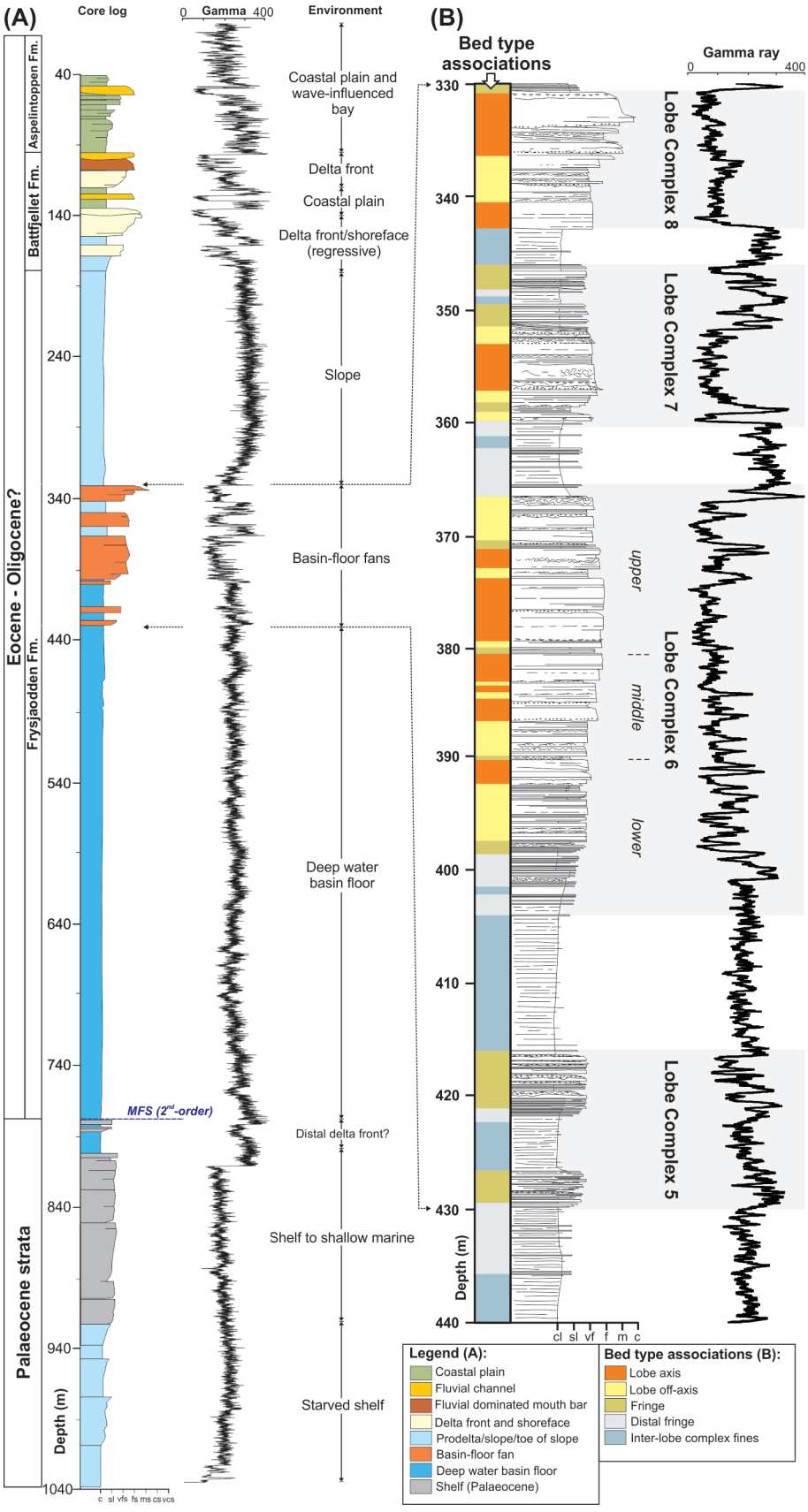

Figure 4_REVISED.tif

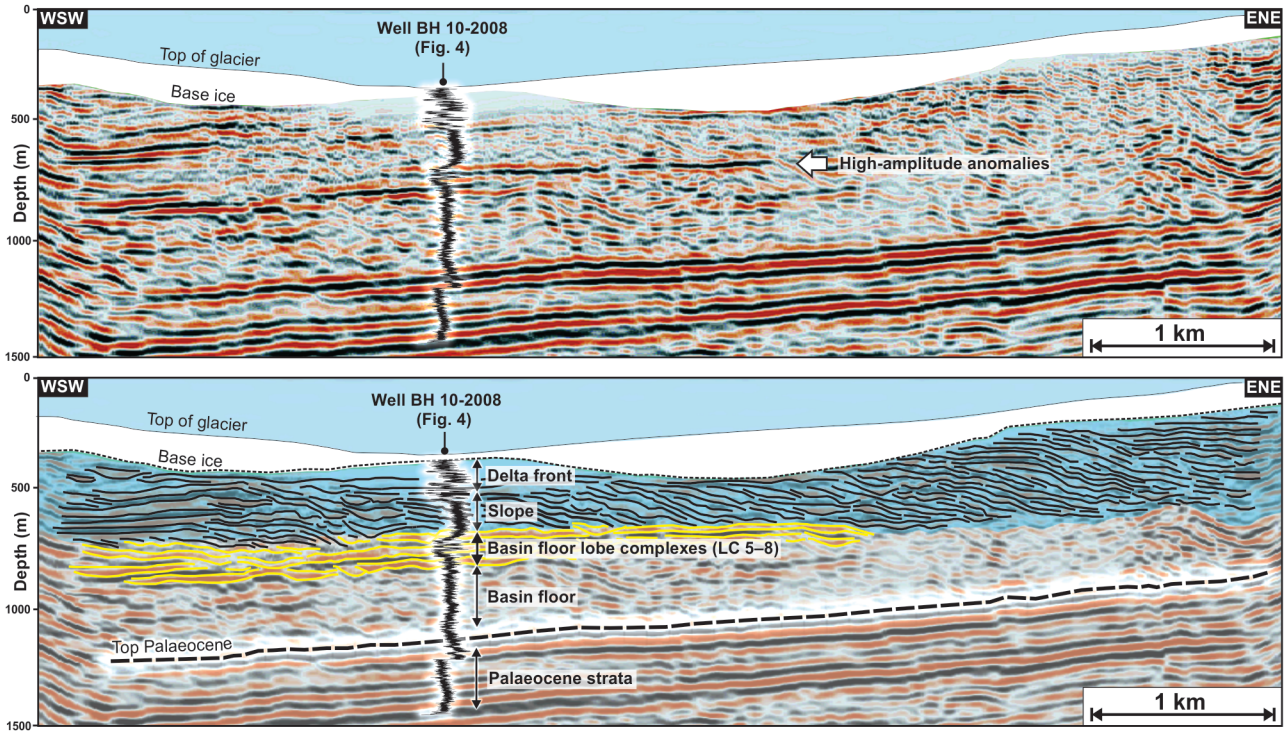

Figure 5_REVISED.tif

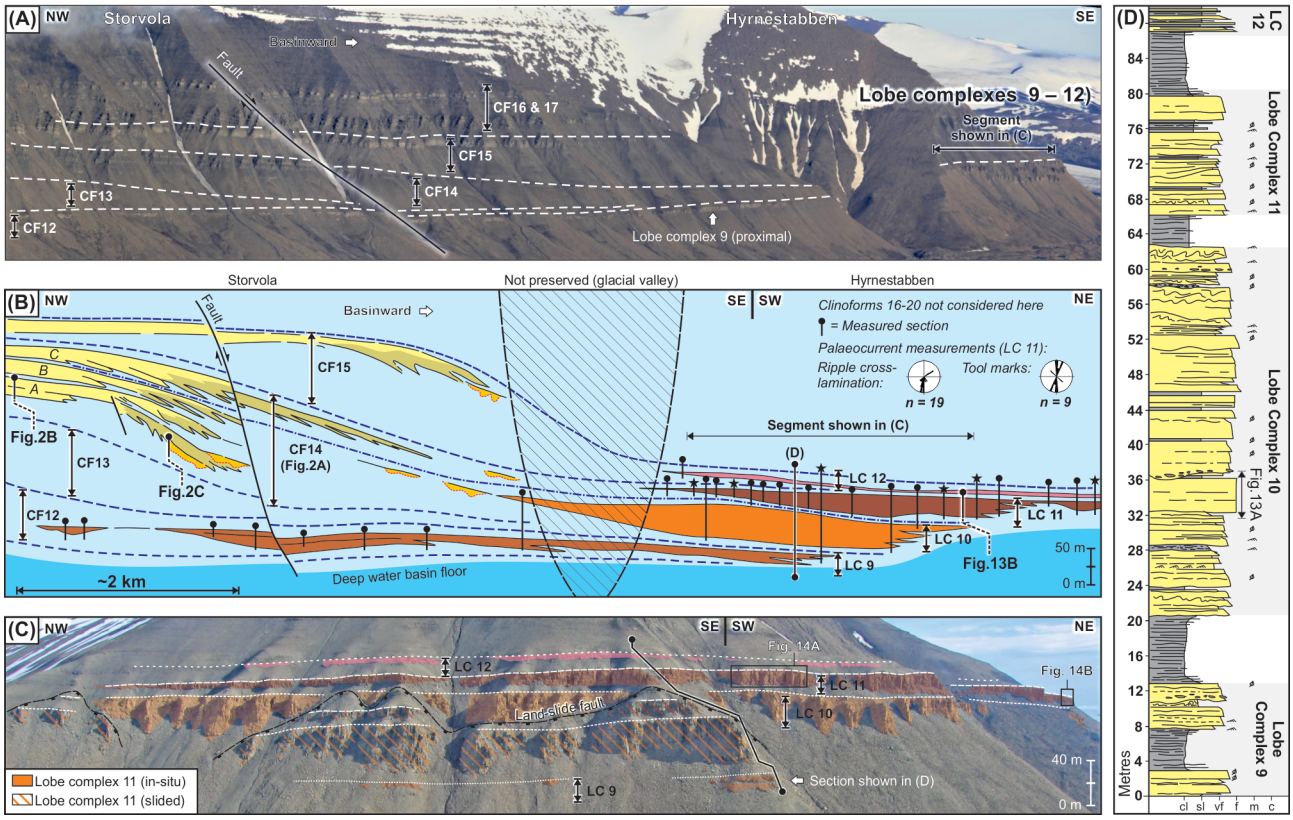

Figure 6_REVISED.tif

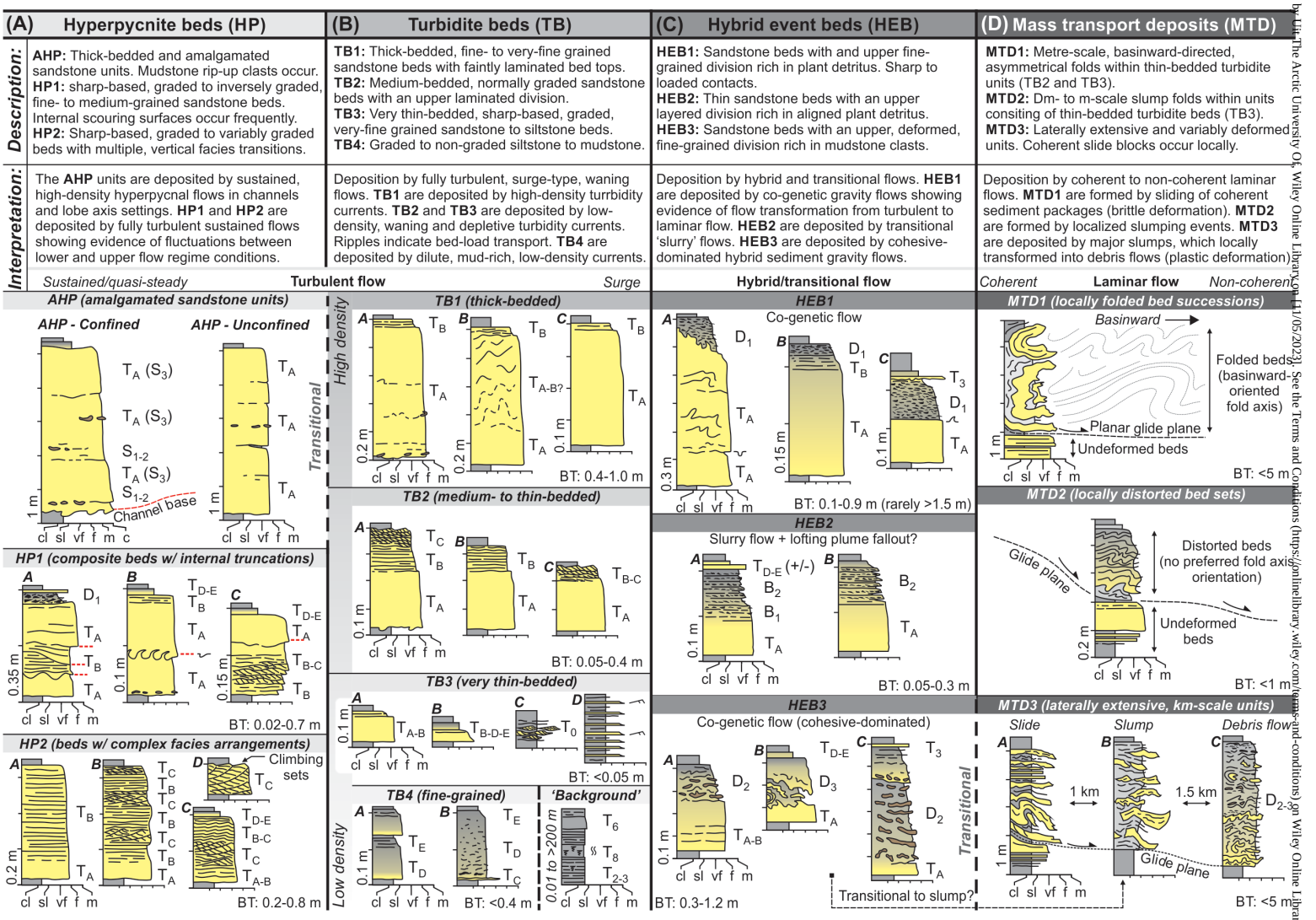

Figure 7_NEW.tif

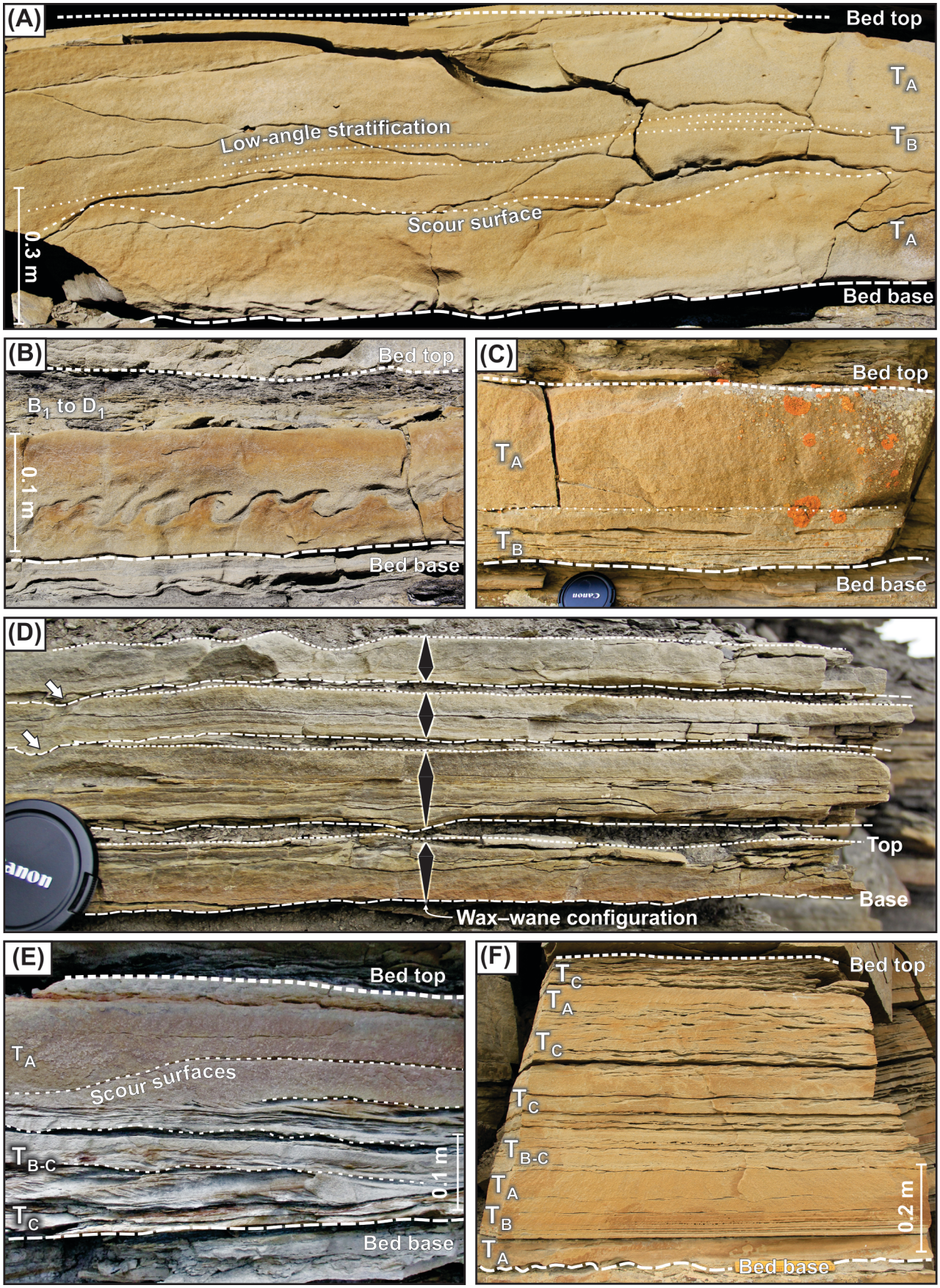

Figure 8_NEW.tif

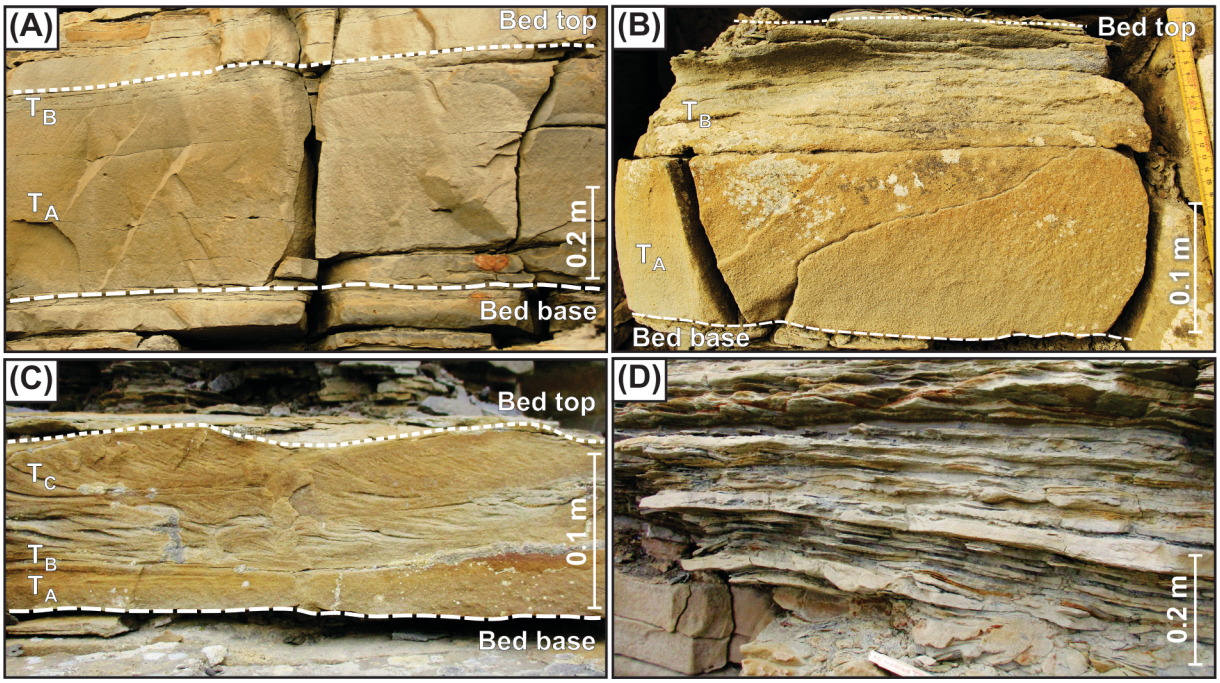

Figure 9_NEW.tif

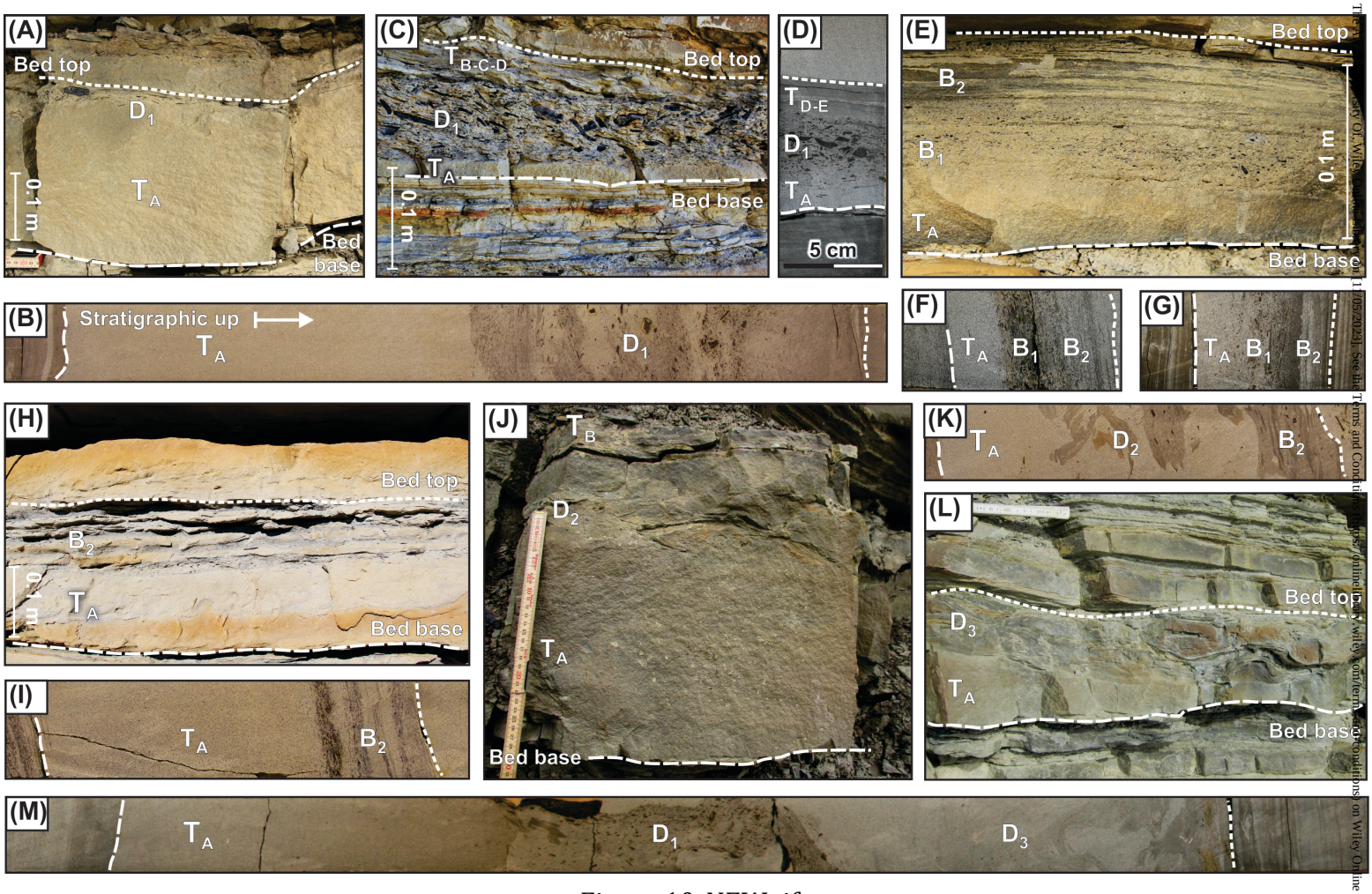

Figure 10_NEW.tif

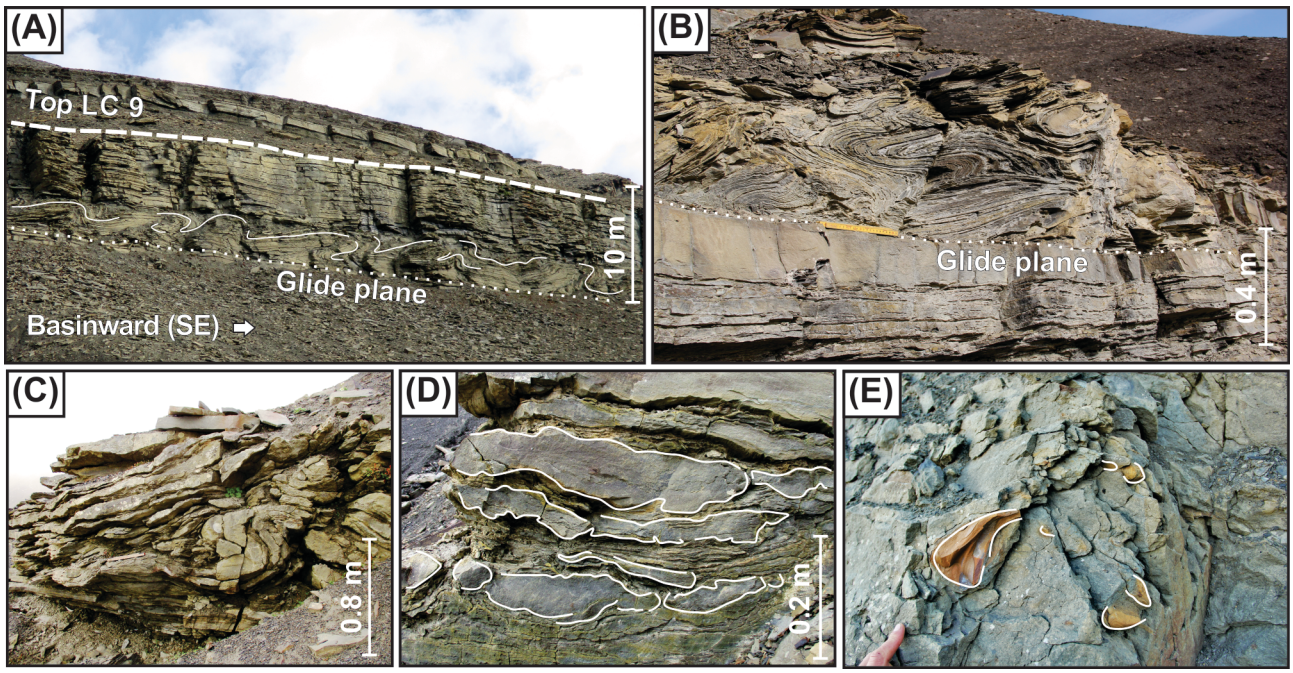

Figure 11_NEW.tif

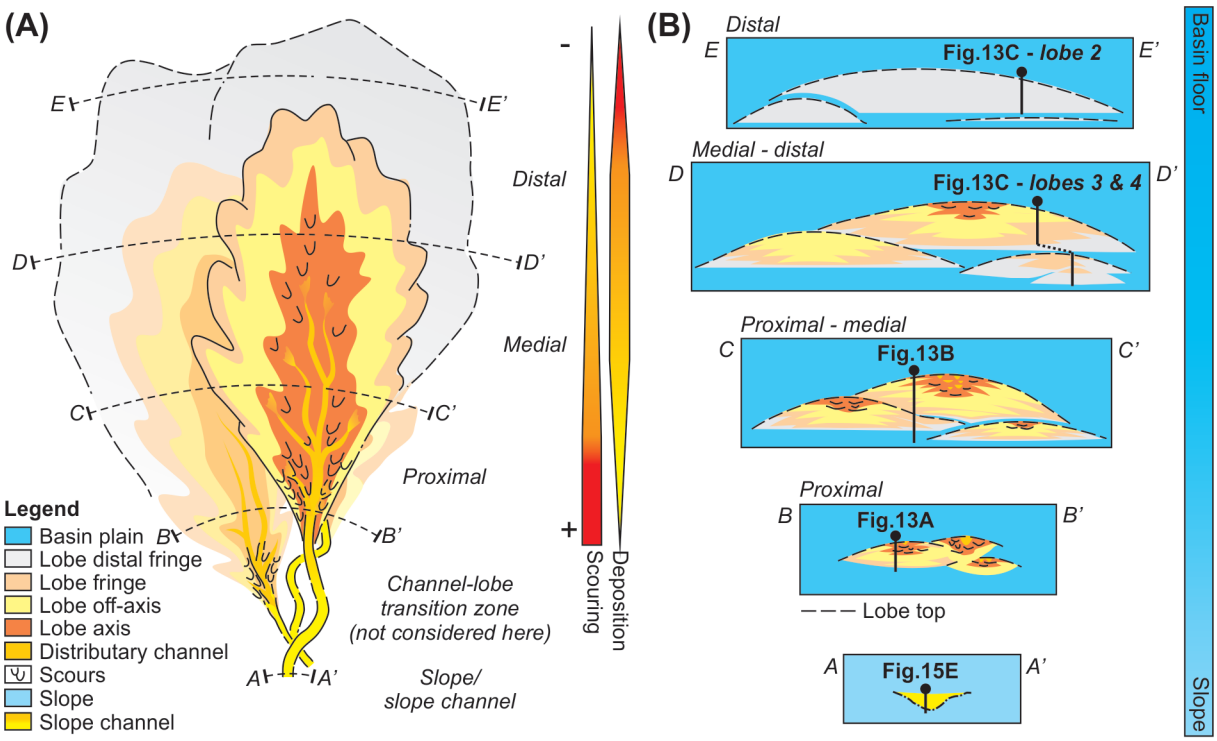

Figure 12_NEW.tif

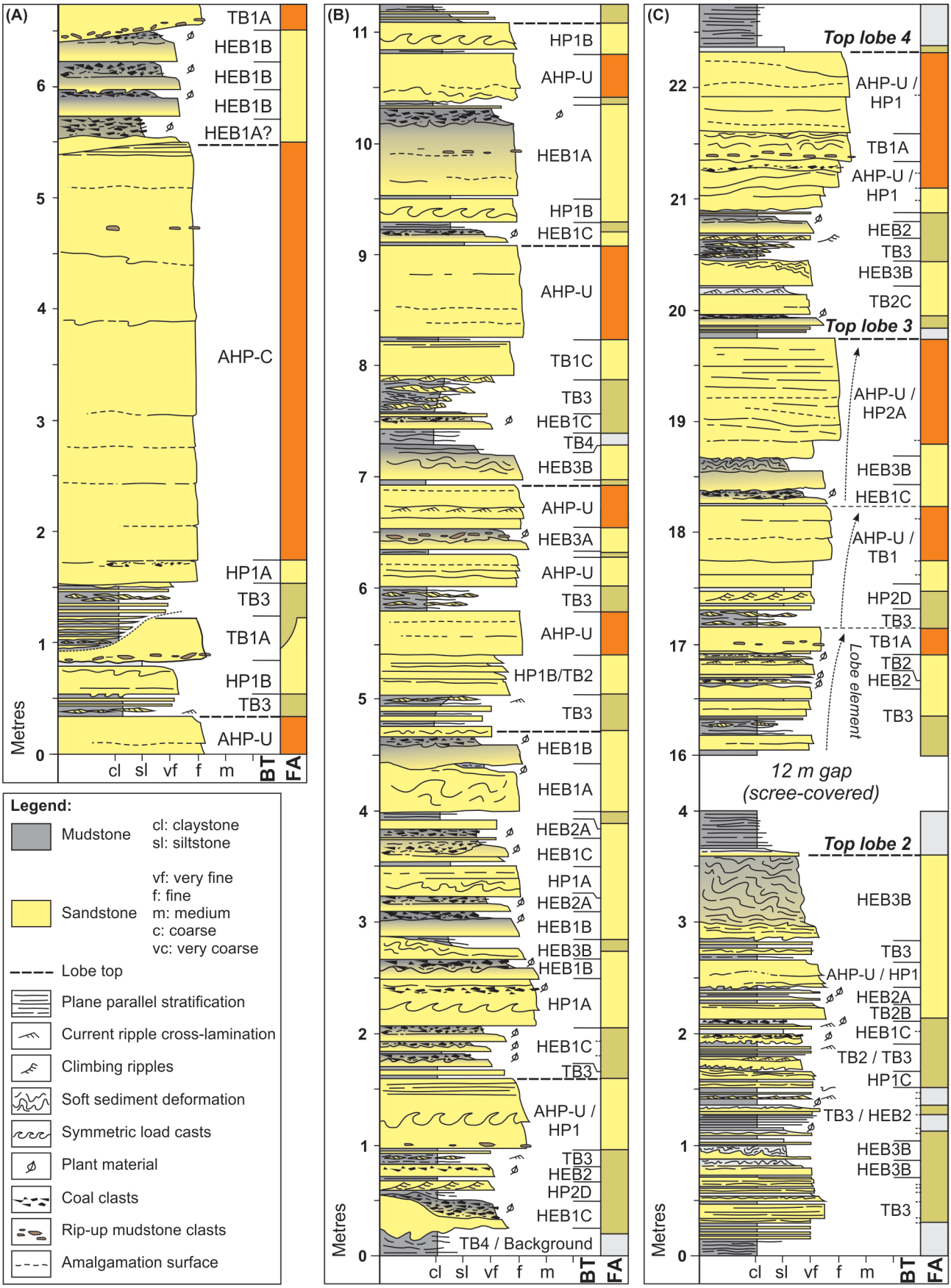

Figure 13_NEW.tif

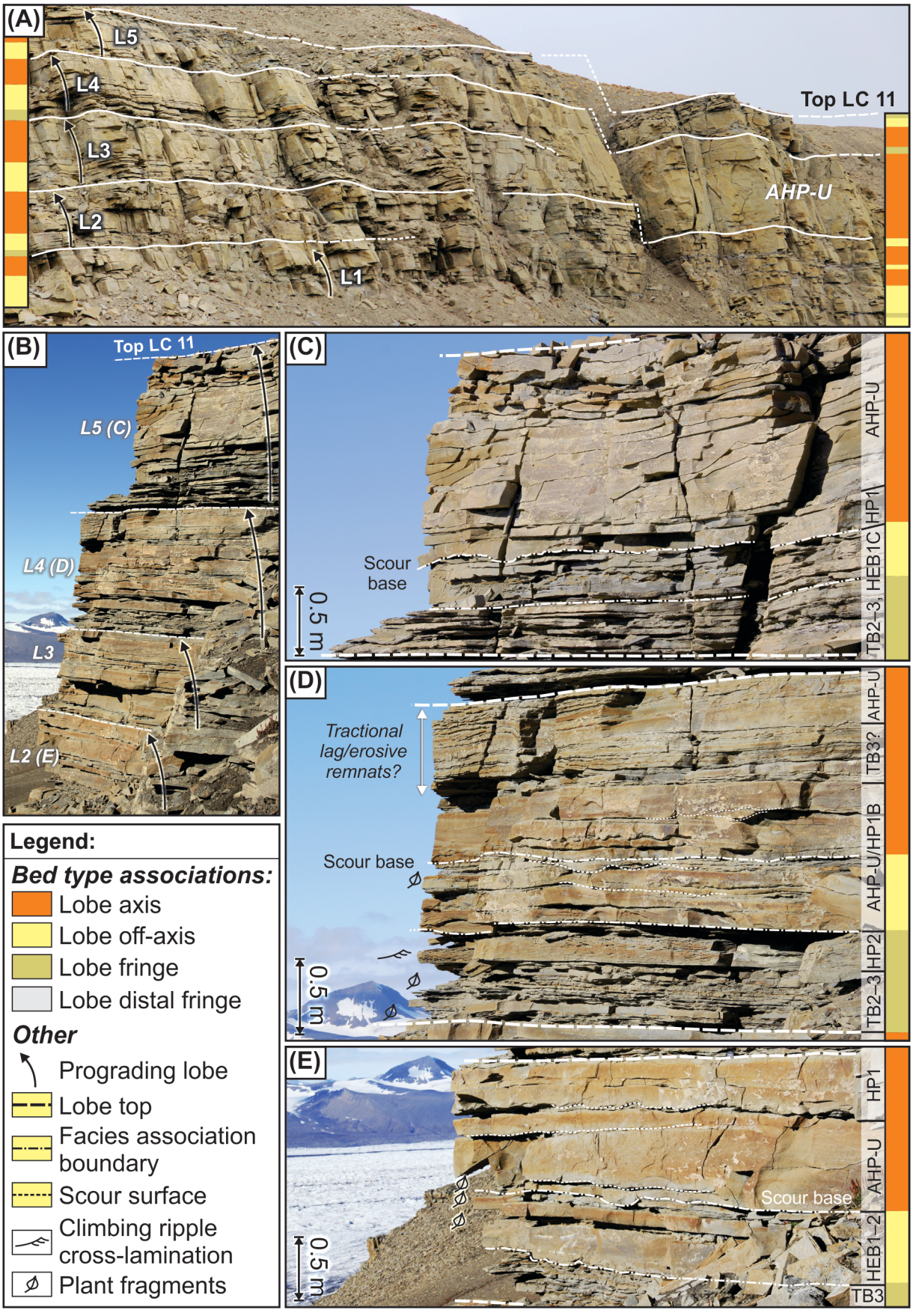

Figure 14_NEW.tif

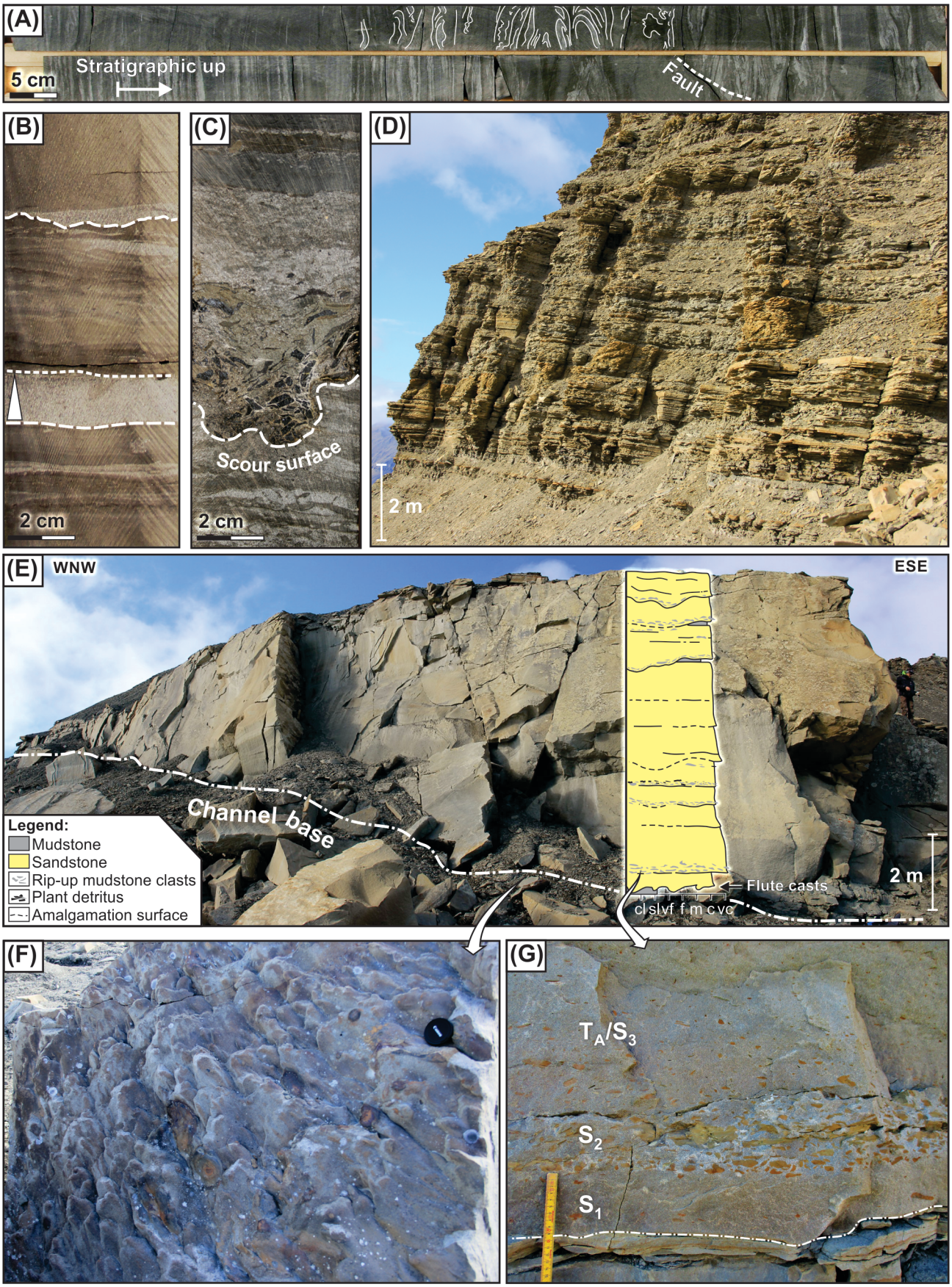

Figure 15_NEW.tif

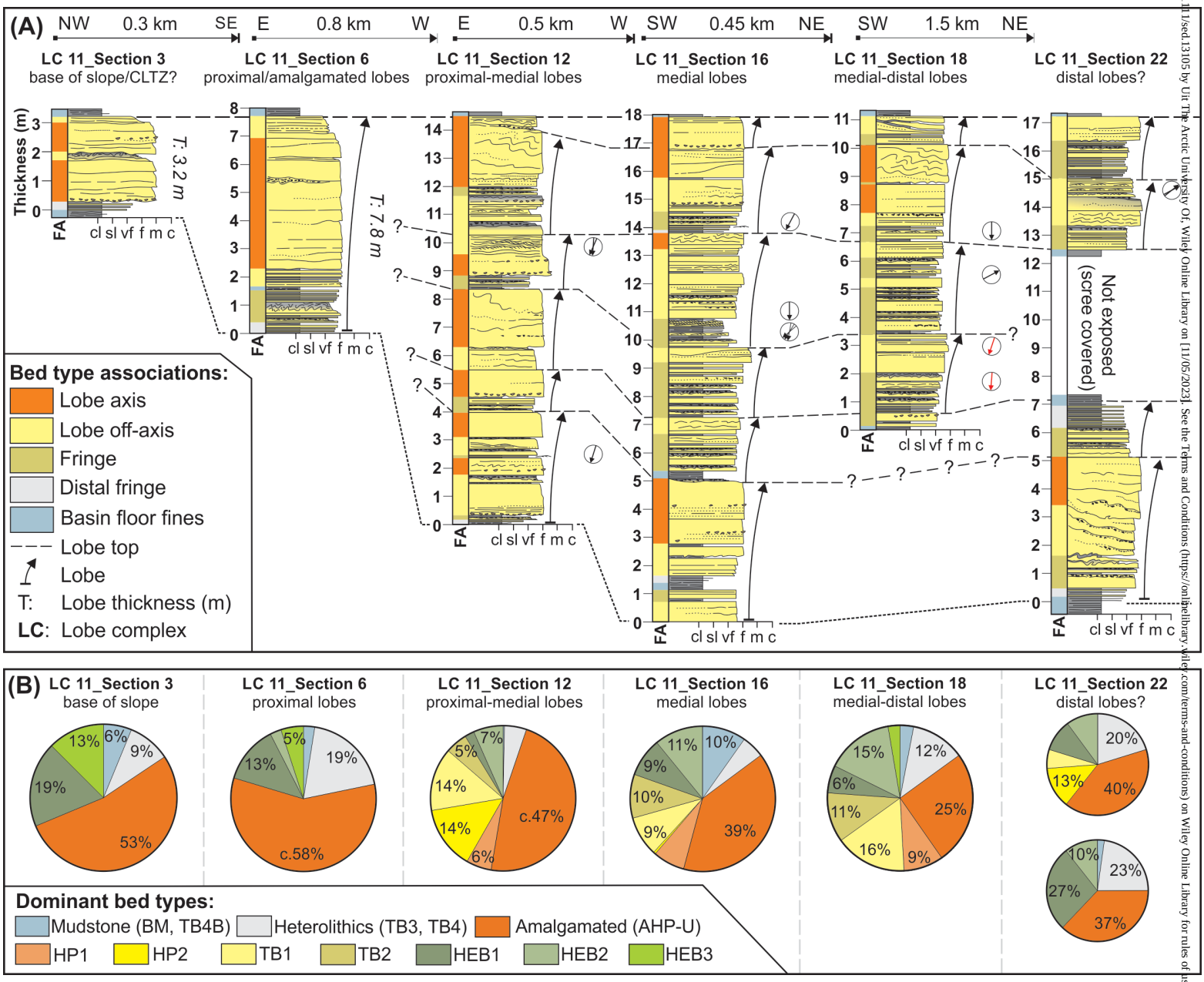

Figure 16_REVISED.tif

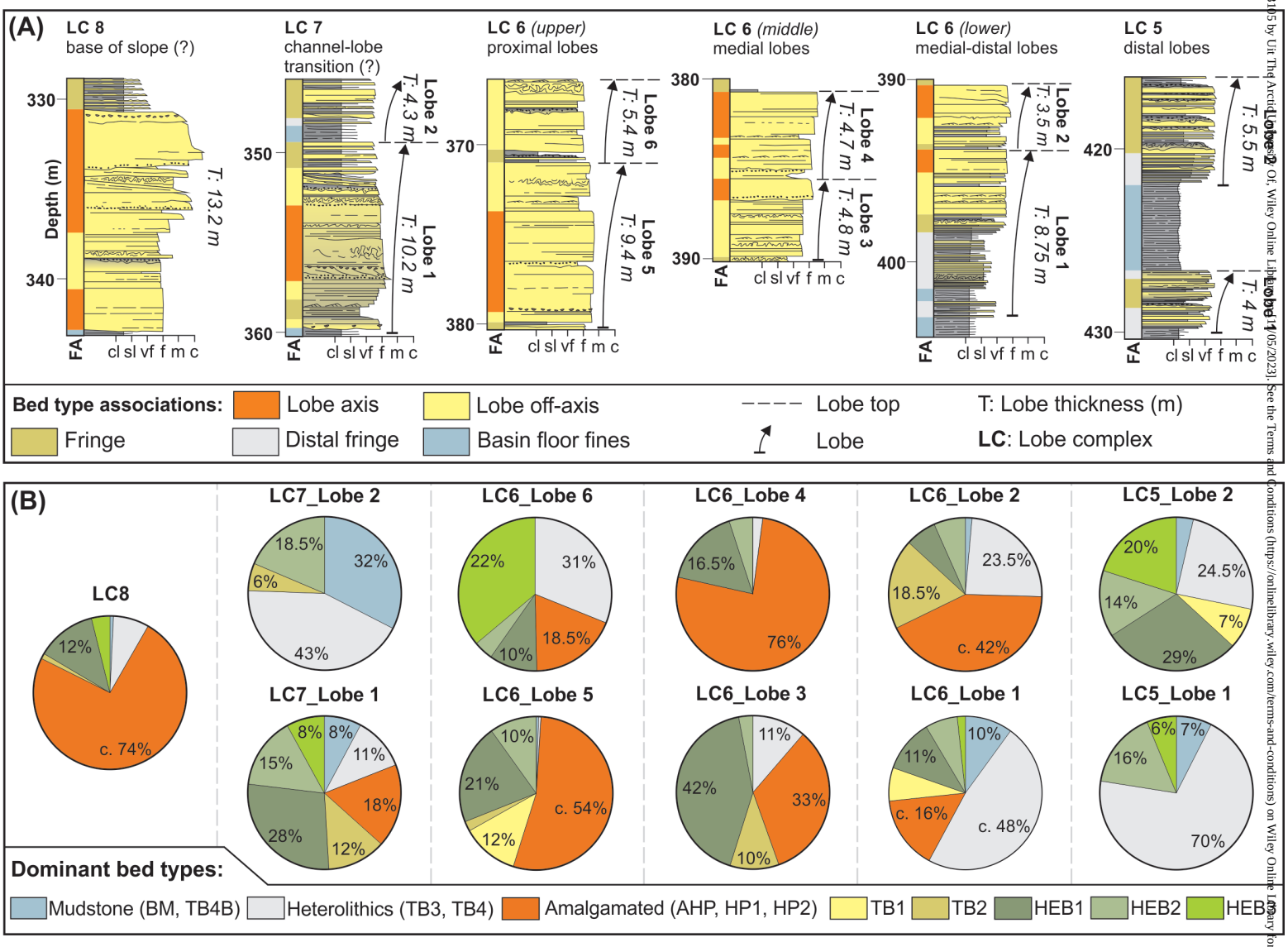

Figure 17_NEW.tif

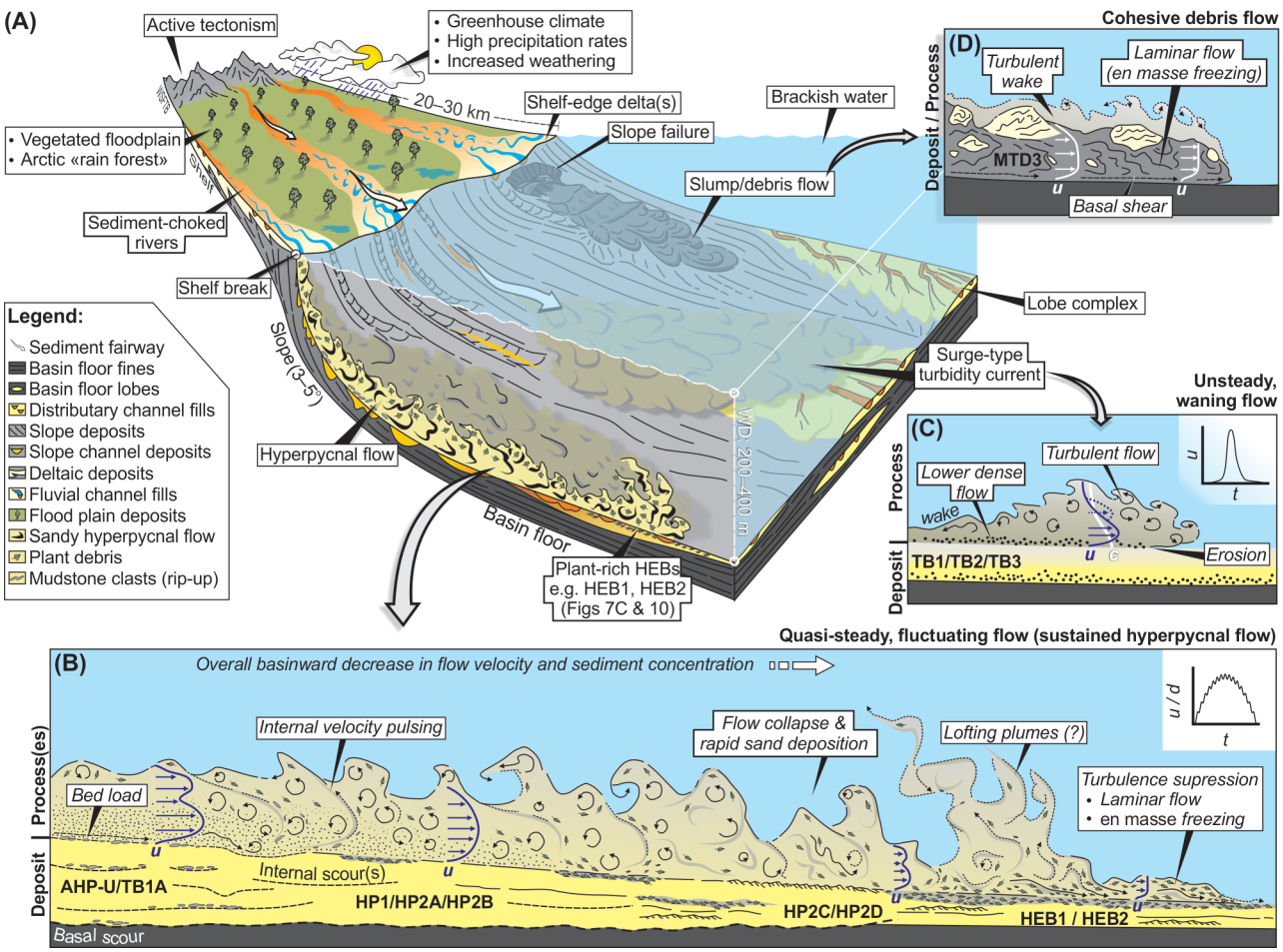

Figure 18_REVISED.tif